Tesi di Dottorato

Università degli Studi di Napoli "Federico II"

Dipartimento di Ingegneria Biomedica
Elettronica e delle Telecomunicazioni

Dottorato di Ricerca in
Ingegneria Elettronica e delle Telecomunicazioni

Radar Waveform Design via Convex Optimization

Marco Piezzo

Il Coordinatore del Corso di Dottorato
Ch.mo Prof. Niccoló Rinaldi

Il Tutore
Ch.mo Prof. Antonio De Maio

A. A. 2012–2013

Contents

List of Figures

List of Algorithms

List of Tables

Introduction

As sanctioned by the IEEE Radar Standard P686/D2 (January 2008), the term *waveform diversity* indicates:
Adaptivity of the radar waveform to dynamically optimize the radar performance for the particular scenario and tasks. May also exploit adaptivity in other domains, including the antenna radiation pattern (both on transmit and receive), time domain, frequency domain, coding domain, and polarization domain.
This paradigm is, undoubtedly, the expression of the revolutionary technological advances in the radar signal processing field (such as new flexible waveform generators, high speed signal processing hardware, digital array technology, and so on), which have made attainable the actual stressing performance requirements; indeed, its basics are in measurement diversity, knowledge-aided processing and design, and transmitter adaptivity, which only in the last decades have become fully accessible. The waveform diversity paradigm arises from the insatiable demands for remote sensing performance that are always present, especially in military applications. We recall here that increasing complex operating scenarios call for more and more sophisticated algorithms with the ability to adapt and diversify dynamically the waveform to the operating environment: it represents, indeed, the key ingredient to achieve a significant performance gain with respect to classic radar waveforms. Nevertheless, this flexibility demands for renewed strategies of modeling waveform properties and optimizing waveform design.

All these aspects highly justify the interest of the research herein conducted, whose main aim has been to investigate the *potentiality* offered by waveform design and waveform diversity. In particular, the essence of the present work of thesis is the possible application of the Optimization Theory so as to the devise high performing transmit signal/receive filter design techniques. Verily, once a certain figure of merit has been cho-

sen and properly described by the mathematical language, and once the necessary data have been collected, many problems of practical interest in radar field can be modeled in terms of an optimization problem, where the main purpose is to optimize the system performance under some constraints imposed by interference, clutter and, more in general, the operating environment. The optimization theory and its tools are not unfamiliar to the signal processing community, although only with the technological growth of the last years they become approachable and computationally reasonable.

Therefore, the thesis is organized as follows:

- In Chapter 1, a waveform design algorithm attempting to jointly optimize the radar detection performance and the region of achievable values for the Doppler estimation accuracy (for a fixed target Doppler frequency) in the presence of colored Gaussian noise is proposed, under a constraint on the transmitted energy and on the degree of similarity with a pre-fixed radar code. Precisely, the resulting waveform design problem can be formulated in terms of a non-convex multi-objective optimization problem. Thus, a family of optimal solutions is constructed, through the use of the Pareto-optimal theory and the introduction of the Pareto weights.

- In Chapter 2, the uncertainty over the prior knowledge of the target Doppler shift is dealt with. The starting point is the realization that many among the algorithms and design techniques in the open literature optimize the radar signal in correspondence of a given target frequency, which is actually an unknown parameter: therefore, even small mismatches between the presumed and the actual value may result in extremely poor performance. Thus, a max-min approach is employed, and a robust waveform design algorithm with polynomial computational complexity is proposed to devise *good* sub-optimal transmit signals, relying on the Semidefinite Programming (SDP) relaxation technique and the theory of trigonometric polynomials, and assuming colored Gaussian disturbance and under a similarity and an energy constraint.

- In Chapter 3, the imposition of a Peak-to-Average power Ratio (PAR) constraint is investigated, which is appealing also from a technical point of view, and very reasonable for radar applications. Specifically, it permits to keep under control the dynamic range of

the transmitted waveform, which is be a primal issue since linear amplifiers with a large dynamic range may be difficult to obtain. Design algorithms maximizing the Signal-to-Noise Ratio (SNR), for both the cases of a given and an unknown target Doppler frequency, are synthesized, and their phase quantized versions (which force the waveform phase to lie within a finite alphabet) are devised. All the problems are formulated in terms of non-convex NP-hard quadratic optimization programs, and thus high-quality sub-optimal solutions, relying on SDP relaxation and randomization as well as on the theory of trigonometric polynomials, are proposed.

- In Chapter 4, the problem of cognitive transmit signal and receive filter design for a point-like target embedded in a high reverberating environment is considered, focusing on phase-only waveforms sharing either a continuous or a finite alphabet phase (so as to comply with the technological limits of the current radar amplifiers); moreover, a similarity constraint is enforced, so as to keep under control the auto-ambiguity properties of the sought transmit code. In particular, the Signal-to-Interference-plus-Noise Ratio (SINR) is considered as figure of merit, and an iterative procedure, requiring the solution fo both a convex and an NP-hard quadratic fractional problem, is proposed to sequentially improve it. As for the NP-hard problem, a relaxation and randomization approach is applied so as to find good-quality sub-optimal solutions.

At the end of each Chapter, some conclusions and possible future tracks are given.

Notation

$\boldsymbol{a}$	column vector;
$a(i)$	i-th element of the column vector $\boldsymbol{a}$;
$\boldsymbol{a}_i$	i-th column vector;
$\boldsymbol{A}$	matrix;
$A(i,k)$	(i,k)-th entry of the matrix $\boldsymbol{A}$;
$(\cdot)^T$	transpose operator;
$(\cdot)^*$	complex conjugate operator (component-wise complex conjugate if the argument is a matrix or a vector);
$(\cdot)^\dagger$	transpose conjugate operator;
$\lfloor \cdot \rfloor$	integer floor operation;
$\mathrm{tr}(\cdot)$	trace of the square matrix argument;
$\det(\cdot)$	determinant of the square matrix argument;
$\mathbf{diag}(\cdot)$	vector formed by the diagonal elements of the matrix argument;
$\mathbf{Diag}(\cdot)$	diagonal matrix formed by the components of the vector argument;
$\lambda_{\min}(\cdot)$	minimum eigenvalue of the square matrix argument;
$\lambda_{\max}(\cdot)$	maximum eigenvalue of the square matrix argument;
$\boldsymbol{I}$	identity matrix;
$\mathbf{0}$	matrix with zero entries;
$\boldsymbol{e}_k$	vector with all zeros except 1 in the k-h position;
j	imaginary unit (i.e., $j = \sqrt{-1}$);
$\mathbb{R}$	set of real numbers;
$\mathbb{C}$	set of complex numbers;

$\Re\{\cdot\}$	real part of the argument;
$\Im\{\cdot\}$	imaginary part of the argument;
$\|\cdot\|$	Euclidean norm of the argument vector;
$\|\cdot\|_\infty$	l_∞ norm of the vector argument, defined as $\|\boldsymbol{a}\|_\infty = \max_{k\in(1,\ldots,N)} \|x(k)\|$;
$\|\cdot\|$	modulus of a complex number;
$\arg(\cdot)$	argument of a complex number;
$\odot$	Hadamard element-wise product;
$E[\cdot]$	expected value operator;
$\succeq$	generalized inequality: $\boldsymbol{A} \succeq \boldsymbol{B}$ means that $\boldsymbol{A} - \boldsymbol{B}$ is an Hermitian positive semidefinite matrix;
$\succ$	generalized inequality: $\boldsymbol{A} \succ \boldsymbol{B}$ means that $\boldsymbol{A} - \boldsymbol{B}$ is an Hermitian positive definite matrix.

System Model

In the following, the model for both the transmitted and the received coded signals is presented, which will be the basic assumption in most part of the thesis.

It is consider a radar which transmits a coherent burst of pulses, such as in [1]:

$$s(t) = a_t u(t) \exp[j(2\pi f_0 t + \phi)]\,,$$

where a_t is the transmit signal amplitude, $j = \sqrt{-1}$,

$$u(t) = \sum_{i=0}^{N-1} a(i) p(t - iT_r)\,,$$

is the signal's complex envelope (see Figure 1), $p(t)$ is the signature of the transmitted pulse, T_r is the Pulse Repetition Time (PRT), $[a(0), a(1), \ldots, a(N-1)] \in \mathbb{C}^N$ is the radar code, $\mathbb{C}$ denotes the set of complex numbers, f_0 is the carrier frequency, and ϕ is a random phase. Moreover, the pulse waveform $p(t)$ is of duration $T_p \leq T_r$ and has unit energy, i.e.

$$\int_0^{T_p} |p(t)|^2 dt = 1\,.$$

The signal backscattered by a target with a two-way time delay τ and received by the radar is

$$r(t) = \alpha_r e^{j2\pi(f_0+f_d)(t-\tau)} u(t-\tau) + i(t) + n(t)\,,$$

where α_r is the complex echo amplitude (accounting for the transmit amplitude, phase, target reflectivity, and channels propagation effects), f_d is the target Doppler frequency, and the term $n(t) + i(t)$ is overall additive disturbance due to the interference (it may be clutter or other source of interference) and thermal noise. This signal is down-converted

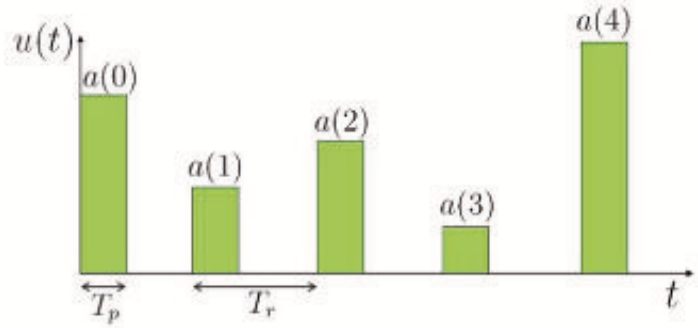

Figure 1: Coded pulse train $u(t)$ for $N = 5$ and $p(t)$ with rectangular shape.

to baseband and filtered through a linear system with impulse response $h(t) = p^*(-t)$. Let the filter output be

$$v(t) = \alpha_r e^{-j2\pi f_0 \tau} \sum_{i=0}^{N-1} a(i) e^{j2\pi i f_d T_r} \chi_p(t - iT_r - \tau, f_d) + w(t)\,,$$

where $\chi_p(\lambda, f)$ is the pulse waveform ambiguity function [2], i.e.

$$\chi_p(\lambda, f) = \int_{-\infty}^{+\infty} p(\beta) p^*(\beta - \lambda) e^{j2\pi f \beta} d\beta,$$

and $w(t)$ is the down-converted and filtered disturbance component. The signal $v(t)$ is sampled at $t_k = \tau + kT_r$, $k = 0, \ldots, N-1$, providing the observables[1]

$$v(t_k) = \frac{\alpha}{\sqrt{N}} a(k) e^{j2\pi k f_d T_r} \chi_p(0, f_d) + w(t_k), \qquad k = 0, \ldots, N-1\,,$$

where $\alpha = \sqrt{N}\alpha_r e^{-j2\pi f_0 \tau}$. Assuming that the pulse waveform time-bandwidth product and the expected range of target Doppler frequencies are such that the single pulse waveform is insensitive to target Doppler shift[2], namely $\chi_p(0, f_d) \sim \chi_p(0, 0) = 1$, it is possible to rewrite the

[1] Range straddling losses are neglected; also, the assumption is that there are no target range ambiguities.

[2] Notice that this assumption might be restrictive for the cases of very fast moving targets such as fighters and ballistic missiles.

samples $v(t_k)$ as

$$v(t_k) = \frac{\alpha}{\sqrt{N}} a(k) e^{j2\pi k f_d T_r} + w(t_k), \qquad k = 0, \ldots, N-1\,.$$

Moreover, denoting by $\boldsymbol{c} = [a(0), a(1), \ldots, a(N-1)]^T$ the N-dimensional column vector containing the code elements, $\boldsymbol{p} = \frac{1}{\sqrt{N}} \left[1, e^{j2\pi\nu_d}, \ldots, e^{j2\pi(N-1)\nu_d}\right]^T$ the normalized temporal steering vector, $\nu_d = f_d T_r$ the normalized Doppler frequency, $\boldsymbol{v} = [v(t_0), v(t_1), \ldots, v(t_{N-1})]^T$, and $\boldsymbol{w} = [w(t_0),\ w(t_1), \ldots, w(t_{N-1})]^T$, the following vectorial model for the backscattered signal is obtained [3]

$$\boldsymbol{v} = \alpha \boldsymbol{c} \odot \boldsymbol{p} + \boldsymbol{w}\,. \tag{1}$$

In the following the disturbance $\boldsymbol{w}$ will generally be modeled as a zero-mean complex circular Gaussian vector with known positive-definite covariance matrix

$$E[\boldsymbol{w}\boldsymbol{w}^\dagger] = \boldsymbol{M}\,; \tag{2}$$

further details will be given in case model (2) no longer subsists.

Chapter 1

Pareto-Optimal Radar Waveform Design

1.1 Introduction

More and more sophisticated algorithms for radar waveform design have been recently developed, due to the considerable advances in high speed signal processing hardware and digital array technology, as well as the growing interest for better and better radar performances [4, 5].

Some recent studies concerning waveform optimization in the presence of colored disturbance can be found in [6]. Therein, some algorithms, exploiting the degrees of freedom provided by a possibly rank deficient clutter covariance matrix, are developed. In [7], a signal design approach relying on the maximization of the SNR under a similarity constraint with a given waveform is proposed and assessed. In [1], focusing on the class of linearly coded pulse trains (both in amplitude and in phase), the authors introduce a code selection algorithm which maximizes the detection performance but, at the same time, is capable of controlling both the region of achievable values for the Doppler estimation accuracy and the degree of similarity with a pre-fixed radar code. Further algorithms are also available attempting to determine the radar waveforms optimizing P_d under structural constraints (for instance a phase-only modulation) [8, 9] or possibly for airborne Space Time Adaptive Processing (STAP) scenarios [10].
In this Chapter, the focus is still focus on constrained code optimization, in the presence of colored Gaussian disturbance, assuming the same sig-

nal model as in [1]. At the design stage, it is proposed a waveform design algorithm based on the following criterion: joint optimization of the detection performance and of the region of achievable values for the Doppler estimation accuracy, under a constraint on the transmitted energy and on the degree of similarity with a pre-fixed radar code. This is tantamount to jointly maximizing two quadratic forms, so that the resulting waveform design problem can be formulated in terms of a non-convex multi-objective optimization problem. In order to solve it, the scalarization technique is invoked, where the original vectorial problem is reduced to a scalar one through the use of the Pareto-optimal theory. Thus, the proposed codes are chosen as *Pareto-optimal points*[1] of the previously mentioned multi-objective optimization problem. Previous applications of the multi-objective optimization theory to radar waveform design can be found in [12, 13], where Multi-Objective Evolutionary Algorithms (MOEA) are applied to approximate the Pareto optimal set. In the present specific application, it is not necessary to approximate the Pareto set via MOEA, because the proposed deterministic and non-iterative procedure, exploiting scalarization, is capable of providing the exact Pareto-optimal points.

At the analysis stage, the performance of the new encoding algorithm are assessed in terms of detection performance, region of achievable Doppler estimation accuracy, and ambiguity function, highlighting the role of the Pareto weight in the optimization. The results show that it is possible to trade-off the aforementioned performance metrics. Precisely, detection capabilities can be swaped for desirable properties of the waveform ambiguity function and/or for an enlarged region of achievable Doppler estimation accuracies. Furthermore, the trade-off is ruled by both the similarity constraint and the Pareto weight. Indeed, this last parameter defines the relative importance of the two objectives in the optimization problem. Otherwise stated, it represents the cost required for improving a given objective (namely the CRLB) making worse the other (namely the detection probability).

Thus, the Chapter is organized as follows. In Section 1.2, resorting to the system model previously presented, the mathematical formulation for the performance measures is given. In Section 1.3, the code design

[1] A Pareto-optimal solution of a multi-objective optimization problem is defined as any solution that can't be improved with respect to a component without worsening the others [11].

problem is formulated, and the algorithm which provides Pareto-optimal waveforms is presented. In Section 1.4, the performance of the proposed encoding method are assessed also in comparison with a standard radar code. Finally, in Section 1.5, the conclusions and outline possible future research tracks are drawn.

1.2 System Model and Performance Measures

In the following, assuming, for the backscattered signal, the same model as in (1), the focus is on the key performance measures which are to be optimized or controlled during the selection of the radar code.

1.2.1 Detection Probability

It is well known that the problem of detecting a target in the presence of observables described by the model (1) can be formulated in terms of the following binary hypotheses test

$$\begin{cases} H_0: \ \boldsymbol{v} = \boldsymbol{w} \\ \\ H_1: \ \boldsymbol{v} = \alpha \boldsymbol{c} \odot \boldsymbol{p} + \boldsymbol{w} \end{cases} . \tag{1.1}$$

Under the assumption (2), the Generalized Likelihood Ratio Test (GLRT) detector over α for (1.1), which coincides with the optimum test (according to the Neyman-Pearson criterion) if the phase of α is uniformly distributed in $[0, 2\pi)$ [14, 15], is given by

$$|\boldsymbol{v}^{\dagger} \boldsymbol{M}^{-1} (\boldsymbol{c} \odot \boldsymbol{p})|^2 \underset{H_0}{\overset{H_1}{\gtrless}} G \,, \tag{1.2}$$

where G is the detection threshold set according to a desired value of the false alarm Probability (P_{fa}). An analytical expression of the detection Probability (P_d), for a given value of P_{fa}, is available both for the cases of nonfluctuating and fluctuating target. In the former case (NFT)

$$P_d = Q\left(\sqrt{2|\alpha|^2 (\boldsymbol{c} \odot \boldsymbol{p})^{\dagger} \boldsymbol{M}^{-1} (\boldsymbol{c} \odot \boldsymbol{p})}, \sqrt{-2 \ln P_{fa}} \right), \tag{1.3}$$

while, for the case of Rayleigh fluctuating target (RFT) with $E\left[|\alpha|^2\right] = \sigma_a^2$,

$$P_d = \exp\left(\frac{\ln P_{fa}}{1+\sigma_a^2(\boldsymbol{c}\odot\boldsymbol{p})^\dagger \boldsymbol{M}^{-1}(\boldsymbol{c}\odot\boldsymbol{p})}\right), \tag{1.4}$$

where $Q(\cdot,\cdot)$ denotes the Marcum Q function of order 1. This expression shows that, given P_{fa}, P_d depends on the radar code, the disturbance covariance matrix and the temporal steering vector only through the SNR [1], defined as:

$$\text{SNR} = \begin{cases} |\alpha|^2(\boldsymbol{c}\odot\boldsymbol{p})^\dagger \boldsymbol{M}^{-1}(\boldsymbol{c}\odot\boldsymbol{p}) & \text{NFT} \\ \sigma_a^2(\boldsymbol{c}\odot\boldsymbol{p})^\dagger \boldsymbol{M}^{-1}(\boldsymbol{c}\odot\boldsymbol{p}) & \text{RFT} \end{cases}. \tag{1.5}$$

Moreover, P_d is an increasing function of SNR and, as a consequence, the maximization of P_d can be obtained optimizing the SNR over the radar code.

1.2.2 Doppler Accuracy

The Doppler accuracy is bounded below by CRLB and CRLB-like techniques which provide lower bounds for the variances of unbiased estimates. A reliable measurement of the Doppler frequency is very important in radar signal processing because it is directly related to the target radial velocity useful to speed the track initiation, to improve the track accuracy [16], and to classify the dangerousness of the target; hence it is clear that it has to be taken in account in the code design operation. It can be shown that the CRLB for known α is given by [1]:

$$\Delta_{CR}(f_d) = \frac{\psi}{\frac{\partial \boldsymbol{h}^\dagger}{\partial f_d}\boldsymbol{M}^{-1}\frac{\partial \boldsymbol{h}}{\partial f_d}} \tag{1.6}$$

where $\boldsymbol{h} = \boldsymbol{c}\odot\boldsymbol{p}$ and $\psi = \frac{1}{2|\alpha|^2}$. Notice that

$$\frac{\partial \boldsymbol{h}}{\partial f_d} = T_r \boldsymbol{c}\odot\boldsymbol{p}\odot\boldsymbol{u},$$

with $\boldsymbol{u} = [0, j2\pi, ..., j2\pi\,(N-1)]^T$, so that (1.6) can be rewritten as

$$\Delta_{CR}(f_d) = \frac{\psi}{T_r^2\,(\boldsymbol{c}\odot\boldsymbol{p}\odot\boldsymbol{u})^\dagger\,\boldsymbol{M}^{-1}\,(\boldsymbol{c}\odot\boldsymbol{p}\odot\boldsymbol{u})}. \tag{1.7}$$

1.2.3 Similarity Constraint

Designing a code which just optimizes the detection performance does not provide any kind of control on the shape of the resulting coded waveform. Precisely, it can lead to signals with significant modulus variations, poor range resolution, high peak sidelobe levels, and more in general with an undesired ambiguity function behavior. These drawbacks can be partially circumvented imposing a further constraint to the sought radar code. In other words, it is required that the solution to be similar to a known code $\boldsymbol{c}_0$ (with $||c_0||^2 = 1$), which shares constant modulus, reasonable range resolution and peak sidelobe level. This is tantamount to imposing that [7]:

$$||\boldsymbol{c} - \boldsymbol{c}_0||^2 \leq \epsilon, \tag{1.8}$$

where the parameter $\epsilon \geq 0$ rules the size of the similarity region. In other words, (1.8) permits to indirectly control the ambiguity function of the considered coded pulse train: the smaller ϵ the higher the degree of similarity between the ambiguity functions of the designed radar code and of the reference sequence.

1.3 Problem Formulation and Pareto-optimal Code Design

The idea pursued in this Chapter is to design a radar code which optimizes jointly the detection performance and the CRLB on the Doppler estimation accuracy, under a similarity constraint with a known radar code $\boldsymbol{c}_0$ and an energy constraint. Specifically, exploiting the following relationships

$$(\boldsymbol{c} \odot \boldsymbol{p})^\dagger \boldsymbol{M}^{-1} (\boldsymbol{c} \odot \boldsymbol{p}) = \boldsymbol{c}^\dagger \boldsymbol{R} \boldsymbol{c} \tag{1.9}$$

and

$$(\boldsymbol{c} \odot \boldsymbol{p} \odot \boldsymbol{u})^\dagger \boldsymbol{M}^{-1} (\boldsymbol{c} \odot \boldsymbol{p} \odot \boldsymbol{u}) = \boldsymbol{c}^\dagger \boldsymbol{R}_1 \boldsymbol{c}, \tag{1.10}$$

where $\boldsymbol{R} = \boldsymbol{M}^{-1} \odot \left(\boldsymbol{p}\boldsymbol{p}^\dagger\right)^*$ and $\boldsymbol{R}_1 = \boldsymbol{M}^{-1} \odot \left(\boldsymbol{p}\boldsymbol{p}^\dagger\right)^* \odot \left(\boldsymbol{u}\boldsymbol{u}^\dagger\right)^*$ are positive semidefinite [17, pag. 1352, A. 77] (in particular, notice that $\boldsymbol{R}$ is positive definite since $\boldsymbol{x}^H \boldsymbol{R} \boldsymbol{x} = (\boldsymbol{x} \odot \boldsymbol{p})^H \boldsymbol{M}^{-1} (\boldsymbol{x} \odot \boldsymbol{p}) > 0$ for any $\boldsymbol{x} \neq \boldsymbol{0}$, which is equivalent to $\boldsymbol{x} \odot \boldsymbol{p} \neq \boldsymbol{0}$), it appears that P_d is an increasing function of $\boldsymbol{c}^\dagger \boldsymbol{R} \boldsymbol{c}$, while the CRLB is a decreasing function of $\boldsymbol{c}^\dagger \boldsymbol{R}_1 \boldsymbol{c}$. As a consequence, the joint optimization of the P_d and CRLB

can be formulated in terms of a non-convex multi-objective optimization problem [11, pp. 174-187]:

$$\begin{array}{ll} \max\limits_{\boldsymbol{c}} & (\boldsymbol{c}^\dagger \boldsymbol{R}\boldsymbol{c}\,,\, \boldsymbol{c}^\dagger \boldsymbol{R}_1 \boldsymbol{c}) \\ \text{s.t.} & ||\boldsymbol{c}-\boldsymbol{c}_0||^2 \leq \epsilon \\ & ||\boldsymbol{c}||^2 = 1. \end{array} \tag{1.11}$$

assuming the standard component-wise partial ordering in $\mathbb{R}^2$.

In the following, radar codes are designed which are Pareto-optimal solutions to (1.11), through the scalarization technique (this technique is thoroughly explained in some specific books such as [11, 18], and shortly summarized in Appendix A for reader's ease and to give self-consistency to this paper). Precisely, consider the scalarized problem

$$\begin{array}{ll} \max\limits_{\boldsymbol{c}} & \boldsymbol{c}^\dagger \left[\frac{\alpha_1}{\lambda_{max}(\boldsymbol{R})} \boldsymbol{R} + \frac{\alpha_2}{\lambda_{max}(\boldsymbol{R}_1)} \boldsymbol{R}_1 \right] \boldsymbol{c} \\ \text{s.t.} & ||\boldsymbol{c}-\boldsymbol{c}_0||^2 \leq \epsilon \\ & ||\boldsymbol{c}||^2 = 1 \end{array} \quad , \tag{1.12}$$

where $\frac{\alpha_1}{\lambda_{max}(\boldsymbol{R})} > 0$ and $\frac{\alpha_2}{\lambda_{max}(\boldsymbol{R}_1)} > 0$ are the weights. A code $\boldsymbol{c}$ is an optimal solution of (1.12) if and only if it is an optimal solution of

$$\begin{array}{ll} \max\limits_{\boldsymbol{c}} & \boldsymbol{c}^\dagger \boldsymbol{Q}(\gamma)\, \boldsymbol{c} \\ \text{s.t.} & ||\boldsymbol{c}-\boldsymbol{c}_0||^2 \leq \epsilon \\ & ||\boldsymbol{c}||^2 = 1 \end{array} \quad , \tag{1.13}$$

where $\boldsymbol{Q}(\gamma) = \boldsymbol{R} + \gamma \boldsymbol{R}_1$, $\gamma = \frac{\alpha_2}{\alpha_1} \frac{\lambda_{max}(\boldsymbol{R})}{\lambda_{max}(\boldsymbol{R}_1)} > 0$. This claim is evident since the objective functions of problem (1.12) and (1.13) are proportional and the constraint sets are the same.

Given γ, an optimal solution to the previous scalarized problem can be found through the procedure proposed in [7]. Precisely, the Pareto-optimal point corresponding to γ can be constructed according to Algorithm 1.

The parameter γ can be interpreted as the *weight* given to the second objective (namely, the CRLB) with respect to the first one (namely, the P_d); otherwise stated, it represents the cost required for improving a component making worse the other.

A final remark concerns the applicability of the proposed framework in real scenarios. Evidently, the objective functions require the specification of ν_d; as a consequence, the solution depends on this pre-assigned

Algorithm 1 Determination of a solution to problem (1.13)

Require: $\boldsymbol{c}_0$, ϵ, $\boldsymbol{R}$, $\boldsymbol{R}_1$, γ;
Ensure: an optimal solution $\hat{\boldsymbol{c}}$ of problem (1.13);
1: let $\boldsymbol{Q}(\gamma) \triangleq \boldsymbol{R} + \gamma \boldsymbol{R}_1$
2: let $\tilde{\boldsymbol{c}}$ be the unit norm eigenvector corresponding to the greatest eigenvalue of $\boldsymbol{Q}(\gamma)$;
3: define $\hat{\boldsymbol{c}} = \tilde{\boldsymbol{c}} e^{j \arg\left(\tilde{\boldsymbol{c}}^\dagger \boldsymbol{c}_0\right)}$ (where $\arg(x)$ defines the argument of x);
4: **if** $\Re(\boldsymbol{c}_0^\dagger \hat{\boldsymbol{c}}) \geq 1 - \epsilon/2$ (where $\Re(x)$ defines the real part of x) **then**
5: $\quad \boldsymbol{c}_{opt}(\gamma) \equiv \hat{\boldsymbol{c}}$;
6: **else if** $\Re(\boldsymbol{c}_0^\dagger \hat{\boldsymbol{c}}) \leq 1 - \epsilon/2$ **then**
7: $\quad$ let $\lambda_{min}(\boldsymbol{Q}(\gamma))$ and $\lambda_{max}(\boldsymbol{Q}(\gamma))$ be, respectively, the smallest and the greatest eigenvalue of $\boldsymbol{Q}(\gamma)$;
8: $\quad$ define:

- $\rho \triangleq \frac{1}{(1-\epsilon/2)^2}$;
- $\eta_1 \triangleq \lambda_{max}(\boldsymbol{Q}(\gamma))$;
- $\eta_2 \triangleq \frac{\rho^{1/2}\left(\lambda_{max}(\boldsymbol{Q}(\gamma))\right) - \lambda_{min}(\boldsymbol{Q}(\gamma))}{\left(\rho^{1/2}-1\right)}$;

9: $\quad$ consider the equation $\frac{\boldsymbol{c}_0^\dagger \left(-\boldsymbol{Q}(\gamma)+\bar{\lambda}\boldsymbol{I}\right)^{-2} \boldsymbol{c}_0}{\left[\boldsymbol{c}_0^\dagger \left(-\boldsymbol{Q}(\gamma)+\bar{\lambda}\boldsymbol{I}\right)^{-1} \boldsymbol{c}_0\right]^2} = \rho$;
10: $\quad$ solve the equation above, via Newton's method, respect to $\bar{\lambda}$, with $\eta_1 < \bar{\lambda} \leq \eta_2$;
11: $\quad \boldsymbol{c}_{opt}(\gamma) = \left(1 - \frac{\epsilon}{2}\right) \frac{\left(-\boldsymbol{Q}(\gamma)+\bar{\lambda}\boldsymbol{I}\right)^{-1} \boldsymbol{c}_0}{\boldsymbol{c}_0^\dagger \left(-\boldsymbol{Q}(\gamma)+\bar{\lambda}\boldsymbol{I}\right)^{-1} \boldsymbol{c}_0}$;
12: **end if**

value. It is thus necessary to provide some guidelines to set ν_d in practical scenarios. To this end, it is important to highlight that:

- a single coded waveform designed for the challenging condition of slowly moving targets (i.e. $\nu_d \simeq 0$) can be devised;
- a single coded waveform optimized over an average scenario may be designed. Specifically, the code might be chosen so as to maximize the objectives with $\boldsymbol{R}$ replaced by $\boldsymbol{R}_a = \boldsymbol{M}^{-1} \odot \left(E\left[\boldsymbol{p}\boldsymbol{p}^\dagger\right]\right)^*$, where the expectation operator is over the normalized Doppler frequency. If this last quantity is modeled as a uniformly distributed random variable, i.e. $\nu_d \sim \mathcal{U}(-\epsilon, \epsilon)$, with $0 < \epsilon < 1/2$, the expectation can be readily evaluated, leading to

$$\boldsymbol{R}_a = \boldsymbol{M}^{-1} \odot \boldsymbol{\Sigma}_\epsilon \,, \tag{1.14}$$

  where $\boldsymbol{\Sigma}_\epsilon(m,n) = \mathrm{sinc}\left[2\epsilon(m-n)\right]$, and $\mathrm{sinc}(x) = \frac{\sin(\pi x)}{\pi x}$.

1.4 Performance Analysis

In this Section, the quality of the proposed waveform design technique are investigated. The analysis is conducted in terms of P_d, CRLB for Doppler estimation accuracy, and ambiguity function of the pulse train modulated with the designed code. Additionally, the Pareto-optimal curve are provided, i.e.

$$\begin{cases} F_1(\boldsymbol{c}_{\mathrm{opt}}(\gamma)) \triangleq \boldsymbol{c}_{\mathrm{opt}}^\dagger(\gamma)\boldsymbol{R}\boldsymbol{c}_{\mathrm{opt}}(\gamma) \\ F_2(\boldsymbol{c}_{\mathrm{opt}}(\gamma)) \triangleq \boldsymbol{c}_{\mathrm{opt}}^\dagger(\gamma)\boldsymbol{R}_1\boldsymbol{c}_{\mathrm{opt}}(\gamma) \end{cases} \tag{1.15}$$

(where, according to (1.3) and (1.7), F_1 and F_2 rule, respectively, P_d and CRLB. Specifically, they respectively play the role of a normalized SNR and a normalized inverse CRLB); namely the set of Pareto-optimal values, obtained through scalarization and varying the relative weight γ, for the considered optimization problem. Finally, the Pareto trade-off between P_d and CRLB, arising through the variation of γ, is explored.

The analysis is developed assuming a disturbance covariance matrix $\boldsymbol{M}$ with the following structure:

$$\boldsymbol{M} = \boldsymbol{M}_{\mathrm{clutter}} + 10^{-2}\boldsymbol{I}$$

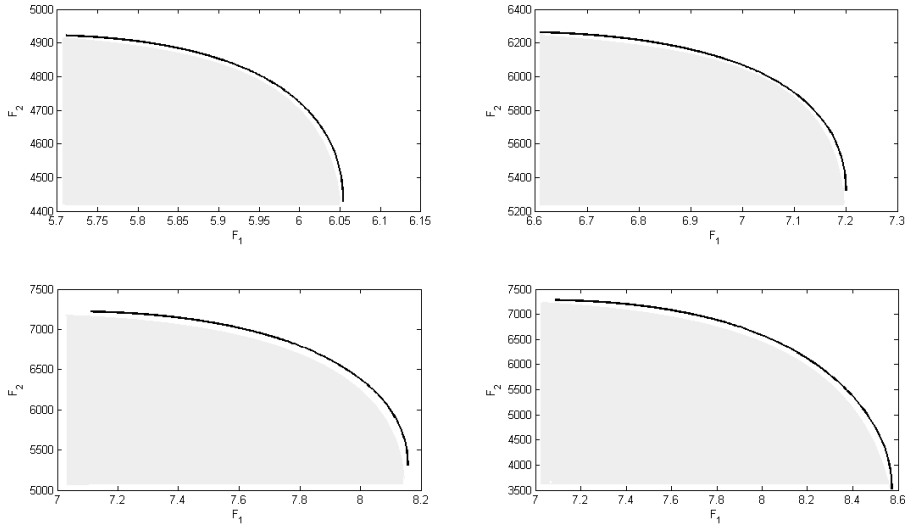

Figure 1.1: Pareto-optimal curves for $\gamma \in]0, 10]$, $\epsilon = 0.1$ (top-left), $\epsilon = 0.3$ (top-right), $\epsilon = 0.7$ (bottom-left) and $\epsilon = 1.9998$ (bottom-right), with the polyphase Barker code of length $N = 7$ as reference code. The set of achievable values under the curves is shaded in gray.

where $\boldsymbol{M}_{\text{clutter}} = \rho^{|m-n|}$, with $\rho = 0.9$. Moreover, the P_{fa} of the receiver is fixed to 10^{-6}, $\nu_d = 0$; a NFT is considered, and the reference code is the generalized Barker sequence of length $N = 7$ [2, pp. 109-113] $\boldsymbol{c}_0 = [0.3780, 0.3780, -0.1072 - j0.3624, -0.0202 - j0.3774, 0.2752 + j0.2591, 0.1855 - j0.3293, 0.0057 + j0.3779]$, properly normalized in order to obtain a unitary norm vector. Indeed, the choice for this is mainly because it shares a good ambiguity function[2]. In Figure 1.1, the Pareto-optimal curve for several values of ϵ is plotter; namely, different degrees of similarity between the devised and the pre-fixed code are considered, assuming that γ ranges in the interval $]0, 10]$. This curve is also referred to as *optimal trade-off curve*, because it highlights the connection between the two objectives, F_1 and F_2, emphasizing the role of the weight γ in the determination of their Pareto-optimal values and the cost paid for increasing one component with respect to the other. The shaded re-

[2]Similar results, not reported in the Chapter, have been obtained with a Frank code. In fact, other similarity codes may exist that, with respect to the analyzed scenari,o might perform better than the generalized Barker code in terms of P_d and/or CRLB.

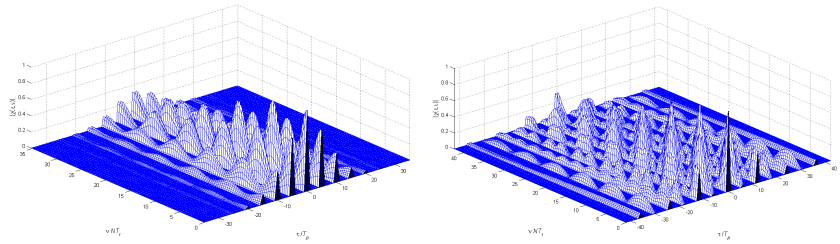

(a) $\epsilon = 1.9998$ and $\gamma = 1$.

(b) $\epsilon = 0.3$ and $\gamma = 1$.

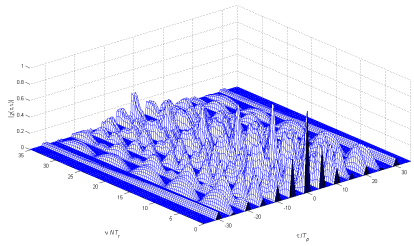

(c) $\epsilon = 0.1561$ and $\gamma = 1$.

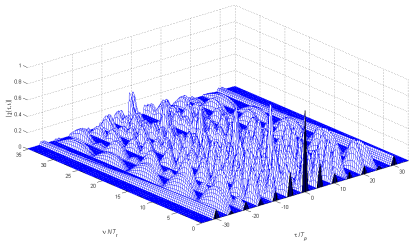

(d) $\epsilon = 0.0506$ and $\gamma = 1$.

Figure 1.2: Ambiguity function modulus of the designed code with $N = 7$, $T_r = 5T_p$.

gion indicates the set of all the achievable values (F_1, F_2); for example, intercepting the curve with the vertical line $F_1 = \eta$ (thus considering a certain value for P_d), it can be observed how small F_2 (thus how large the corresponding CRLB) has to be in order to achieve $F_1 \geq \eta$. The same interpretation arises intercepting the curve with an horizontal line $F_2 = \beta$ (thus considering a certain value for the CRLB), which makes evident how small F_1 (thus the corresponding P_d) has to be in order to achieve $F_2 \geq \beta$. The slope of the optimal trade-off curve at a Pareto-optimal value shows the *local* optimal trade-off between the two objectives; steep slopes lead to large variations of F_2 in correspondence of small changes in F_1 (this is actually what happens in the lower right region of the curves in Figure 1.1).

Notice also how a reduction of ϵ (or, equivalently, an increase in the degree of similarity) leads to worse and worse optimal values for both F_1 and F_2, namely to lower and lower Pareto-optimal curves. This result can be explained observing that decreasing ϵ is tantamount to reducing the size of the feasible set. However, the resulting loss (both in terms of detection capability and estimation accuracy) is compensated for an improvement of the coded pulse train ambiguity function, which appears

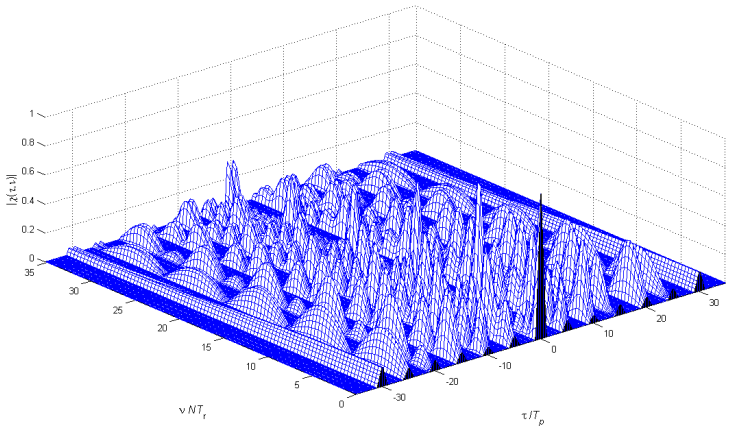

Figure 1.3: Ambiguity function modulus of the generalized Barker code $\boldsymbol{c}_0$ of length $N = 7$ with $T_r = 5T_p$.

more and more similar to that of the reference code. This is shown in Figures 1.2a-d, where the ambiguity function modulus is plotted, for $\gamma = 1$ and some values of the similarity parameter ϵ. Comparing them with the ambiguity function of the code $\boldsymbol{c}_0$, plotted in Figure 1.3, it can be easily recognized a greater and greater degree of similarity as ϵ decreases.

The effects of the similarity parameter ϵ on the detection capability and the Doppler estimation accuracy are analyzed in Figures 1.4a-b. Therein, setting $\gamma = 0.05$, the P_d (Figure 1.4a) and the normalized CRLB ($\text{CRLB}_n = T_r^2\text{CRLB}$, Figure 1.4b) versus $|\alpha|^2$ are plotted for several values of ϵ ($\epsilon = \{0.1, 0.3, 0.7, 1.9998\}$). In order to compare the performance of the sought code with that of the similarity sequence, the P_d and CRLB_n obtained through the use of $\boldsymbol{c}_0$ are evaluated too. As benchmark code, instead, it is consider the sequence which maximizes the unconstrained (namely without forcing the similarity constraint) P_d or CRLB , i.e.

$$\boldsymbol{c}_{\text{benchmark}}^{P_d} = \arg\max_{\boldsymbol{c}} \left\{ \boldsymbol{c}^\dagger \boldsymbol{R} \boldsymbol{c} \;/\; ||\boldsymbol{c}||^2 = 1 \right\} , \tag{1.16}$$

$$\boldsymbol{c}_{benchmark}^{CRLB} = \arg\max_{\boldsymbol{c}} \left\{ \boldsymbol{c}^\dagger \boldsymbol{R}_1 \boldsymbol{c} \;/\; ||\boldsymbol{c}||^2 = 1 \right\} . \tag{1.17}$$

The corresponding P_d and CRLB are referred to in the following as $P_d^{\text{benchmark}}$ and $\text{CRLB}_n^{\text{benchmark}}$. Usually, they are are not obtained in correspondence of the same code.

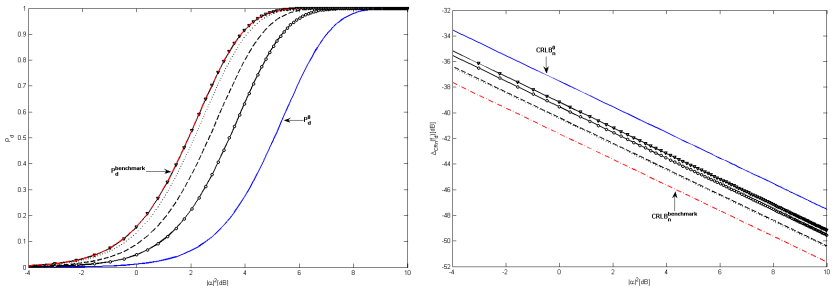

(a) P_d versus $|\alpha|^2$ for non-fluctuating target.

(b) CRLB_n versus $|\alpha|^2$ for non-fluctuating target.

Figure 1.4: $P_{fa} = 10^{-6}$, $N = 7$, $\gamma = 0.05$, and: $\epsilon = 0.1$ (solid-circle curve), $\epsilon = 0.3$ (dashed curve), $\epsilon = 0.7$ (dotted curve) and $\epsilon = 1.9998$ (solid-down triangle curve). The curves related to $\boldsymbol{c}_0$ (solid curve) and $\boldsymbol{c}_{benchmark}$ (dash-dotted curve) are highlighted directly on the figure; notice that the curve for $\epsilon = 1.9998$ overlaps with the benchmark one (P_d vs $|\alpha|^2$).

The curves in Figure 1.4a show that, decreasing ϵ, worse and worse P_d values are obtained. This behavior can be explained observing that reducing ϵ is tantamount to reducing the size of the similarity region. Nevertheless, the quoted P_d loss is compensated for an improvement in the coded pulse train ambiguity function, which is forced to be more similar to the reference sequence. Different considerations apply to the curves of Figure 1.4b, representing the CRLB behavior for the same values of ϵ as in Figure 1.4a. In this case, due to the small value of the relative weight γ, the scalarization places almost all the emphasis on the P_d objective, which substantially rules the choice of the optimum code for the scalarized problem. As a consequence, enlarging the similarity region, we can find a new code improving P_d, but such a code can also lead to a degradation of the CRLB because the two objectives are competing.

Now the effects of the Pareto weight γ, on the performance of the designed code, fixing the similarity constraint ϵ, are analyzed. To this end, in Figure 1.5, the Pareto-optimal curve obtained for $\epsilon = 0.1561$ are plotted, highlighting six different Pareto-optimal values (operating points in the following), related to six different weights. In Figures 1.6a and 1.6b, the impact of the Pareto weight on the optimization of the detection capability and Doppler estimation accuracy is studied. Specifically, the P_d and CRLB_n versus $|\alpha|^2$ are plotted for the six operating points of Figure 1.5. The performance follows the same qualitative behavior explained in

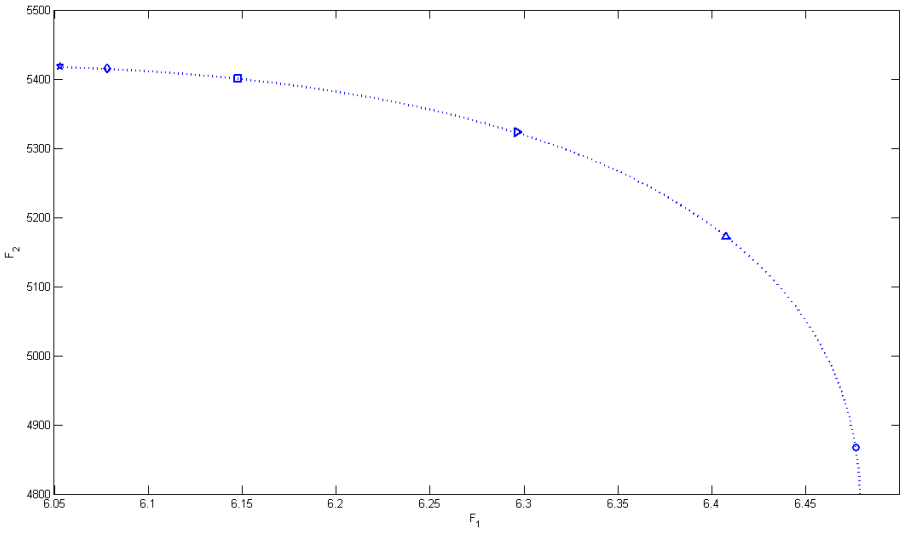

Figure 1.5: Pareto-optimal curve for $\epsilon = 0.1561$ and $\gamma \in]0, 10]$. Each marker represents an operative point for a given γ; $\gamma = 0.05$ (circle), $\gamma = 0.4$ (up-triangle), $\gamma = 1$ (right-triangle), $\gamma = 3$ (square), $\gamma = 6.5$ (diamond) and $\gamma = 10$ (star).

Figure 1.1; namely, P_d and CRLB are both decreasing functions of γ. Finally, it is important to point out that, although tied up to the same similarity value ϵ, the codes resulting from the optimization problem (1.13) are clearly affected by the chosen value for the weight γ. As a consequence, the corresponding pulse trains will exhibit different ambiguity functions as shown in Figures 1.7a-d.

1.5 Conclusions

In this Chapter, the radar waveform design, in the presence of colored Gaussian disturbance, forcing an energy and a similarity constraints, has been addressed. The considered design criterion has been the joint constrained optimization of the detection performance and CRLB on Doppler estimation accuracy. The problem has been formulated in terms of a non-convex multi-objective optimization problem with two quadratic constraints. Hence, radar codes been have constructed as Pareto-optimal points of the aforementioned problem through the scalarization procedure.

At the analysis stage, the performances of the new algorithm have

been evaluated in terms of detection performance, CRLB for Doppler estimation accuracy, and ambiguity function. Additionally, the Pareto-optimal curve has been studied showing the effects of the Pareto weight on the performance trade-off. Finally, the impact of the similarity constraint on the performance, for a given value of the Pareto weight, has been analyzed.

Possible future research tracks might concern the extension of the framework to situations where it is necessary to optimize more than two objectives (performance measures) and/or where it is necessary to force additional constraints on the structure of the radar waveform.

1.6 Acknowledgment

The effort of the author of the present Chapter is sponsored by the Air Force Office of Scientific Research, Air Force Material Command, USAF, under grant number FA8655-09-1-3006. The U.S. Governmental purpose notwithstanding any copyright notation thereon.

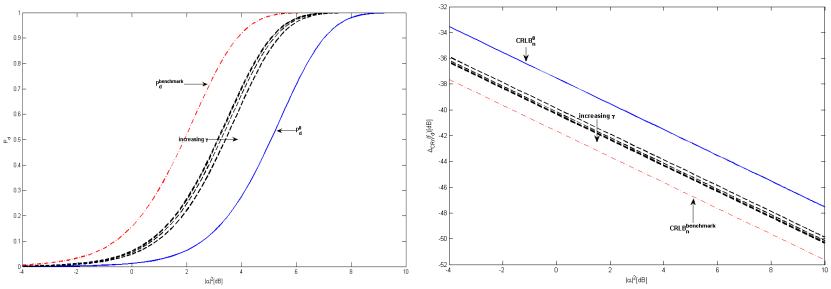

(a) P_d versus $|\alpha|^2$ for non-fluctuating target

(b) CRLB_n versus $|\alpha|^2$ for non-fluctuating target

Figure 1.6: $P_{fa} = 10^{-6}$, $N = 7$, $\epsilon = 0.1561$ and $\gamma = [0.05, 0.4, 1, 3, 6.5, 10]$. Generalized Barker code (solid curve). Designed codes (dashed curves). Benchmark code (dash-dotted curve).

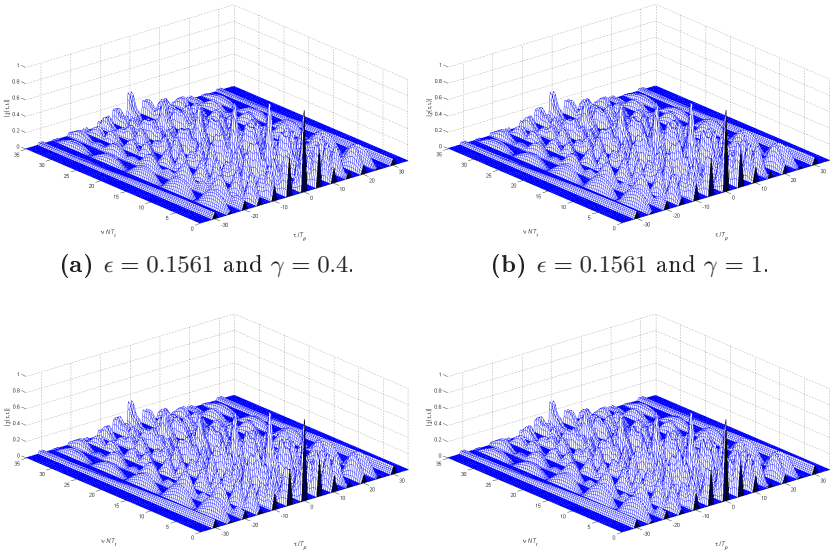

(a) $\epsilon = 0.1561$ and $\gamma = 0.4$.

(b) $\epsilon = 0.1561$ and $\gamma = 1$.

(c) $\epsilon = 0.1561$ and $\gamma = 3$.

(d) $\epsilon = 0.1561$ and $\gamma = 10$.

Figure 1.7: Ambiguity function modulus of the designed code with $N = 7$, $T_r = 5T_p$.

Chapter 2

A Doppler Robust Max-Min Approach to Radar Code Design

2.1 Introduction

The advent of adaptive radar transmitters, which permit the use of advanced and flexible pulse shaping techniques, and the significant achievements in high speed signal processing hardware are paving the way to the development of very innovative and computational demanding techniques for radar waveform design [4, 19]. The idea is to adapt and diversify dynamically the transmitted signal to the operating environment in order to achieve a performance gain over classic radar waveforms [5, 20, 21, 22, 6, 7].

In [1], focusing on the class of linearly coded pulse trains (both in amplitude and in phase), the authors introduce a code selection algorithm which maximizes the detection performance but, at the same time, is capable of controlling both the region of achievable values for the Doppler estimation accuracy and the degree of similarity with a pre-fixed radar code. However, since in several practical situations, the radar amplifiers might work in saturation conditions and hence an amplitude modulation might be difficult to perform, in [8], the authors also consider the synthesis of constant modulus phase coding schemes for radar coherent pulse trains. Finally, in [10], the problem of constrained code optimization for radar Space-Time Adaptive Processing (STAP) in the presence

of colored Gaussian disturbance, under two accuracy constraints (on the temporal and the spatial Doppler frequency) and a similarity constraint, is addressed.

Many among the previously mentioned algorithms optimize the radar signal in correspondence of a given target Doppler frequency. Hence, they can be easily applied to situations where it is required a confirmation of an initial detection in a certain Doppler bin, namely when some knowledge about the Doppler frequency is available. In other situations, the Doppler parameter is usually unknown and a practical application of the techniques can be obtained either tuning the design Doppler to a challenging condition, dictated by the clutter Power Spectral Density (PSD) shape, or optimizing the waveform to an average scenario, namely considering as objective function the average SNR over the possible target Doppler shifts. The present Chapter moves another step towards the synthesis of radar waveforms when no prior knowledge about the actual Doppler is available. Specifically, resorting to the max-min criterion, the waveform design problem is formulated as the constrained maximization of the worst case (over the set of possible Doppler frequencies) detection performance. The constraints considered here are an energy constraint, imposed by the finite transmission resources, and a similarity constraint, important to equip the waveform with desirable properties such as small modulus variations, good range resolution, low peak sidelobe levels, and more in general with a good ambiguity function. The resulting problem is a non-convex Quadratically Constrained Quadratic Program (QCQP) with infinitely many quadratic constraints. This class of QCQP's, is known to be NP-hard in general, and as a consequence, finding a global optimal solution is often very difficult [23]. Hence, the aim is the construction of a *good* sub-optimal solution for the quoted problem with the goodness in the sense that the produced solution leads to an high-quality radar code for the considered robust radar waveform design problem, as supported also by the simulations in Section 2.4.

The Chapter is organized as follows. In Section 2.2, the waveform design problem is formulated according to the max-min criterion, based on system model (1)-(2); in Section 2.3, the new algorithm for the considered problem is presented; in Section 2.4, the performance of the proposed technique is analyzed, and numerical results assessing the quality of the produced sub-optimal solution are provided. Finally, conclusions are given in Section 2.5.

2.2 System Model and Waveform Design Problem

The same signal model as in eq. (1) is herein considered. The main goal is to find radar waveforms optimizing the worst case detection performance, under an energy constraint and a similarity constraint with a given radar code exhibiting a good ambiguity function. In this Section, the problem is formulated mathematically, showing how the worst case detection probability can be maximized and the constraints can be enforced, under the assumption (2) for the disturbance. With reference to the case of non-fluctuating target[1], as already shown in eq. (1.2), the detection probability P_d of the GLRT, for a given value of the false alarm Probability P_{fa}, depends on the radar code, the disturbance covariance matrix, and the temporal steering vector only through the SNR, defined as in eq. (1.4), which is a function of the actual Doppler frequency due to the dependence of $\boldsymbol{p}$ over ν_d. Moreover, P_d is an increasing function of SNR and, as a consequence, the maximization of P_d can be obtained maximizing the quadratic form

$$(\boldsymbol{c} \odot \boldsymbol{p})^\dagger \boldsymbol{M}^{-1} (\boldsymbol{c} \odot \boldsymbol{p}) = \boldsymbol{c}^\dagger \left(\boldsymbol{M}^{-1} \odot (\boldsymbol{p}\boldsymbol{p}^\dagger)^* \right) \boldsymbol{c}\,, \tag{2.1}$$

over the radar code, as already shown in eq. (1.8). It is important to highlight that $\boldsymbol{M}^{-1} \odot (\boldsymbol{p}\boldsymbol{p}^\dagger)^*$ is the Hadamard product of two positive semidefinite matrices, and hence it is itself positive semidefinite [17, p. 1352, A.77].

Performing the maximization of (2.1), possibly under some constraints [1] (for instance accuracy, similarity, and energy constraints), leads to a code vector which depends on the specific value of the Doppler frequency present in the definition of $\boldsymbol{p}$. In order to get a transmit radar waveform independent of the Doppler frequency, it is proposed here a max-min approach attempting at maximizing the worst case (over the possible target Doppler frequencies) SNR. In other words, the following objective function, to maximize over the radar code, is considered:

$$\min_{\nu_d \in [0,1]} \boldsymbol{c}^\dagger (\boldsymbol{M}^{-1} \odot (\boldsymbol{p}\boldsymbol{p}^\dagger)^*) \boldsymbol{c}\,.$$

Adding the similarity constraint with a code $\boldsymbol{c}_0$ [7], important to confer desirable properties to the radar waveform, as well as an energy con-

[1] The conclusions may be easily extended to the case of fluctuating target.

straint (accounting for the limited transmission power), the following optimization problem arises:

$$\max_{\boldsymbol{c}\in\Omega}\min_{\nu_d\in[0,1]} \boldsymbol{c}^{\dagger}(\boldsymbol{M}^{-1}\odot(\boldsymbol{p}\boldsymbol{p}^{\dagger})^{*})\boldsymbol{c}, \tag{2.2}$$

where the set Ω is defined as $\Omega = \{\boldsymbol{c}|\ ||\boldsymbol{c}|| = 1, ||\boldsymbol{c}-\boldsymbol{c}_0||^2 \leq \epsilon\}$ with $||\boldsymbol{c}_0|| = 1$, and the parameter $\epsilon \geq 0$ ruling the size of the similarity region. Indeed, the smaller ϵ is, the higher the degree of similarity between the ambiguity functions of the designed radar code and $\boldsymbol{c}_0$ is.

Before presenting the new algorithm, it is worth to point out the differences between this optimization problem and those formulated and solved in [1] and [8]. To this end, observe that the objective function in [1] and [8] depends on a specific design Doppler value, while in the present problem the worst case SNR (over the Doppler frequency) is optimized (2.2). [1] accounts for a Doppler dependent constraint on the estimation accuracy of f_d, while in the present case, only a similarity and an energy constraint are considered. [8] accounts for a phase-only constraint on the devised code, while in this Chapter a general amplitude-phase coding is considered. In other words, (2.2) optimizes a robust objective function with respect to [1] and [8], but the former forces one less quadratic constraint than the problem in [1], and the constraints of the problem specified in [8] look very different from those in (2.2) . From the optimization theory point of view, the three formulations lead to different optimization problems:

- that in [1] is a homogeneous QCQP with three constraints, a global optimal solution for which can be found in polynomial time (namely for this problem the SDP relaxation is tight or, equivalently, the problem shares an hidden convexity);

- that in [8] is an NP-hard QCQP optimization problem due to the phase-only and the possibly finite alphabet constraint, whose optimal solution is approximated using the relaxation and randomization approach typical of the max-cut-like problems.

- that in the current Chapter is a QCQP with infinitely many constraints, for which we establish a deterministic approximation procedure, with polynomial time computational complexity, to output a solution leading to high-quality radar waveforms.

2.3 Approximate Solution to the Max-Min Optimization Problem

The max-min problem (2.2) can be recast as

$$\begin{array}{ll} \max\limits_{\boldsymbol{c},t} & t \\ \text{s.t.} & t \leq \boldsymbol{p}^\dagger(\boldsymbol{M}^{-1} \odot (\boldsymbol{c}\boldsymbol{c}^\dagger)^*)\boldsymbol{p}, \qquad \forall \nu_d \in [0,1], \\ & ||\boldsymbol{c} - \boldsymbol{c}_0||^2 \leq \epsilon, \\ & ||\boldsymbol{c}|| = 1. \end{array} \tag{2.3}$$

Moreover, elaborating on the similarity constraint, problem (2.3) can be equivalently rewritten as

$$\begin{array}{ll} \max\limits_{\boldsymbol{c},t} & t \\ \text{s.t.} & t \leq \boldsymbol{p}^\dagger(\boldsymbol{M}^{-1} \odot (\boldsymbol{c}\boldsymbol{c}^\dagger)^*)\boldsymbol{p}, \qquad \forall \nu_d \in [0,1], \\ & \Re\left(\boldsymbol{c}^\dagger \boldsymbol{c}_0\right) \geq 1 - \epsilon/2, \\ & ||\boldsymbol{c}||^2 = 1\,. \end{array} \tag{2.4}$$

Observing that a rotation of $\boldsymbol{c}$ does not change the first constraint, it is possible to claim that problem (2.4) is equivalent to

$$\begin{array}{ll} \max\limits_{\boldsymbol{c},t} & t \\ \text{s.t.} & t \leq \boldsymbol{p}^\dagger(\boldsymbol{M}^{-1} \odot (\boldsymbol{c}\boldsymbol{c}^\dagger)^*)\boldsymbol{p}, \qquad \forall \nu_d \in [0,1], \\ & \boldsymbol{c}^\dagger \boldsymbol{c}_0 \boldsymbol{c}_0^\dagger \boldsymbol{c} \geq \delta_\epsilon, \\ & ||\boldsymbol{c}||^2 = 1, \end{array} \tag{2.5}$$

where $\delta_\epsilon = (1 - \epsilon/2)^2$, in the sense that if $(\boldsymbol{c}^\star, t^\star)$ is an optimal solution of problem (2.5), then $(\boldsymbol{c}^\star e^{j \arg \boldsymbol{c}^{\star\dagger}\boldsymbol{c}_0}, t^\star)$ is an optimal solution of (2.4). Therefore, from now on the focus will be on problem (2.5).

It can be easily seen that problem (2.5) is a QCQP with infinitely many constraints. As already highlighted, this class of problems is known to be NP-hard in general (see [23]) and hence difficult to solve. In other words, the convex relaxation of the class of QCQP problem may or may not be tight, in particular, its SDP relaxation may have only optimal solutions of rank higher than one, or may have optimal solutions of rank higher than one as well as equal to one. Futher, to retrieve a rank-one optimal solution of the SDP relaxation problem from an optimal solution of general rank is usually a non-trivial task. In the following, an approximation scheme is presented to produce a feasible solution for the problem

(2.5), based on the techniques of SDP relaxation, SDP representation of trigonometric polynomials, and a specific rank-one matrix decomposition. It turns out by the numerical simulations that the algorithm provides high-quality radar codes for the proposed robust waveform design problem. Additionally, if the SDP relaxation is tight (namely, the SDP has always a rank-one optimal solution) than the devised code is also optimal for the original non-convex problem.

The SDP relaxation of (2.5) is

$$\begin{array}{ll} \max\limits_{\boldsymbol{C},t} & t \\ \text{s.t.} & t \le \boldsymbol{p}^\dagger(\boldsymbol{M}^{-1} \odot \boldsymbol{C}^*)\boldsymbol{p}, \qquad \forall \nu_d \in [0,1], \\ & \mathrm{tr}\,(\boldsymbol{c}_0\boldsymbol{c}_0^\dagger \boldsymbol{C}) \ge \delta_\epsilon, \\ & \mathrm{tr}\,(\boldsymbol{C}) = 1, \\ & \boldsymbol{C} \succeq \boldsymbol{0}\,. \end{array} \tag{2.6}$$

Clearly, the constraint function $\boldsymbol{p}^\dagger(\boldsymbol{M}^{-1} \odot \boldsymbol{C}^*)\boldsymbol{p} - t$ is a trigonometric polynomial [24] of degree $N-1$, that is,

$$\boldsymbol{p}^\dagger(\boldsymbol{M}^{-1} \odot \boldsymbol{C}^*)\boldsymbol{p} - t = x(0) - t + 2\mathrm{Re}\,\left(\sum_{k=1}^{N-1} x(k)e^{-jk\omega}\right),$$

where $\omega = 2\pi\nu_d$ and

$$x(k) = \frac{1}{N}\sum_{i=1}^{N-k}(\boldsymbol{M}^{-1} \odot \boldsymbol{C}^*)(i+k,i), \qquad k = 0,1,\ldots,N-1, \tag{2.7}$$

with the notation $(\boldsymbol{M}^{-1} \odot \boldsymbol{C}^*)(i+k,i)$ being the $(i+k,i)$-th entry of $\boldsymbol{M}^{-1} \odot \boldsymbol{C}^*$.

It is known that the nonnegativity constraint of a trigonometric polynomial has an equivalent SDP representation. Specifically, the following result derived in [25, Theorem 3.1] is quoted here as a lemma.

Lemma 2.3.1. *The trigonometric polynomial* $f(\omega) = x(0) + 2\Re\left(\sum_{k=1}^{N-1} x(k)e^{-jk\omega}\right)$ *is nonnegative over* $[0, 2\pi]$*, if and only if there exists an* $N \times N$ *Hermitian matrix* $\boldsymbol{X}$ *such that*

$$\boldsymbol{x} = \boldsymbol{W}^\dagger \mathbf{diag}(\boldsymbol{W}\boldsymbol{X}\boldsymbol{W}^\dagger), \qquad \boldsymbol{X} \succeq \boldsymbol{0}, \tag{2.8}$$

where $\boldsymbol{x} = [x(0),\ldots,x(N-1)]^T$*,* $\boldsymbol{W} = [\boldsymbol{w}_0,\ldots,\boldsymbol{w}_{N-1}] \in C^{M\times N}$*, and* $\boldsymbol{w}_k = [1, e^{-jk\theta},\ldots,e^{-j(M-1)k\theta}]^T$*,* $k = 0,\ldots,N-1$*,* $\theta = 2\pi/M$*,* $M \ge 2N-1$*.*

It follows by Lemma 2.3.1 that SDP (2.6) is equivalent to the following SDP

$$\begin{array}{ll} \max\limits_{\boldsymbol{X},\boldsymbol{C},t} & t \\ \text{s.t.} & \boldsymbol{W}^{\dagger}\mathbf{diag}(\boldsymbol{W}\boldsymbol{X}\boldsymbol{W}^{\dagger}) + t\boldsymbol{e}_1 = \boldsymbol{x}, \\ & \mathrm{tr}\,(\boldsymbol{c}_0\boldsymbol{c}_0^{\dagger}\boldsymbol{C}) \geq \delta_{\epsilon}, \\ & \mathrm{tr}\,(\boldsymbol{C}) = 1, \\ & \boldsymbol{C} \succeq \boldsymbol{0}, \\ & \boldsymbol{X} \succeq \boldsymbol{0}\,, \end{array} \tag{2.9}$$

where $\boldsymbol{x}$ is defined by (2.7), $\boldsymbol{W}$ is the same as the one defined in Lemma 2.3.1 by taking $M = 2N-1$. In order to proceed further it is necessary to show the following

Lemma 2.3.2. *It holds that SDP problem* (2.9) *is solvable*[2].

Proof. See Appendix B □

Let $(\boldsymbol{X}^{\star}, \boldsymbol{C}^{\star}, t^{\star})$ be an optimal solution of (2.9). It is easily seen that $(\boldsymbol{C}^{\star}, t^{\star})$ is an optimal solution of SDP (2.6) with

$$t^{\star} = \min_{\nu_d \in [0,1]} \boldsymbol{p}^{\dagger}(\boldsymbol{M}^{-1} \odot (\boldsymbol{C}^{\star})^{*})\boldsymbol{p}. \tag{2.10}$$

Problem (2.10) is one dimensional optimization problem with sufficiently smooth objective function, therefore it is possible to apply Newton method to solve it. Letting

$$\nu_d^{\star} = \arg \min_{\nu_d \in [0,1]} \boldsymbol{p}^{\dagger}(\boldsymbol{M}^{-1} \odot (\boldsymbol{C}^{\star})^{*})\boldsymbol{p}, \tag{2.11}$$

namely a value of $\nu_d \in [0,1]$ minimizing the argument and

$$\boldsymbol{p}^{\star} = \frac{1}{\sqrt{N}}[1, e^{j2\pi\nu_d^{\star}}, \ldots, e^{j(N-1)2\pi\nu_d^{\star}}]^T\,, \tag{2.12}$$

it follows that

$$t^{\star} = \boldsymbol{p}^{\star\dagger}(\boldsymbol{M}^{-1} \odot (\boldsymbol{C}^{\star})^{*})\boldsymbol{p}^{\star} = \mathrm{tr}\,\left[\left(\boldsymbol{M}^{-1} \odot \left(\boldsymbol{p}^{\star}\boldsymbol{p}^{\star\dagger}\right)^{*}\right)\boldsymbol{C}^{\star}\right].$$

Now if $\boldsymbol{C}^{\star}$ is rank-one, namely $\boldsymbol{C}^{\star} = \boldsymbol{c}_1\boldsymbol{c}_1^{\dagger}$, then $\boldsymbol{c}^{\star} = \boldsymbol{c}_1 e^{j\arg \boldsymbol{c}_1^{\dagger}\boldsymbol{c}_0}$ and $\nu_d^{\star}$ are optimal for the original max-min problem, i.e. the SDP relaxation is

[2]By saying *solvable*, it means that the problem is feasible, bounded, and the optimal value is attained (see [26, page 13]).

tight. Otherwise, an approximate solution to (2.2) can be provided. To this end, it is necessary to find a rank-one matrix $\boldsymbol{cc}^\dagger$ such that

$$\begin{aligned} \mathrm{tr}\left[\left(\boldsymbol{M}^{-1}\odot\left(\boldsymbol{p}^\star\boldsymbol{p}^{\star\dagger}\right)^*\right)\boldsymbol{cc}^\dagger\right] &= \mathrm{tr}\left[\left(\boldsymbol{M}^{-1}\odot\left(\boldsymbol{p}^\star\boldsymbol{p}^{\star\dagger}\right)^*\right)\boldsymbol{C}^\star\right] && (2.13)\\ &= t^\star, && (2.14)\\ \mathrm{tr}\left(\boldsymbol{c}_0\boldsymbol{c}_0^\dagger\boldsymbol{cc}^\dagger\right) &= \mathrm{tr}\left(\boldsymbol{c}_0\boldsymbol{c}_0^\dagger\boldsymbol{C}^\star\right)=s, && (2.15)\\ \mathrm{tr}\left(\boldsymbol{cc}^\dagger\right) &= \mathrm{tr}\left(\boldsymbol{C}^\star\right)=1, && (2.16)\end{aligned}$$

as long as $\boldsymbol{C}^\star$ is of rank higher than one. If it is possible to find a rank-one solution $\boldsymbol{cc}^\dagger$ satisfying (2.13)-(2.16), then the following one-dimensional search yields a feasible solution of problem (2.5):

$$\nu_d=\arg\min_{\nu_d\in[0,1]}\boldsymbol{p}^\dagger(\boldsymbol{M}^{-1}\odot(\boldsymbol{cc}^\dagger)^*)\boldsymbol{p}, \tag{2.17}$$

with the optimal value

$$t=\min_{\nu_d\in[0,1]}\boldsymbol{p}^\dagger(\boldsymbol{M}\odot(\boldsymbol{cc}^\dagger)^*)\boldsymbol{p}. \tag{2.18}$$

In other words, $(\boldsymbol{c},t)$ is a sub-optimal solution of problem (2.5). To find a rank-one solution of (2.13)-(2.16), the following rank-one decomposition theorem [27] is invoked.

Lemma 2.3.3. *Suppose that $\boldsymbol{X}$ is an $N\times N$ complex Hermitian positive semidefinite matrix of rank R, and $\boldsymbol{A}_1,\boldsymbol{A}_2$ are two $N\times N$ given Hermitian matrices. Then, there is a rank-one decomposition of $\boldsymbol{X}$ (synthetically denoted as $\mathcal{D}(\boldsymbol{X},\boldsymbol{A}_1,\boldsymbol{A}_2)$), $\boldsymbol{X}=\sum_{r=1}^R\boldsymbol{x}_r\boldsymbol{x}_r^\dagger$, such that*

$$\boldsymbol{x}_r^\dagger\boldsymbol{A}_1\boldsymbol{x}_r=\frac{\mathrm{tr}\left(\boldsymbol{XA}_1\right)}{R}\quad\textit{and}\quad\boldsymbol{x}_r^\dagger\boldsymbol{A}_2\boldsymbol{x}_r=\frac{\mathrm{tr}\left(\boldsymbol{XA}_2\right)}{R},\ r=1,\ldots,R.$$

In the present context, it is necessary to perform $\mathcal{D}\left(\boldsymbol{C}^\star,\boldsymbol{M}^{-1}\odot\left(\boldsymbol{p}^\star\boldsymbol{p}^{\star\dagger}\right)^*-t^\star\boldsymbol{I},\boldsymbol{c}_0\boldsymbol{c}_0^\dagger-s\boldsymbol{I}\right)$ obtaining $\boldsymbol{C}^\star=\sum_{i=1}^R\boldsymbol{c}_i\boldsymbol{c}_i^\dagger$, where $R=\mathrm{Rank}\left(\boldsymbol{C}^\star\right)$. Then, it is easily verified that each $\boldsymbol{c}_i\boldsymbol{c}_i^\dagger/||\boldsymbol{c}_i||^2$ for $i=1,\ldots,R$, fulfills (2.13)-(2.16). In fact,

$$\begin{aligned}\frac{1}{R}\mathrm{tr}\left[\left(\boldsymbol{M}^{-1}\odot\left(\boldsymbol{p}^\star\boldsymbol{p}^{\star\dagger}\right)^*-t^\star\boldsymbol{I}\right)\boldsymbol{c}_i\boldsymbol{c}_i^\dagger\right]=&\mathrm{tr}\left[\left(\boldsymbol{M}^{-1}\odot\left(\boldsymbol{p}^\star\boldsymbol{p}^{\star\dagger}\right)^*-\right.\right.\\ &\left.\left.t^\star\boldsymbol{I}\right)\boldsymbol{C}^\star\right]=0, && (2.19)\\ \frac{1}{R}\mathrm{tr}\left[\left(\boldsymbol{c}_0\boldsymbol{c}_0^\dagger-s\boldsymbol{I}\right)\boldsymbol{c}_i\boldsymbol{c}_i^\dagger\right]=&\mathrm{tr}\left[\left(\boldsymbol{c}_0\boldsymbol{c}_0^\dagger-s\boldsymbol{I}\right)\boldsymbol{C}^\star\right]=0, && (2.20)\end{aligned}$$

which imply

$$\text{tr}\left[\left(\boldsymbol{M}^{-1}\odot\left(\boldsymbol{p}^{\star}\boldsymbol{p}^{\star\dagger}\right)^{*}\right)\boldsymbol{c}_i\boldsymbol{c}_i^{\dagger}\right] = t^{\star}\|\boldsymbol{c}_i\|^2, \tag{2.21}$$

$$\text{tr}\left[\left(\boldsymbol{c}_0\boldsymbol{c}_0^{\dagger}\right)\boldsymbol{c}_i\boldsymbol{c}_i^{\dagger}\right] = s\|\boldsymbol{c}_i\|^2\,. \tag{2.22}$$

As a consequence, $\boldsymbol{c}_i\boldsymbol{c}_i^{\dagger}/||\boldsymbol{c}_i||^2$, for $i=1,\ldots,R$, complies with (2.13)-(2.16). Performing the one-dimensional optimization problem (2.18) gives the sub-optimal solutions $(\boldsymbol{c}_i/||\boldsymbol{c}_i||, t_i)$, where t_i is the optimal value of problem (2.18) corresponding to $\boldsymbol{c}_i/||\boldsymbol{c}_i||$. Take the maximal value of $\{t_1,\ldots,t_R\}$, say t_1, and output $(\boldsymbol{c}_1/||\boldsymbol{c}_1||, t_1)$ as the sub-optimal solution (namely the best among the couples $(\boldsymbol{c}_i/||\boldsymbol{c}_i||, t_i)$).

Summarizing, a sub-optimal solution for problem (2.2) can be summarized as in Algorithm 2.

Algorithm 2 Approximation procedure for the max-min problem (2.2)

Require: $\boldsymbol{c}_0$, ϵ, $\boldsymbol{M}$, N;
Ensure: a sub-optimal solution $(\boldsymbol{c}^{\star}, \nu_d^{\star})$ of problem (2.2);

1: solve SDP (2.9) finding $(\boldsymbol{X}^{\star}, \boldsymbol{C}^{\star}, t^{\star})$;
2: solve problem (2.10) obtaining $\nu_d^{\star}$; compute $\boldsymbol{p}^{\star}$ like (2.12);
3: let $\text{tr}\left(\boldsymbol{c}_0\boldsymbol{c}_0^{\dagger}\boldsymbol{C}^{\star}\right) = s$, and perform $\mathcal{D}\left(\boldsymbol{C}^{\star}, \boldsymbol{M}^{-1}\odot\left(\boldsymbol{p}^{\star}\boldsymbol{p}^{\star\dagger}\right)^{*} - t^{\star}\boldsymbol{I}, \boldsymbol{c}_0\boldsymbol{c}_0^{\dagger} - s\boldsymbol{I}\right)$ getting $\boldsymbol{C}^{\star} = \sum_{i=1}^{R}\boldsymbol{c}_i\boldsymbol{c}_i^{\dagger}$;
4: let $\boldsymbol{c}_i = \boldsymbol{c}_i/||\boldsymbol{c}_i||$, $i=1,\ldots,R$, and solve problem (2.18) with parameter $\boldsymbol{c}_i$, obtaining the optimal values $\{t(1),\ldots,t(R)\}$ and the optimums $\{\nu_{d,1},\ldots,\nu_{d,R}\}$.
5: choose $\boldsymbol{c}_i$ such that $t(i)=\max\{t(1),\ldots,t(R)\}$, say $\boldsymbol{c}_i=\boldsymbol{c}_1$, and let $\boldsymbol{c}^{\star}=\boldsymbol{c}_1 e^{j\arg \boldsymbol{c}_1^{\dagger}\boldsymbol{c}_0}$ and $\nu_d^{\star}=\nu_{d,1}$.

As to the computational complexity of the above algorithm, it is dictated by the solution of the SDP problem (2.9) [3], which has a worst-case complexity of $O\left(N^{4.5}\log\frac{1}{\eta}\right)$ (see [26]), since the specific rank-one decomposition involved requires $O(N^3)$ operations and the cost of the one dimensional optimization problem[4] is very low compared to the cost

[3] An SDP problem can be efficiently solved in polynomial time through *interior point methods*, and the number of iterations necessary to achieve convergence usually ranges between 10 and 100 (see [11]).

[4] In the later numerical simulation, the Matlab command `fminbnd` is used.

of the computations in the other steps.

Before concluding, it is interesting to highlight that a possible extension of the encoding algorithm aimed at optimizing the minimum SNR (over ν_d) in a sub-interval of $[0,1]$ (or even in the union of more than one of such sub-intervals) can be easily conceived exploiting [25, Theorem 3.2] in place of [25, Theorem 3.1] to express the nonnegativity of the trigonometric polynomial in the considered sub-interval.

2.4 Performance Analysis

This Section is devoted to the performance analysis of the proposed scheme for the robust waveform design. To this end, the assumption is that the (l,k)-th entry disturbance covariance matrix is given by $\boldsymbol{M}(l,k) = \rho_1^{|l-k|}\exp\left[j2\pi\gamma(l-k)\right] + 10\rho^{|l-k|} + 10^{-2}\boldsymbol{I}(l,k)$, which is a structure accounting for the simultaneous presence of sea clutter, land clutter, and thermal noise. Moreover, the P_{fa} of the GLRT receiver if fixed to 10^{-6}, $\rho_1 = 0.8$, $\rho = 0.9$, and $\gamma = 0.2$. The analysis is conducted in terms of P_d, robustness with respect to Doppler shifts, and ambiguity function of the coded pulse train which results exploiting the proposed algorithm, i.e.

$$\begin{aligned}\chi(\lambda,f) &= \int_{-\infty}^{\infty} u(\beta)u^*(\beta-\lambda)e^{j2\pi f\beta}d\beta \\ &= \sum_{l=0}^{N-1}\sum_{m=0}^{N-1}\bar{a}(l)\bar{a}^*(m)\chi_p[\lambda-(l-m)T_r,f]\,.\end{aligned}$$

The convex optimization MATLAB toolbox SElf-DUal-MInimization (SeDuMi) [28] is exploited for solving the SDP relaxation. The decomposition $\mathcal{D}(\cdot,\cdot,\cdot)$ of the SeDuMi solution is performed using the technique described in [27]. Finally, the MATLAB toolbox of [2] is used to plot the ambiguity functions of the coded pulse trains. In the following, the generalized Barker sequence [2, pp. 109-113] of length $N = 10$ is considered as similarity code (namely, $\boldsymbol{c}_0 = [0.3162, 0.3162, 0.1724+0.2651j, -0.1905+0.2524j, -0.2322+0.2147j, 0.3084+0.0697j, 0.3141+0.0367j, -0.2250-0.2222j, 0.29851+0.1044j, -0.1881-0.2542j]^T$).

In Figure 2.1, the P_d of the optimized code (according to the max-min criterion) versus $|\alpha|^2$ is plotted for several values of δ_ϵ, together with P_d of the similarity code for $\nu_d = \nu_d^\star$. The curves show that increasing δ_ϵ

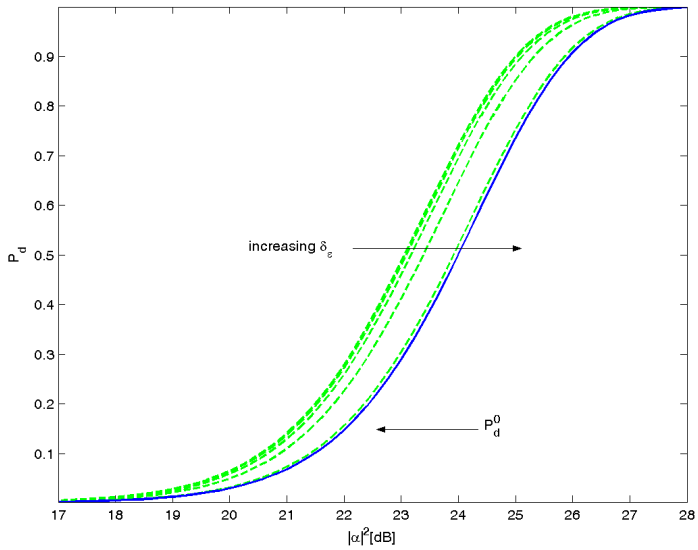

Figure 2.1: P_d versus $|\alpha|^2$ for non-fluctuating target, $P_{fa} = 10^{-6}$, $N = 10$, $\nu_d = \nu_d^\star$, and $\delta_\epsilon = \{0.1, 0.4, 0.7, 0.9, 0.9801, 0.9999\}$. Generalized Barker code (solid curve). Max-min code (dashed curves).

worse and worse P_d values are obtained; this behavior can be explained observing that the smaller δ_ϵ, the larger ϵ, the larger the size of the similarity region. However, this detection loss is compensated for an improvement of the coded pulse train ambiguity function. This is shown in Figures 2.2a-2.2d, where such function is plotted assuming rectangular pulses, $T_r = 5T_p$. The plots highlight that the closer δ_ϵ to 1 the higher the degree of similarity between the ambiguity functions of the devised and the pre-fixed code. This is due to the fact that increasing δ_ϵ is tantamount to reducing the size of the similarity region. In other words, the devised code is forced to be similar and similar to the pre-fixed one and, as a consequence, we get similar and similar ambiguity functions. The last analysis of this Section concerns the robustness of P_d with respect to Doppler shifts. Specifically, in Figure 2.3, the P_d versus ν_d for the max-min code and the similarity code $\boldsymbol{c}_0$ are plotted, assuming $|\alpha|^2 = 23$ dB. Inspection of the curves highlights that, for values of $\delta_\epsilon \leq 0.9$, P_d of the optimized code exhibits a quite flat behavior with respect to Doppler frequencies. On the contrary, P_d of the similarity code is very sensitive

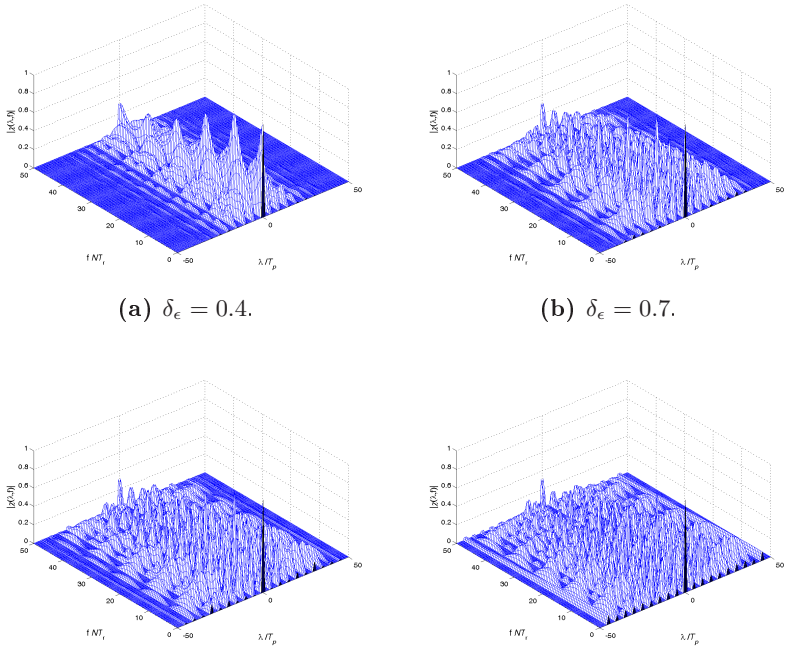

(a) $\delta_\epsilon = 0.4$. **(b)** $\delta_\epsilon = 0.7$.

(c) $\delta_\epsilon = 0.9$. **(d)** $\delta_\epsilon = 0.9999$.

Figure 2.2: Ambiguity function modulus of the max-min code with $N = 10$, $T_r = 5T_p$.

to the Doppler shift and exhibits significant variations. Moreover, for a wide range of Doppler shifts the max-min code outperforms the similarity sequence. Actually, the smaller δ_ϵ, the wider the Doppler interval where the max-min code performs better than the similarity code $\boldsymbol{c}_0$.

A numerical analysis, aimed at assessing the quality of the solution produced by the new algorithm, is now proposed. Specifically, the normalized gap Δ_g between the optimal value of the SDP problem and t_1 is evaluated, i.e. $\Delta_g = \frac{t^\star - t_1}{t^\star}$. Observing the second row of Table 2.1, it is possible to see that, for the considered values of the parameters, the devised algorithm provides high-quality solutions. Notice that, for all the simulated $\delta_\epsilon \geq 0.7$ or $0.15 \leq \delta_\epsilon < 0.4$, it even outputs the optimal solution to the max-min problem (i.e. the SDP relaxation problem has always a rank-one optimal solution).

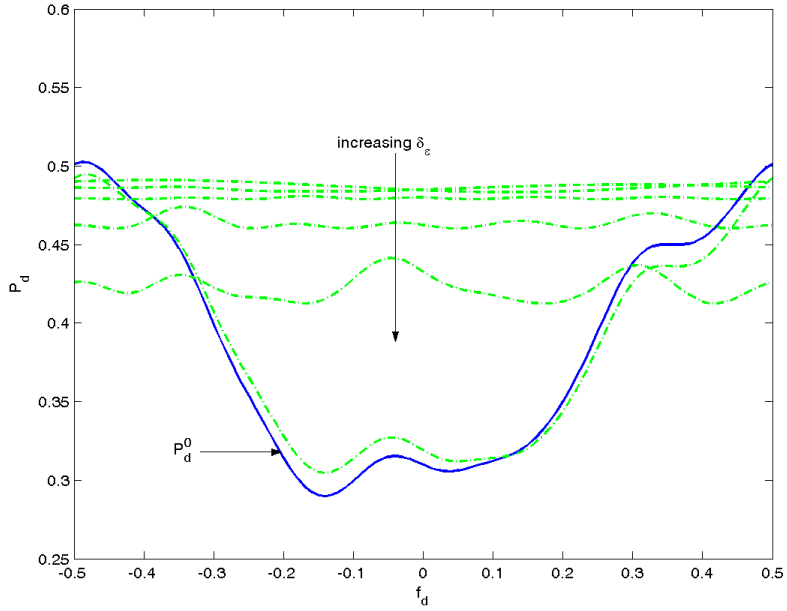

Figure 2.3: P_d versus ν_d for $|\alpha|^2 = 23$ dB, non-fluctuating target, $N = 10$, and $\delta_\epsilon = \{0.1, 0.4, 0.7, 0.9, 0.9801, 0.9999\}$. Generalized Barker code (solid curves), Max-min code (dash curves).

2.5 Conclusions

In the present Chapter, a max-min algorithm for radar waveform design, in the presence of colored Gaussian disturbance, and forcing energy and similarity constraints, has been proposed and analyzed. The waveform synthesis has been formulated as a non-convex quadratic optimization problem with infinitely many quadratic constraints. Through a clever technique, exploiting SDP relaxation techniques and some results from the theory of nonnegative trigonometric polynomials, a procedure capable of providing an high-quality waveform from an optimal solution of the SDP relaxation has been devised. The technique is based on a suitable rank-one decomposition and its implementation requires a polynomial computational complexity. At the analysis stage, the performance of the new algorithm in terms of detection performance, ambiguity function and robustness of P_d with respect to Doppler shifts, have

Table 2.1: Δ_g for $N = 10$, several values of δ_ϵ, and Generalized Barker code as similarity sequence.

δ_ϵ	0.4	0.45	0.47	0.5	0.53	0.55
Δ_g	0.22%	1.39%	1.89%	2.69%	3.56%	4.08%
δ_ϵ	0.57	0.6	0.63	0.65	0.67	//
Δ_g	4.54%	5.16%	5.67%	5.15%	2.75%	//

been evaluated. The effect of the similarity parameter has been studied. Precisely, if there are sufficient degrees of freedom for the optimization problem, namely the similarity parameter is not close to 1, then the max-min algorithm is capable of ensuring a very robust detection performance with respect to target Doppler shifts. Moreover, this robust behavior can be traded off with ambiguity function peculiarities.

Chapter 3

Design of Optimized Radar Codes with a Peak to Average Power Ratio Constraint

3.1 Introduction

Modern digital technology and adaptive transmitters now give the ability to generate high-accuracy, sophisticated, broad-bandwidth radar waveforms, dynamically adaptable to and optimized for a range of different tasks (detection, tracking, target recognition, etc.) potentially on a pulse-by-pulse and channel-by-channel basis. For instance, a modern multifunction phased array radar can adapt the waveform, dwell time, and update interval according to the nature of the surrounding clutter environment, the Signal to Noise Ratio (SNR), and the particular target (the most likely type of target, the threat that it may represent, and the degree to which it is manoeuvering, etc.). This is essentially the subject of waveform diversity [4, 19, 5, 29, 30], namely a new flexibility and dynamic adaptation which demands new ways of characterizing waveform properties and optimizing waveform design.

The possibility of modulating adaptively the radar signal depending on the surrounding environment and on the expected target characteristics has lead to the concept of matched-illumination [31, 20, 21], which determines the optimized transmission waveform and the corresponding receiver response through the maximization of SNR. This concept is also thoroughly investigated in [22], with reference to a Gaussian point-like

target and stationary Gaussian clutter, showing that the optimum allocation procedure places the signal energy in the noise band having minimum power. Recent studies concerning waveform optimization in the presence of colored disturbance can be found in [7], where a signal design approach relying on the maximization of the SNR under a similarity constraint with a given waveform is proposed and assessed. In [1], focusing on the class of linearly coded pulse trains (both in amplitude and in phase), the authors introduce a code selection algorithm which maximizes the detection performance and, at the same time, is capable of controlling both the region of achievable values for the Doppler estimation accuracy and the degree of similarity with a pre-fixed radar code. In [10] and [32], the approach is extended to account for a Space-Time Adaptive Processing and an unknown target Doppler frequency respectively. However, since in several practical situations, the radar amplifiers might work in saturation conditions and hence an amplitude modulation might be difficult to perform, in [8], the authors also consider the synthesis of constant modulus (unimodular) phase coding schemes for radar coherent pulse trains.

In this Chapter, a new waveform design approach relying on the maximization of the detection performance under a more general constraint than unimodularity is intriduced. Specifically, waveforms are designed with a bounded transmitted Peak-to-Average power Ratio (PAR). This constraint is very reasonable for radar applications and includes, as a special case, the phase only modulation condition. Indeed, it has also been imposed in [33] for the synthesis of waveforms with stopband and correlation constraints. Actually, controlling the PAR permits to constrain the excursions of the squared code elements around their mean value. This also allows to keep under control the dynamic range of the transmitted waveform which is an important practical issue (for the current technology) because high PAR values necessitate a linear amplifier having a large dynamic range and this may be difficult to accommodate. Finally, the PAR control is also a crucial task in OFDM (Orthogonal Frequency-Division Multiplexing) systems and the interested reader might refer to [34] and references therein where this issue is addressed.

Firstly, the focus is on the selection of the radar waveform optimizing the SNR in correspondence of a given expected target Doppler frequency, under a PAR and an energy constraint (Algorithm 3). Notice that this problem is of practical importance when it is required a confirmation of

an initial detection in a certain Doppler bin, namely when some knowledge about the Doppler frequency is available. Besides, when the Doppler parameter is unknown, the practical application of Algorithm 3 can be obtained either tuning the design Doppler to a challenging condition, dictated by the clutter Power Spectral Density (PSD) shape, or optimizing the waveform to an average scenario. This is tantamount to considering as objective function the average SNR over the possible target Doppler shifts.

Afterward, the technique is made robust with respect to the received target target Doppler frequency resorting to a max-min approach (Algorithm 4). Otherwise stated, the worst case (over the target Doppler) SNR is optimized under the same constraints as in the previous problem. Since Algorithms 3 and 4 do not impose any condition on the waveform phase (i.e. the waveform phase can range within the continuous interval $[0, 2\pi)$), their phase quantized versions (Algorithms 5 and 6 respectively) are devise too, which force the waveform phase to belong to a finite alphabet.

All the problems are formulated in terms of non-convex quadratic optimization problems with a finite (cases of Algorithms 3 and 5) or an infinite (cases of Algorithms 4 and 6) number of quadratic constraints. These problems are proved to be NP-hard and, hence, design techniques, relying on Semidefinite Programming (SDP) relaxation and randomization[1] as well as on the theory of trigonometric polynomials [25], are introduced, which approximate the optimal solution with a polynomial time computational complexity. For Algorithms 3 and 5, an analytical expression of the approximation bound which quantifies the quality of the obtained waveforms is provided.

At the analysis stage, the performance of the new technique are assessed in terms of detection probability achievable by the Neyman-Pearson receiver and robust behavior of the detection performance with respect to the target Doppler frequency. The results show that the new algorithms trade off detection performance and SNR robustness with small desirable values of the PAR as well as (Algorithms 5 and 6) with the number of quantization levels used to represent the waveform phase.

The Chapter is organized as follows. In Section 3.2, under the as-

[1]SDP relaxation and randomization techniques have also been used in other signal processing fields. For instance, in maximum likelihood multiuser detection [35] and transmit beamforming [36].

sumptions of the system model (1)-(2), the formulation of the waveform design problems is presented; in Sections 3.3-3.6, solution algorithms for the considered problems are devised; in Section 3.7, the performance of the new waveform design techniques are analyzed, providing numerical results aimed at assessing their quality. Finally, conclusions are given in Section 3.8.

3.2 System Model and Formulation of the Problems

The focus is on a monostatic radar transmitting a linearly encoded pulse train and consider the signal model of eq. (1) [1], with the only difference that $\boldsymbol{p} = [1, e^{j2\pi\nu_d}, \ldots, e^{j2\pi(N-1)\nu_d}]^T$.

The main goal is to find codes optimizing the SNR (either in the matched case, namely in correspondence of a given normalized target Doppler frequency, or in the worst normalized Doppler case), under a constraint on the transmitted energy, namely $\|\boldsymbol{c}\|^2 = N$, and forcing an upper bound to the PAR, i.e.

$$\text{PAR} = \frac{\max\limits_{i=1,\ldots,N} |c(i)|^2}{\frac{1}{N}\|\boldsymbol{c}\|^2} = \max_{i=1,\ldots,N} |c(i)|^2, \tag{3.1}$$

where $\boldsymbol{c} = [c(1), \ldots, c(N)]^T \in \mathbb{C}^N$. Evidently, a bound on the PAR is tantamount to imposing a more general constraint than the phase-only condition, which can be obtained letting PAR=1.

In the following, the waveform design problems are formulated mathematically, showing how the matched or worst case SNR can be optimized and the constraints can be enforced, under the assumption of eq. (2) for the disturbance vector $\boldsymbol{w}$. First of all, focusing (without loss of generality) on the case of non-fluctuating target, the SNR can be again defined as in eq. (1.8). Hence, for a given normalized target Doppler ν_d, the Waveform Design Problem (WDP) can be formulated in terms of the following complex quadratic optimization program

$$\begin{aligned} \max_{\boldsymbol{c}} \quad & \boldsymbol{c}^\dagger \boldsymbol{R} \boldsymbol{c} \\ \text{s.t.} \quad & \text{PAR} = \max_{i=1,\ldots,N} |c(i)|^2 \leq \gamma \\ & \|\boldsymbol{c}\|^2 = N \end{aligned} \tag{3.2}$$

(PAR constrained WDP) where $1 \leq \gamma \leq N$ rules the maximum allowable PAR. The resulting waveform optimizes the radar performance in correspondence of the specific design Doppler. From a practical point of view, this is of interest during the confirmation process, i.e. when it is required to confirm an initial detection in a certain Doppler bin (obtained using a possibly standard non-optimized waveform) so as to improve the quality of detection. Alternatively, the practical application of the criterion can be obtained either tuning the design Doppler to a challenging condition, dictated by the clutter Power Spectral Density (PSD) shape (i.e. design Doppler in correspondence of the PSD peak), or optimizing the waveform to an average scenario.

If the target Doppler is not a-priori known, it makes sense to consider the waveform optimizing the worst case SNR. By doing so, it is possible to get a single transmitted signal capable of ensuring a robust behavior of the detection performance with respect to the actual Doppler frequency. This criterion leads to the following Robust PAR constrained WDP

$$\begin{array}{ll} \max\limits_{\boldsymbol{c}} & \min\limits_{\nu_d \in [0,1]} \boldsymbol{c}^\dagger \boldsymbol{R} \boldsymbol{c} \\ \text{s.t.} & \text{PAR} = \max\limits_{i=1,\ldots,N} |c(i)|^2 \leq \gamma, \\ & \|\boldsymbol{c}\|^2 = N. \end{array} \tag{3.3}$$

Since problems (3.2) and (3.3) do not impose any condition on the waveform phase (i.e. the waveform phase can range within the continuous interval $[0, 2\pi)$), it is of interest to consider also their phase quantized versions, forcing the waveform phase to belong to a finite set. This observation leads to PAR constrained and phase quantized WDP

$$\begin{array}{ll} \max\limits_{\boldsymbol{c}} & \boldsymbol{c}^\dagger \boldsymbol{R} \boldsymbol{c} \\ \text{s.t.} & \text{PAR} = \max\limits_{i=1,\ldots,N} |c(i)|^2 \leq \gamma \\ & \arg\left(c(i)\right) \in \{0, \frac{1}{M} 2\pi, \ldots, \frac{M-1}{M} 2\pi\},\ i = 1, \ldots, N \\ & \|\boldsymbol{c}\|^2 = N \end{array} \tag{3.4}$$

(where the number of quantization levels M is an integer such that $M \geq 2$) and robust PAR constrained and phased quantized WDP:

$$\begin{array}{ll} \max\limits_{\boldsymbol{c}} & \min\limits_{\nu_d \in [0,1]} \boldsymbol{c}^\dagger \boldsymbol{R} \boldsymbol{c} \\ \text{s.t.} & \text{PAR} = \max\limits_{i=1,\ldots,N} |c(i)|^2 \leq \gamma, \\ & \arg\left(c(i)\right) \in \{0, \frac{1}{M} 2\pi, \ldots, \frac{M-1}{M} 2\pi\},\ i = 1, \ldots, N \\ & \|\boldsymbol{c}\|^2 = N \end{array} \tag{3.5}$$

which respectively refer to the case of known and unknown normalized target Doppler.

Before proceeding with the design of solution techniques for (3.2), (3.3), (3.4), and (3.5), it is worth to address the differences between them and the optimization problems formulated and solved in some of the previous works:

1. the problem in [1] is a non-convex homogeneous Quadratically Constrained Quadratic Programming (QCQP) with three constraints, the strong duality holds for the problem, and a polynomial-time algorithm is established based on a suitable rank-one decomposition;

2. the problem in [10] is a non-convex homogeneous QCQP with four constraints for which strong duality does not hold in general. Nevertheless, the authors have shown how to construct an optimal solution in polynomial-time, provided only that the SDP relaxation of the original problem gives an optimal solution with rank not equal to two;

3. the problem in [8] is an NP-hard QCQP optimization problem due to the phase-only and the possibly finite alphabet constraint, whose optimal solution is approximated using the relaxation and randomization approach typical of the boolean Quadratic Programming (QP) problems;

4. the problem in [32] is a QCQP with infinitely many constraints, for which the authors establish a *deterministic* approximation procedure, with polynomial time computational complexity, to output a solution leading to high-quality radar waveforms.

In this Chapter, new randomized approximation algorithms for the WDP (3.2) and its phase-quantized version (3.4) are established, respectively. Due to the PAR constraint considered in (3.2), which is quite different in nature from the constraint (the similarity constraint under the infinite norm) in the optimization problem considered in [8], the approximation procedures for (3.2) and (3.4) must be re-designed and the mathematical analysis for the approximation bounds has to be re-assessed. For the robust PAR constrained WDPs (3.3) and (3.5), respective randomized approximation algorithms will be proposed, in contrast to the determin-

istic approximation algorithm built in [32], according to some convex optimization techniques and the new randomization procedures.

3.3 PAR Constrained WDP

Problem (3.2) can be equivalently reformulated as

$$\begin{array}{ll} \max\limits_{\boldsymbol{c}} & \boldsymbol{c}^{\dagger}\boldsymbol{R}\boldsymbol{c} \\ \text{s.t.} & |c(i)|^2 \leq \gamma,\ i = 1, \ldots, N \\ & \|\boldsymbol{c}\|^2 = N. \end{array} \tag{3.6}$$

Notice that when $\gamma = 1$, a feasible point for (3.6) has the property that $|c(i)| = 1\ \forall i$, and thus the norm constraint $\|\boldsymbol{c}\|^2 = N$ is redundant, i.e., (3.6) reduces to

$$\begin{array}{ll} \max\limits_{\boldsymbol{c}} & \boldsymbol{c}^{\dagger}\boldsymbol{R}\boldsymbol{c} \\ \text{s.t.} & |c(i)|^2 \leq 1,\ i = 1, \ldots, N. \end{array} \tag{3.7}$$

Problem (3.7) has been proven NP-hard in [37][2] (see related works [38], [39], [40]) and approximation algorithms for (3.7) are established in [37] (see [41] also). An interesting application for (3.7) with all parameters and design variable being real-valued can be found with reference to blind Maximum-Likelihood (ML) detection of Orthogonal Space-Time Block Codes (OSTBCs) with unknown Channel State Information (CSI) in Multiple-Input-Multiple-Output (MIMO) transmissions [42].

In this Section, problem (3.6) is considered with $\gamma > 1$, which means that the norm constraint does not vanish. Clearly, problem (3.6) is a non-convex QCQP with multiple constraints[3]. It is possible to claim that problem (3.6) with γ greater than one is NP-hard by a reduction from an even partition problem which is known to be NP-complete.

[2] Indeed, problem (3.7) is equivalent to (3.7) with all the inequality constraints becoming equality constraints, due to the fact that the maximal value of a convex function is attained only at the boundary of a convex region. In other words, replacing the inequality constraints in (3.7) into equality ones, neither the optimal value nor the optimal solution set of problem (3.7) would be changed. It has been shown in [37] that the problem (3.7) with all equality constraints is NP-hard, thus problem (3.7) is NP-hard, as it stands now.

[3] For a QCQP, non-convexity does not imply that it is hard to solve; it turns out that, if the number of constraints is not too high, the QCQP can be solved efficiently; in other words, the SDP relaxation of it is tight. See [27], [43].

Proposition 3.3.1. *The radar code design problem* (3.6) *is NP-hard with parameters* $\boldsymbol{R} \succeq \mathbf{0}$ *and* $\gamma > 1$.

Proof. See Appendix C. □

Due to Proposition 3.3.1, the radar code design problem (3.6) is unlikely to admit a polynomial time solution method (which means (3.6) is computational intractable in general). Thus, efforts will be made in the following toward the design of an approximation algorithm for (3.6).

3.3.1 Approximation algorithm via semidefinite programming relaxation and randomization

To get an approximate solution (alternatively termed as a suboptimal solution) of (3.6), consider its SDP relaxation:

$$\begin{array}{ll} \max\limits_{\boldsymbol{C}} & \mathrm{tr}\,(\boldsymbol{RC}) \\ \text{s.t.} & C(i,i) \le \gamma,\ i = 1, \ldots, N \\ & \mathrm{tr}\,(\boldsymbol{C}) = N \\ & \boldsymbol{C} \succeq \mathbf{0}. \end{array} \tag{3.8}$$

Evidently, problem (3.8) with the additional rank constraint $\mathrm{Rank}\,(\boldsymbol{C}) = 1$ is equivalent to (3.6). It follows from the strong duality theorem [26, Theorem 1.7.1] of SDP that (3.8) is solvable[4], since the SDP (3.8) is feasible (for example, $\boldsymbol{I}$ is a feasible point) and its dual is strictly feasible:

$$\begin{array}{ll} \min\limits_{t(i)} & t(0)N + \gamma \sum_{i=1}^{N} t(i) \\ \text{s.t.} & \boldsymbol{R} - \sum_{i=1}^{N} t(i)\boldsymbol{E}_i - t(0)\boldsymbol{I} \preceq \mathbf{0} \\ & t(i) \ge 0,\ i = 1, \ldots, N \end{array} \tag{3.9}$$

where $\boldsymbol{E}_i$ stands for the $N \times N$ matrix with the ii-th entry being one and all other entries being zero. In practice, an optimal solution of (3.8) can be obtained using public solvers (such as cvx [44] and SeDuMi [28]).

Let $\boldsymbol{C}^\star$ be an optimal solution of (3.8). The main goal is to extract a rank-one feasible solution of (3.8) with mathematically provable quality from $\boldsymbol{C}^\star$, which may or may not be of rank-one. Notice that if $\mathrm{Rank}\,\boldsymbol{C}^\star$ happens to be one, then the radar code design problem (3.6) is optimally solved and the SDP relaxation is tight.

[4] By saying *solvable*, it means that the problem is feasible, bounded, and the optimal value is attained (see [26, page 13]).

However, often, it is not the case that Rank $\boldsymbol{C}^{\star}$ is one, which means that the SDP relaxation (3.8) is not tight for (3.6). Therefore, the design of a suitable procedure to construct in polynomial time a *suboptimal* solution of problem (3.6) is a compromising must. The idea of a Gaussian randomization procedure to produce an approximate solution to an NP-hard optimization problem comes from the seminal work [45] by Goemans and Williamson where the authors proposed a randomized approximation algorithm for the NP-hard max-cut problem, with the approximation bound 0.87856, via the SDP relaxation technique. Since then, a large number of NP-hard optimization problems have been solved by the approximation method of SDP-relaxation-plus-randomization, importantly with theoretically assured approximation bound. For an overview of it from a perspective of signal processing, the reader is invited to refer to the magazine paper [43]. Using the idea (mainly from [45] and [46] and references therein), a Gaussian randomization procedure is presented so as to obtain an approximate solution of problem (3.6), based on the optimal solution $\boldsymbol{C}^{\star}$ of the SDP relaxation problem (3.8). The quoted procedure requires the definition of a suitable "ad hoc" covariance matrix of the Gaussian distribution to be adopted in the randomization step. The basic criterion for selecting such a covariance matrix is that the entire randomization procedure has to lead to a feasible solution of the original problem with probability one and it has also to provide mathematical tractability in assessing the quality of the resulting solution. According to this guideline, denote by

$$\boldsymbol{d} = \sqrt{\mathbf{diag}(\boldsymbol{C}^{\star})}, \tag{3.10}$$

and by $\boldsymbol{d}^{-}$

$$(\boldsymbol{d}^{-})_i = \begin{cases} 1/d(i), & \text{if } d(i) > 0 \\ 1, & \text{if } d(i) = 0 \end{cases} \quad i = 1, \ldots, N. \tag{3.11}$$

Additionally, let

$$\boldsymbol{D} = \mathbf{Diag}(\boldsymbol{d}),\ \boldsymbol{D}^{-} = \mathbf{Diag}(\boldsymbol{d}^{-}), \tag{3.12}$$

and observe that, from (3.10)-(3.12),

$$(\boldsymbol{D}^{-}\boldsymbol{D})(i,i) = \begin{cases} 1, & \text{if } d(i) > 0 \\ 0, & \text{if } d(i) = 0 \end{cases} \quad i = 1, \ldots, N. \tag{3.13}$$

Hence, the entries of the matrix

$$\tilde{\boldsymbol{C}}^{\star} = \boldsymbol{C}^{\star} + (\boldsymbol{I} - \boldsymbol{D}^{-}\boldsymbol{D}) \tag{3.14}$$

comply with

$$\tilde{C}^{\star}(i,k) = \begin{cases} C^{\star}(i,k), & \text{if } i \neq k \\ C^{\star}(i,i), & \text{if } C^{\star}(i,i) > 0 \\ 1, & \text{if } C^{\star}(i,i) = 0 \end{cases} . \tag{3.15}$$

By the construction of $\tilde{\boldsymbol{C}}^{\star}$, it is possible to see that the diagonal elements $\tilde{\boldsymbol{C}}^{\star}$ are positive and that $\tilde{C}^{\star}(i,i) = 1$ provided that $C^{\star}(i,i)$ vanishes. Exploiting the above definitions and observations, further important properties about $\tilde{\boldsymbol{C}}^{\star}$ follow:

Proposition 3.3.2. *Let $\boldsymbol{C}^{\star}$ be a positive semidefinite matrix and $\boldsymbol{d}$, $\boldsymbol{d}^{-}$, $\boldsymbol{D}$, $\boldsymbol{D}^{-}$, $\tilde{\boldsymbol{C}}^{\star}$ be defined as* (3.10)-(3.12), (3.14), *respectively. Then, the matrix $\boldsymbol{D}^{-}\tilde{\boldsymbol{C}}^{\star}\boldsymbol{D}^{-}$ enjoys the following properties:*

(i) $\boldsymbol{D}^{-}\tilde{\boldsymbol{C}}^{\star}\boldsymbol{D}^{-} \succeq \boldsymbol{0}$;

(ii) the diagonal elements of $\boldsymbol{D}^{-}\tilde{\boldsymbol{C}}^{\star}\boldsymbol{D}^{-}$ are one.

Proof. See Appendix D. □

This proposition indicates that $\boldsymbol{D}^{-}\tilde{\boldsymbol{C}}^{\star}\boldsymbol{D}^{-}$ can be a suitable choice for the covariance matrix of a Gaussian distribution to be adopted in the randomized approximation algorithm. Indeed, suppose to take a Gaussian random vector $\boldsymbol{\xi}$ from the distribution $\mathcal{N}_{\mathbb{C}}(\boldsymbol{0}, \boldsymbol{D}^{-}\tilde{\boldsymbol{C}}^{\star}\boldsymbol{D}^{-})$; then each component of $\boldsymbol{\xi}$ is with zero mean and unit variance (according to (ii) of Proposition 3.3.2), i.e., the vector $\boldsymbol{\xi}$ enjoys dependent standard complex Gaussian random components. It can be seen that with probability one, $(\sqrt{C^{\star}(1,1)}\frac{\xi(1)}{|\xi(1)|}, \ldots, \sqrt{C^{\star}(N,N)}\frac{\xi(N)}{|\xi(N)|})$ is feasible for the PAR constrained WDP (3.2). Additionally, such a construction of the covariance $\boldsymbol{D}^{-}\tilde{\boldsymbol{C}}^{\star}\boldsymbol{D}^{-}$ shares some advantages in mathematically assessing the quality of a randomized approximation algorithm (as it can be seen in the next sub-section). Based on these observations, in order to produce an approximate solution (i.e., a suboptimal solution, or a feasible solution) of (3.6), the following randomization procedure (in Algorithm 3) is proposed.

It is worth to remark that in practice the randomization steps 3 and 4 can be repeated many times, in order to obtain a solution with

Algorithm 3 Gaussian randomization procedure for radar code design problem (3.6)

Require: $\boldsymbol{R}$, γ;
Ensure: a randomized approximate solution $\boldsymbol{c}$ of (3.6);
1: solve the SDP (3.8) finding $\boldsymbol{C}^\star$;
2: define $\boldsymbol{d}$, $\boldsymbol{d}^-$, $\boldsymbol{D}$, $\boldsymbol{D}^-$ according to (3.10)-(3.12);
3: draw a random vector $\boldsymbol{\xi} \in \mathbb{C}^N$ from the complex normal distribution $\mathcal{N}_{\mathbb{C}}(\boldsymbol{0}, \boldsymbol{D}^-(\boldsymbol{C}^\star + (\boldsymbol{I} - \boldsymbol{D}^-\boldsymbol{D}))\boldsymbol{D}^-)$;
4: let $c(i) = \sqrt{C^\star(i,i)}e^{j\arg(\xi(i))}$, $i = 1, \ldots, N$.

better quality. As it can be directly seen, the computational cost of Algorithm 3 is dominated by solving SDP (3.8) which has a complexity of $O(N^{3.5}\log(1/\epsilon))$ [43], given a solution accuracy $\epsilon > 0$.

3.3.2 Approximation bound

The approximation bound of an approximation algorithm is a measure characterizing the quality of the algorithm. For a randomized approximation algorithm solving a maximization (minimization) problem, an approximation bound[5] $R \in (0,1]$ ($R \in [1, +\infty)$) means that for all instances of the problem, the algorithm always delivers a feasible solution whose expected objective functional value is at least (at most) R times the optimal value. Such an algorithm is usually called randomized R-approximation algorithm. More precisely, let $v(\cdot)$ be the optimal value of an instance of a given maximization (minimization) problem $(\cdot)$, then a feasible solution z produced by a randomized R-approximation algorithm, complies with

$$E[\text{the objective function evaluated at } z] \geq Rv(\cdot)$$

($E[\text{the objective function evaluated at } z] \leq Rv(\cdot)$ for minimization problem). It is clear that an algorithm produces a *better* approximation (for either maximization problem or minimization problem), if the approximation bound is *closer* to 1. The aim of this subsection is to establish an approximation bound for Algorithm 3. Toward this end, a result proved in [37, Section 3.3, pp. 884] is invoked:

[5]It is also termed as performance guarantee, or worst case ratio in the open literature.

Lemma 3.3.3. *Let $\boldsymbol{Z}$ be a positive semidefinite matrix with all one diagonal elements and $\boldsymbol{z}$ be a randomized vector generated setting $z(i) = e^{j\arg(\xi(i))}$, $i = 1, \ldots, N$, where $\boldsymbol{\xi} \sim \mathcal{N}_{\mathbb{C}}(\boldsymbol{0}, \boldsymbol{Z})$. Then,*

$$E[\boldsymbol{z}\boldsymbol{z}^{\dagger}] = F(\boldsymbol{Z}) = \frac{\pi}{4}\boldsymbol{Z} + \frac{\pi}{2}\sum_{k=1}^{\infty}\frac{((2k)!)^2}{2^{4k+1}(k!)^4(k+1)}(\boldsymbol{Z}^T \odot \boldsymbol{Z})^{(k)} \odot \boldsymbol{Z} \succeq \frac{\pi}{4}\boldsymbol{Z} \tag{3.16}$$

where $(\boldsymbol{A})^{(k)}$ denotes the Hadamard product of k copies of $\boldsymbol{A}$.

Besides, from Proposition 3.3.2, it follows

Proposition 3.3.4. *Let $\boldsymbol{C}^{\star}$ be a positive semidefinite matrix and $\boldsymbol{d}$, $\boldsymbol{d}^{-}$, $\boldsymbol{D}$, $\boldsymbol{D}^{-}$, $\tilde{\boldsymbol{C}}^{\star}$ be defined as* (3.10)-(3.12), (3.14)*, respectively. Then,*

$$\boldsymbol{D}(\boldsymbol{D}^{-}\tilde{\boldsymbol{C}}^{\star}\boldsymbol{D}^{-})\boldsymbol{D} = \boldsymbol{C}^{\star}.$$

Proof. See Appendix E. □

Capitalizing Lemma 3.3.3 and Proposition 3.3.4, the proposition below is obtained showing that the randomized Algorithm 3 has the approximation abound $\frac{\pi}{4}$.

Proposition 3.3.5. *Let $\boldsymbol{c}$ be the randomized solution output by Algorithm 3. Then,*

$$E[\boldsymbol{c}^{\dagger}\boldsymbol{R}\boldsymbol{c}] = \mathrm{tr}\,(\boldsymbol{R}(\boldsymbol{D}F(\boldsymbol{D}^{-}\tilde{\boldsymbol{C}}^{\star}\boldsymbol{D}^{-})\boldsymbol{D})) \geq \frac{\pi}{4}\mathrm{tr}\,(\boldsymbol{R}\boldsymbol{C}^{\star}) \geq \frac{\pi}{4}v((3.6)) \tag{3.17}$$

where $\tilde{\boldsymbol{C}}^{\star}$ is defined in (3.14) *and the function $F(\cdot)$ is defined in* (3.16)*.*

Proof. See Appendix F. □

Before concluding, it is important to remark that problem (3.6) is equivalent to the real-valued quadratic program:

$$\begin{array}{ll} \max\limits_{\boldsymbol{u},\boldsymbol{v}} & [\boldsymbol{u}^T\ \boldsymbol{v}^T]\begin{bmatrix} \Re(\boldsymbol{R}) & -\Im(\boldsymbol{R}) \\ \Im(\boldsymbol{R}) & \Re(\boldsymbol{R}) \end{bmatrix}\begin{bmatrix} \boldsymbol{u} \\ \boldsymbol{v} \end{bmatrix} \\ \text{s.t.} & u(i)^2 + v(i)^2 \leq \gamma,\ i = 1, \ldots, N \\ & \sum_{i=1}^{N}(u(i)^2 + v(i)^2) = N \end{array} \tag{3.18}$$

where $\boldsymbol{u} = \Re(\boldsymbol{c})$ and $\boldsymbol{v} = \Im(\boldsymbol{c})$. The approximation bound for the approximation algorithm solving a real-valued quadratic program like in (3.18) but without any special structure of the positive semidefinite

matrix appearing in the objective function, obtained in [46], is $\frac{2}{\pi}$ ($\approx$ 0.6366), instead of $\frac{\pi}{4}$ (≈ 0.7854). It is easy to see that complex quadratic program (3.6) is a structured real quadratic program (3.18); in other words, the matrix appearing in the objective function of (3.18) has the structure

$$\begin{bmatrix} \Re(\boldsymbol{R}) & -\Im(\boldsymbol{R}) \\ \Im(\boldsymbol{R}) & \Re(\boldsymbol{R}) \end{bmatrix},$$

rather than a general $(2N) \times (2N)$ positive semidefinite matrix. As a consequence, the complex quadratic program (3.6) is equivalent to a subclass of real quadratic programs, and it is reasonable that it shares a tighter approximation bound. Indeed, this phenomenon happens also in related literature as for instance in [37], [38] and [27].

3.4 Robust PAR Constrained WDP

Problem (3.3) can be equivalently expressed as

$$\begin{array}{ll} \max\limits_{\boldsymbol{c},t} & t \\ \text{s.t.} & t \leq \boldsymbol{p}^\dagger(\boldsymbol{M}^{-1} \odot (\boldsymbol{c}\boldsymbol{c}^\dagger)^*)\boldsymbol{p},\ \forall \nu_d \in [0,1] \\ & |c(i)|^2 \leq \gamma,\ i = 1, \ldots, N \\ & \|\boldsymbol{c}\|^2 = N. \end{array} \tag{3.19}$$

The conventional SDP relaxation of (3.19) is

$$\begin{array}{ll} \max\limits_{\boldsymbol{C},t} & t \\ \text{s.t.} & t \leq \boldsymbol{p}^\dagger(\boldsymbol{M}^{-1} \odot (\boldsymbol{C})^*)\boldsymbol{p},\ \forall \nu_d \in [0,1] \\ & C(i,i) \leq \gamma,\ i = 1, \ldots, N \\ & \text{tr}\,(\boldsymbol{C}) = N \\ & \boldsymbol{C} \succeq \boldsymbol{0}. \end{array} \tag{3.20}$$

Problem (3.20) includes the infinitely many quadratic constraints $t \leq \boldsymbol{p}^\dagger(\boldsymbol{M}^{-1} \odot (\boldsymbol{C})^*)\boldsymbol{p}$, $\forall \nu_d \in [0,1]$. However, it can be proved that they can be transformed into a finite number convex constraints, resorting to the SDP representation of nonnegative trigonometric polynomials [25]. To this end, first observe that

$$\boldsymbol{p}^\dagger(\boldsymbol{M}^{-1} \odot (\boldsymbol{C})^*)\boldsymbol{p} - t = x(0) - t + 2\Re\left(\sum_{k=1}^{N-1} x(k)e^{-jk\omega}\right),$$

where $\omega = 2\pi\nu_d$ and

$$x(k) = \sum_{i=1}^{N-k} (\boldsymbol{M} \odot (\boldsymbol{C})^*)(i+k, i), \qquad k = 0, 1, \ldots, N-1. \tag{3.21}$$

Hence, the following theorem, proved in [25, Theorem 3.1] and quoted here as a lemma, is exploited.

Lemma 3.4.1. *The trigonometric polynomial* $f(\omega) = x(0) + 2\Re\left(\sum_{k=1}^{N-1} x(k)e^{-jk\omega}\right)$ *is nonnegative over* $[0, 2\pi]$*, if and only if there exists an* $N \times N$ *Hermitian matrix* $\boldsymbol{X} \succeq \boldsymbol{0}$ *such that*

$$\boldsymbol{x} = \boldsymbol{W}^\dagger \mathbf{diag}(\boldsymbol{W}\boldsymbol{X}\boldsymbol{W}^\dagger), \tag{3.22}$$

where $\boldsymbol{x} = [x(0), \ldots, x(N-1)]^T$*,* $\boldsymbol{W} = [\boldsymbol{w}_0, \ldots, \boldsymbol{w}_{N-1}] \in \mathbb{C}^{L\times N}$*,* $\boldsymbol{w}_k = [1, e^{-jk\theta}, \ldots, e^{-j(L-1)k\theta}]^T$*,* $k = 0, \ldots, N-1$*,* $\theta = 2\pi/L$*,* $L \geq 2N-1$*.*

The above Lemma implies that (3.20) can be recast equivalently as the following SDP:

$$\begin{array}{ll} \max\limits_{\boldsymbol{C}, \boldsymbol{X}, t} & t \\ \text{s.t.} & \boldsymbol{W}^\dagger \mathbf{diag}(\boldsymbol{W}\boldsymbol{X}\boldsymbol{W}^\dagger) + t\boldsymbol{e}_1 = \boldsymbol{x} \\ & C(i,i) \leq \gamma,\ i = 1, \ldots, N \\ & \mathrm{tr}\,(\boldsymbol{C}) = N \\ & \boldsymbol{C} \succeq \boldsymbol{0},\ \boldsymbol{X} \succeq \boldsymbol{0} \end{array} \tag{3.23}$$

where $\boldsymbol{x}$ is defined by (3.21) and $\boldsymbol{W}$ is the same as the one defined in Lemma 3.4.1 by taking $L = 2N-1$.

Proposition 3.4.2. *It holds that SDP problem* (3.23) *is solvable.*

Proof. See Appendix G. □

Let $(\boldsymbol{C}^\star, \boldsymbol{X}^\star, t^\star)$ be an optimal solution of (3.20). Feasible solutions $\boldsymbol{c}_k$, $k = 1, \ldots, K$ (K will be referred to as the number of randomizations), of (3.3) are generated using $\boldsymbol{C}^\star$ in a way similar to Algorithm 3. Then pick $\boldsymbol{c}_k$, say $\boldsymbol{c}_1$, such that the objective function value $t(1)$ is maximal over all

$$t(k) = \min_{\nu_d \in [0,1]} \boldsymbol{p}^\dagger (\boldsymbol{M} \odot (\boldsymbol{c}_k \boldsymbol{c}_k^\dagger)^*)\boldsymbol{p},\ k = 1, \ldots, K. \tag{3.24}$$

The minimization problems (3.24) are one dimensional optimization problem. It is seen that each problem in (3.24) is equivalent to an SDP. In fact, for each k, it follows that

$$t(k) = \max_{s} \; s \;\; \text{s.t. } \boldsymbol{p}^{\dagger}(\boldsymbol{M} \odot (\boldsymbol{c}_k \boldsymbol{c}_k^{\dagger})^*)\boldsymbol{p} \geq s, \, \forall \nu_d \in [0,1]. \tag{3.25}$$

It follows from Lemma 3.4.1 that problem (3.25) is equivalent to

$$\begin{array}{rll} t(k) = & \max\limits_{\boldsymbol{X}_1, s} & s \\ & \text{s.t.} & \boldsymbol{W}^{\dagger}\mathbf{diag}(\boldsymbol{W}\boldsymbol{X}_1\boldsymbol{W}^{\dagger}) + s\boldsymbol{e}_1 = \boldsymbol{x}_k \\ & & \boldsymbol{X}_1 \succeq \mathbf{0}, \, s \in \mathbb{R} \end{array} \tag{3.26}$$

where the l-th element of $\boldsymbol{x}_k$ is similar to that defined in (3.21), i.e.,

$$x_k(l) = \sum_{i=1}^{N-l} (\boldsymbol{M} \odot (\boldsymbol{c}_k \boldsymbol{c}_k^{\dagger})^*)(i+l, i), \qquad l = 0, 1, \ldots, N-1. \tag{3.27}$$

Algorithm 4 summarizes the procedure to generate an approximate solution of (3.3).

Algorithm 4 Gaussian randomization procedure for the code design problem (3.3)

Require: $\boldsymbol{M}$, γ;
Ensure: a randomized approximate solution $\boldsymbol{c}$ of (3.3);
1: solve the SDP (3.23) finding $\boldsymbol{C}^{\star}$;
2: define $\boldsymbol{d}$, $\boldsymbol{d}^{-}$, $\boldsymbol{D}$, $\boldsymbol{D}^{-}$ according to (3.10)-(3.12);
3: draw random vectors $\boldsymbol{\xi}_k \in \mathbb{C}^N$ from the complex normal distribution $\mathcal{N}_{\mathbb{C}}(\mathbf{0}, \boldsymbol{D}^{-}(\boldsymbol{C}^{\star} + (\boldsymbol{I} - \boldsymbol{D}^{-}\boldsymbol{D}))\boldsymbol{D}^{-})$, $k = 1, \ldots, K$;
4: let $c_k(i) = \sqrt{C^{\star}(i,i)} e^{j \arg(\xi_k(i))}$, $i = 1, \ldots, N$, $k = 1, \ldots, K$;
5: compute

$$t(k) = \min_{\nu_d \in [0,1]} \boldsymbol{p}^{\dagger}(\boldsymbol{M} \odot (\boldsymbol{c}_k \boldsymbol{c}_k^{\dagger})^*)\boldsymbol{p},$$

by solving SDP (3.26), $k = 1, \ldots, K$;
6: pick the maximal value over $\{t(1), \ldots, t(K)\}$, say $t(1)$, and output $\boldsymbol{c}_1$.

It is worth to remark that the complexity of the algorithm is dominated by the computation required for solving SDPs (3.23) and (3.26). Lastly, notice that an alternative way to numerically solve the one dimensional problems is to perform one dimension search since each of

the problems has sufficiently smooth objective function and compact feasible interval. In the numerical simulation, we shall use the Matlab ©command `fminbnd` to perform it.

3.5 PAR Constrained and Phase Quantized WDP

In this section, the synthesis of an approximation algorithm for (3.4) has been considered, equivalently reformulated as:

$$\begin{array}{ll} \max\limits_{\boldsymbol{c}} & \boldsymbol{c}^\dagger \boldsymbol{R}\boldsymbol{c} \\ \text{s.t.} & |c(i)|^2 \le \gamma \\ & \arg\left(c(i)\right) \in \{0, \frac{1}{M}2\pi, \ldots, \frac{M-1}{M}2\pi\},\ i = 1, \ldots, N \\ & \|\boldsymbol{c}\|^2 = N. \end{array} \tag{3.28}$$

Clearly, when M goes to infinity, (3.28) becomes (3.6). The claim is that problem (3.28) is also NP-hard, as shown below.

Proposition 3.5.1. *The phase quantized code design problem* (3.28) *is NP-hard with parameters* $\boldsymbol{R} \succeq \boldsymbol{0}$ *and* $\gamma > 1$.

Proof. See Appendix H. □

Due to the hardness of problem (3.28), similar to Algorithm 3, it is proposed a randomized approximation algorithm based on the SDP relaxation technique (as explained in Algorithm 5). Notice that the SDP relaxation problem for (3.28) is (3.8) as well.

Notice that, using the related idea in [46], the approximation algorithm is applicable to the following quadratic program:

$$\begin{array}{ll} \max\limits_{\boldsymbol{c}} & \boldsymbol{c}^\dagger \boldsymbol{R}\boldsymbol{c} \\ \text{s.t.} & \arg\left(c(i)\right) \in \{0, \frac{1}{M}2\pi, \ldots, \frac{M-1}{M}2\pi\},\ i = 1, \ldots, N \\ & [|c(1)|^2, \ldots, |c(N)|^2]^T \in \mathcal{F} \end{array} \tag{3.30}$$

where $\mathcal{F} \subseteq \mathbb{R}_+^N$ is a closed convex set. In this case, the convex relaxation of (3.30) is

$$\begin{array}{ll} \max\limits_{\boldsymbol{C}} & \mathrm{tr}\left(\boldsymbol{R}\boldsymbol{C}\right) \\ \text{s.t.} & \mathbf{diag}(\boldsymbol{C}) \in \mathcal{F} \\ & \boldsymbol{C} \succeq \boldsymbol{0} \end{array} \tag{3.31}$$

which can be solved efficiently due to the convexity of the problem. As to the approximation bound for Algorithm 5, Lemma 3.3 of [37] is quoted as the following lemma.

Algorithm 5 Gaussian randomization procedure for radar code design problem (3.28)

Require: $\boldsymbol{R}$, γ, M;
Ensure: a randomized approximate solution $\boldsymbol{c}$ of (3.28);
1: solve the SDP (3.8) finding $\boldsymbol{C}^\star$;
2: define $\boldsymbol{d}$, $\boldsymbol{d}^-$, $\boldsymbol{D}$, $\boldsymbol{D}^-$ according to (3.10)-(3.12);
3: draw a random vector $\boldsymbol{\xi} \in \mathbb{C}^N$ from the complex normal distribution $\mathcal{N}_{\mathbb{C}}(\boldsymbol{0}, \boldsymbol{D}^-(\boldsymbol{C}^\star + (\boldsymbol{I} - \boldsymbol{D}^-\boldsymbol{D}))\boldsymbol{D}^-)$;
4: let $c(i) = \sqrt{C^\star(i,i)}\mu(\xi(i))$, $i = 1, \ldots, N$. where $\mu(x)$ is defined as

$$\mu(x) = \begin{cases} 1, & \text{if } \arg(x) \in [0, 2\pi\frac{1}{M}) \\ e^{j2\pi\frac{1}{M}}, & \text{if } \arg(x) \in [2\pi\frac{1}{M}, 2\pi\frac{2}{M}) \\ \vdots & \\ e^{j2\pi\frac{M-1}{M}}, & \text{if } \arg(x) \in [2\pi\frac{M-1}{M}, 2\pi) \end{cases}. \tag{3.29}$$

Lemma 3.5.2. *Let $\boldsymbol{Z}$ be a positive semidefinite matrix with all diagonal elements being one, $\boldsymbol{z}$ be a randomized vector generated setting $z(i) = \mu(\xi(i))$, $i = 1, \ldots, N$, where $\boldsymbol{\xi} \sim \mathcal{N}_{\mathbb{C}}(\boldsymbol{0}, \boldsymbol{Z})$, and the rounding function $\mu(x)$ is defined according to* (3.29)*. Then,*

$$E[\boldsymbol{z}\boldsymbol{z}^\dagger] \succeq \frac{2}{\pi}\Re(\boldsymbol{Z}) \text{ for } M = 2, \text{ and } E[\boldsymbol{z}\boldsymbol{z}^\dagger] \succeq \frac{M^2 \sin^2\frac{\pi}{M}}{4\pi}\boldsymbol{Z} \text{ for } M \geq 3. \tag{3.32}$$

Resorting to the above lemma, it can be obtained the following result concerning the approximation bound.

Proposition 3.5.3. *Let $\boldsymbol{c}$ be the randomized solution obtained through Algorithm 3. Then,*

$$E[\boldsymbol{c}^\dagger\boldsymbol{R}\boldsymbol{c}] \geq R(M) \times \mathrm{tr}\,(\boldsymbol{R}\boldsymbol{C}^\star) \geq R(M) \times v((3.28)) \tag{3.33}$$

where

$$R(M) = \begin{cases} \frac{2}{\pi}, & \text{if } M = 2 \\ \frac{M^2 \sin^2\frac{\pi}{M}}{4\pi}, & \text{if } M \geq 3 \end{cases}. \tag{3.34}$$

Proof. The proof is based on Propositions 3.3.2, 3.3.4, and Lemma 3.5.2. It is completely similar to the proof of Proposition 3.3.5 and, thus, it is omitted here. □

In words, Algorithm 5 is a randomized $R(M)$-approximation algorithm for (3.28), where some examples of $R(M)$ are $R(4) = 0.6366$, $R(8) = 0.7458$, $R(16) = 0.7754$, $R(32) = 0.7829$, $R(64) = 0.7848$, $R(128) = 0.7852$.

3.6 Robust PAR Constrained and Phase Quantized WDP

In this Section, the main goal is to solve problem (3.5), which can be equivalently written as

$$\begin{array}{ll} \max\limits_{\boldsymbol{c},\, t} & t \\ \text{s.t.} & t \leq \boldsymbol{p}^{\dagger}(\boldsymbol{M}^{-1} \odot (\boldsymbol{c}\boldsymbol{c}^{\dagger})^{*})\boldsymbol{p},\ \forall \nu_d \in [0,1] \\ & |c(i)|^2 \leq \gamma,\ i = 1, \ldots, N \\ & \arg\left(c(i)\right) \in \{0, \frac{1}{M}2\pi, \ldots, \frac{M-1}{M}2\pi\},\ i = 1, \ldots, N \\ & \|\boldsymbol{c}\|^2 = N. \end{array} \tag{3.35}$$

It is verified that (3.20) is an SDP relaxation of (3.35). Let $(\boldsymbol{C}^{\star}, \boldsymbol{X}^{\star}, t^{\star})$ be an optimal solution of (3.20). Based on $\boldsymbol{C}^{\star}$, approximate solutions of (3.5) are constructed, and then the one with the best performance is selected. Algorithm 6 summarizes the procedure to generate an approximate solution of (3.5).

Notice that, although there is not an analytical approximation bound, the numerical simulations indicate that such an approximate scheme leads to high quality radar waveforms, also with a moderate sample size K. This point will be better elicited in the section addressing numerical results.

3.7 Performance Analysis

This Section is devoted to the performance analysis of the proposed waveform design techniques in correspondence of different values for the design parameters (namely, the PAR constraint γ, the number of randomizations K, the number of phase quantization levels M, etc.). To this end, a disturbance covariance matrix $\boldsymbol{M}$, accounting for both clutter and thermal noise, with the following structure is assumed:

$$\boldsymbol{M} = \sum_{i=1}^{N_c} \beta_i \boldsymbol{p}(\nu_{d,i})\boldsymbol{p}(\nu_{d,i})^{\dagger} + \beta_n \boldsymbol{I}$$

Algorithm 6 Gaussian randomization procedure for radar code design problem (3.5)

Require: $\boldsymbol{M}$, γ, M;
Ensure: a randomized approximate solution $\boldsymbol{c}$ of (3.5);
1: solve the SDP (3.23) finding $\boldsymbol{C}^{\star}$;
2: define $\boldsymbol{d}$, $\boldsymbol{d}^{-}$, $\boldsymbol{D}$, $\boldsymbol{D}^{-}$ according to (3.10)-(3.12);
3: draw random vectors $\boldsymbol{\xi}_k \in \mathbb{C}^N$ from the complex normal distribution $\mathcal{N}_{\mathbb{C}}(\boldsymbol{0}, \boldsymbol{D}^{-}(\boldsymbol{C}^{\star} + (\boldsymbol{I} - \boldsymbol{D}^{-}\boldsymbol{D}))\boldsymbol{D}^{-})$, $k = 1, \ldots, K$;
4: let $c_k(i) = \sqrt{C^{\star}(i,i)}\mu\left(\xi_k(i)\right)$, $i = 1, \ldots, N$, $k = 1, \ldots, K$, where $\mu(x)$ is defined in (3.29);
5: compute

$$t(k) = \min_{\nu_d \in [0,1]} \boldsymbol{p}^{\dagger}(\boldsymbol{M} \odot (\boldsymbol{c}_k \boldsymbol{c}_k^{\dagger})^{*})\boldsymbol{p},$$

by solving SDP (3.26), $k = 1, \ldots, K$;
6: pick the maximal value over $\{t(1), \ldots, t(K)\}$, say $t(1)$, and output $\boldsymbol{c}_1$.

where the number of discrete clutter scatterers $N_c = 10$, their strength $\beta_i = \beta = 10^3$, $\nu_{d,i} = (i-1)/2$, $i = 1, \ldots, 10$, and $\beta_n = 10^{-2}$.

The analysis is conducted in terms of P_d of the GLRT receiver [1] (or equivalently the standard matched filter with pre-whitening, followed by squared modulus operation and threshold comparison) for a prescribed target normalized Doppler frequency $\bar{\nu}_d$ (design parameter for Algorithms 3 and 5), and robustness of the detection capabilities with respect to Doppler shifts for a fixed $\bar{\alpha}$:

$$P_d(\alpha, \bar{\nu}_d) = Q\left(\sqrt{2|\alpha|^2 \boldsymbol{c}^{\dagger}\boldsymbol{R}(\bar{\nu}_d)\boldsymbol{c}}, \sqrt{-2\ln P_{fa}}\right),$$

$$P_{d,rob} = P_d(\bar{\alpha}, \nu_d), \qquad \nu_d = -\frac{1}{2}, \ldots, \frac{1}{2}, \ \alpha = \bar{\alpha},$$

where $Q(\cdot,\cdot)$ is the Marcum Q function [47], assuming a false alarm probability $P_{fa} = 10^{-6}$. Additionally, due to the randomization procedures involved into Algorithms 3-6, the aforementioned performance metrics have been averaged over 500 independent trials. It is important to highlight that, for Algorithms 3 and 5, $P_{d,rob} = P_d(\bar{\alpha}, \nu_d)$ is the detection performance obtained when the code is designed for the given $\bar{\nu}_d$, while the actual target and the receiver steering vectors are matched to the same Doppler ν_d.

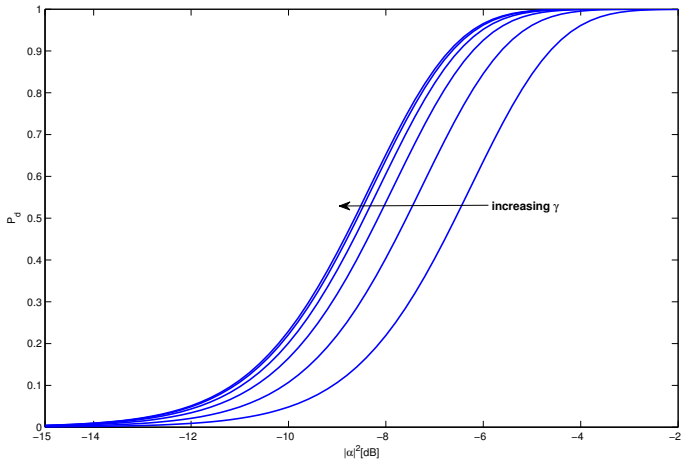

Figure 3.1: P_d versus $|\alpha|^2$ for $P_{fa} = 10^{-6}$, $\bar{\nu}_d = 0.1$, $N = 10$ and $\gamma \in \{1, 1.3, 1.6, 1.9, 2.2, 2.5\}$. Algorithm 3 - PAR constrained code.

In Figure 3.1, the P_d, achieved using the code devised according to Algorithm 3, versus $|\alpha|^2$, in plotted, for $N = 10$, some values of γ (precisely, $\gamma \in \{1, 1.3, 1.6, 1.9, 2.2, 2.5\}$), and $\bar{\nu}_d = 0.1$. The curves highlight that greater and greater PAR parameters lead to better and better P_d values. Such behaviour was indeed expected, because increasing γ (namely, imposing a less restrictive PAR constraint on the devised code) is tantamount to increasing the size of the feasible set of the problem. However, it is also evident that, after a threshold value for γ, depending on the maximum eigenvalue of the covariance matrix $\boldsymbol{M}$, no additional performance improvements can be observed. This phenomenon has a clear analytical interpretation. In fact, for γ greater than the threshold value, the PAR constraint becomes inactive and an optimal solution to (3.2) coincides with an optimal solution to

$$\begin{array}{ll} \max\limits_{\boldsymbol{c}} & \boldsymbol{c}^{\dagger}\boldsymbol{R}\boldsymbol{c} \\ \text{s.t.} & \|\boldsymbol{c}\|^2 = N. \end{array} \tag{3.36}$$

In other words, the optimal waveform is proportional to the eigenvector of $\boldsymbol{R}$ corresponding to the maximum eigenvalue.

The robustness of Algorithms 3 and 4 with respect to target Doppler shifts is studied in Figure 3.2. Therein, the $P_{d,rob}$ versus the actual ν_d is

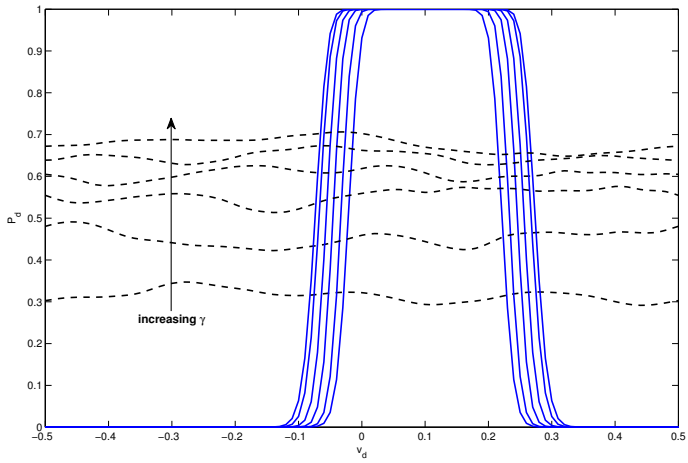

Figure 3.2: P_d versus ν_d for $P_{fa} = 10^{-6}$, $|\bar{\alpha}|^2 = 0$ dB, $\bar{\nu}_d = 0.1$, $K = 10$, $N = 10$, and $\gamma \in \{1, 1.3, 1.6, 1.9, 2.2\}$. Algorithm 1 - PAR constrained code (solid curves). Algorithm 4 - Robust PAR constrained code (dashed curves).

plotted for the PAR constrained (Algorithm 3) and the Robust PAR constrained (Algorithm 4) codes, assuming $N = 10$, $K = 10$, $|\bar{\alpha}|^2 = 0$ dB, and $\gamma = \{1, 1.3, 1.6, 1.9, 2.2\}$. The nominal target Doppler for Algorithm 3 is set to $\bar{\nu}_d = 0.1$, while Algorithm 4 does not require this information. Inspection of the curves shows that Algorithm 3 outperforms Algorithm 4 when the actual target Doppler is sufficiently close to the nominal one. However, in the presence of significant Doppler mismatches, $P_{d,rob}$ of Algorithm 3 exhibits a significant deterioration, approaching values very close to zero. Besides, the transition from the Doppler interval with close to 1 detection rates to the undetectability region is quite sharp. On the contrary, the performance curves of Algorithm 4 show a quite flat shape with respect to Doppler variations, outperforming Algorithm 3 for a wide range of Doppler shifts. This feature is far more evident as γ increases, leading (for the considered values of the parameters) to codes with greater and greater detection capabilities, due to the less restrictive constraints enforced in the optimization problem.

In Figure 3.3, the impact of the number of randomizations K on the detection performance of Algorithm 4 is analyzed. Specifically, the worst case P_d versus $|\alpha|^2$ is plotted for $N = 10$, $\gamma = 1.3$, and several values of K ($K \in \{1, 5, 10, 25\}$). It is easy to notice a performance improvement as K

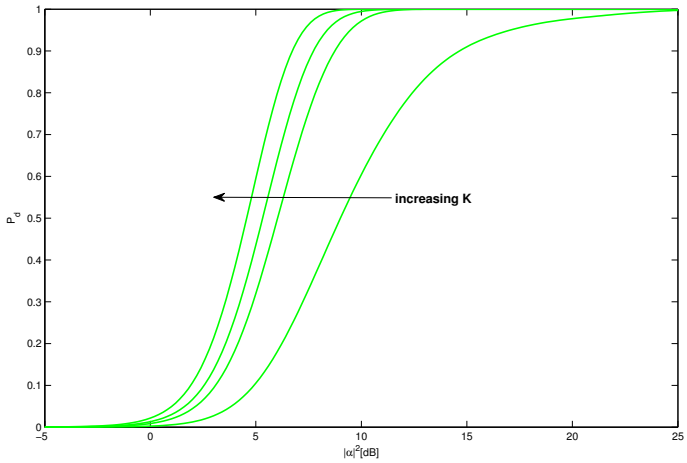

Figure 3.3: Worst case P_d versus $|\alpha|^2$ for $P_{fa} = 10^{-6}$, $\gamma = 1.3$, $N = 10$, and $K \in \{1, 5, 10, 25\}$ randomizations. Algorithm 4 - Robust PAR constrained code.

increases. This behavior can be explained based on Step 6 of Algorithm 4, which selects the code ensuring the best performance among all the K randomization experiments. It is also worth pointing out that, for a quite moderate number of randomizations, $K = 5, 10$, the performance can be considered satisfactory, in the sense that an additional increase in K does not lead to additional sensible improvements in P_d.

In Figures 3.4 and 3.5, the same analysis developed in Figures 3.1 and 3.2 (for Algorithms 3 and 4), with reference to the performance of Algorithms 5 and 6, has been conducted. Precisely, in Figure 3.4, the P_d of the code designed according to Algorithm 5 versus $|\alpha|^2$ is plotted for $N = 10$, $\bar{\nu}_d = 0.1$, some values of the PAR parameter $\gamma \in \{1, 1.3, 1.6, 1.9, 2.2\}$, and $M = 4$ levels for the phase quantization. As in Figure 3.1, increasing γ leads to better and better detection levels. In Figure 3.5, the $P_{d,rob}$s versus the actual ν_d for the PAR constrained Phase quantized (Algorithm 5) and the Robust PAR constrained Phase quantized (Algorithm 6) codes are plotted, assuming $N = 10$, $K = 10$, $|\bar{\alpha}|^2 = 0$ dB, $M = 4$ and $\gamma \in \{1, 1.3, 1.6, 1.9, 2.2\}$. The nominal target Doppler for Algorithm 3 is set to $\bar{\nu}_d = 0.1$, while Algorithm 4 does not require this information. Analyzing the curves, the same considerations as in Figure 3.2 can be repeated.

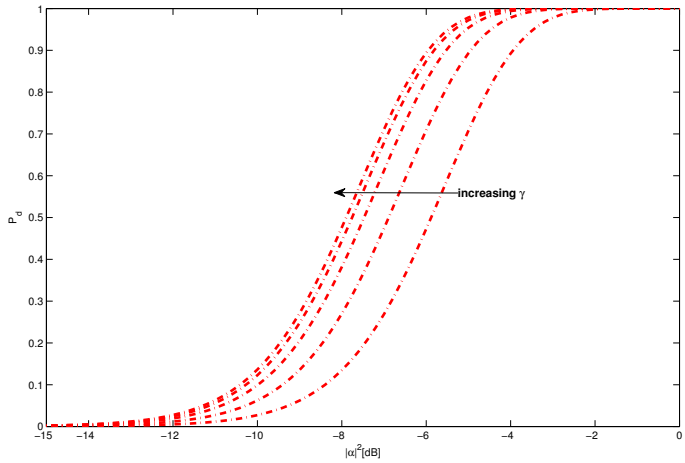

Figure 3.4: P_d versus $|\alpha|^2$ for $P_{fa} = 10^{-6}$, $\bar{\nu}_d = 0.1$, $M = 4$, $N = 10$, and $\gamma \in \{1, 1.3, 1.6, 1.9, 2.2\}$. Algorithm 5 - PAR constrained Phase quantized code.

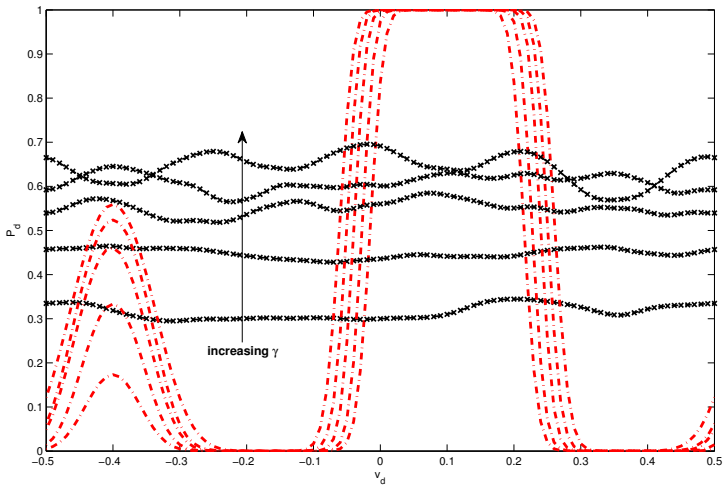

Figure 3.5: P_d versus ν_d for $P_{fa} = 10^{-6}$, $|\bar{\alpha}|^2 = 0$ dB, $\bar{\nu}_d = 0.1$, $K = 10$, $M = 4$, $N = 10$, and $\gamma \in \{1, 1.3, 1.6, 1.9, 2.2\}$. Algorithm 5 - PAR constrained Phase quantized code (dashed-dotted curves). Algorithm 6 - Robust PAR constrained Phase quantized code (dashed x-marked curves).

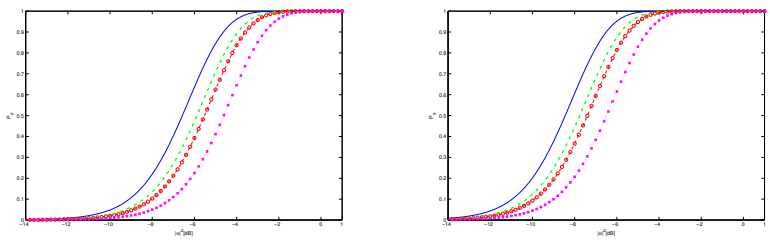

(a) $\gamma = 1$ **(b)** $\gamma = 1.9$

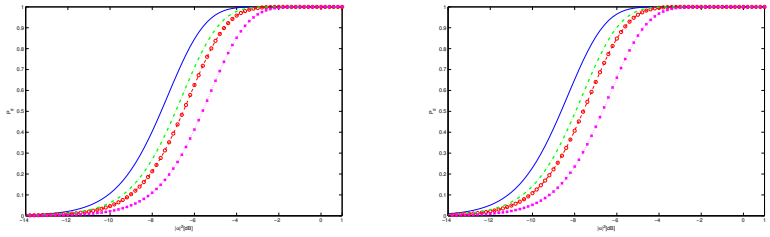

(c) $\gamma = 1.3$ **(d)** $\gamma = 2.5$

Figure 3.6: P_d versus $|\alpha|^2$ for $P_{fa} = 10^{-6}$, $\bar{\nu}_d = 0.1$, $M = 4$, $K = 10$, $N = 10$. Algorithm 3 - PAR constrained code (solid line). Approximation Bound of Algorithm 3 (dashed o-marked curve). Algorithm 5 - PAR constrained Phase quantized code (dashed-dotted line). Approximation Bound of Algorithm 5 (dotted x-marked curve).

The focus is now on Algorithms 3 and 5 and the corresponding approximation bounds. In Figures 3.6, assuming $N = 10$, $\bar{\nu}_d = 0.1$, $K = 10$, and $M = 4$, the performance of Algorithms 3 and 3 are compared with the P_d curves obtained exploiting their approximation bounds defined by (3.17) and (3.33) respectively (i.e. using (3.17) or (3.33) in the first argument of the Marcum Q function in place of the respective quadratic form). Each subplot refers to a specific value of the PAR parameter γ. The plots highlight that Algorithm 3 performs better than Algorithm 5, which quantizes the phase of the transmitted waveform on four different levels. The performance loss of the latter with respect to the former is kept within 1 dB, for $P_d = 0.9$, and is quite acceptable considering also the less demanding hardware implementation of a phase quantized waveform. It is also interesting to observe that the P_d curves obtained using the approximation bound provide a quite good approximation of the actual detection performance, for all the considered values of the parameter γ and for both the considered algorithms. As a matter

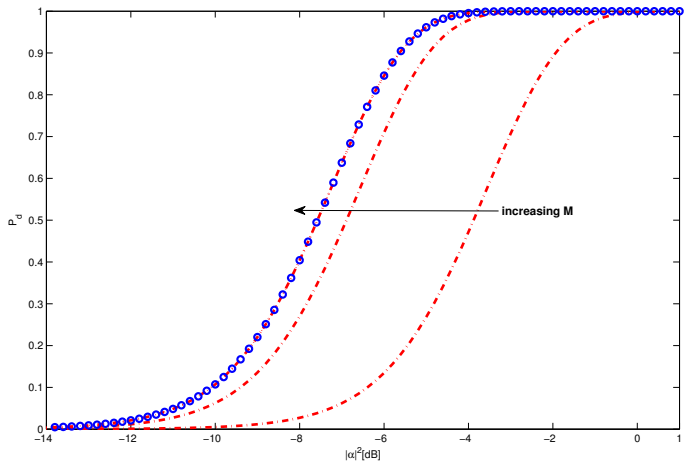

Figure 3.7: P_d versus $|\alpha|^2$ for $P_{fa} = 10^{-6}$, $\bar{\nu}_d = 0.1$, $\gamma = 1.3$, $K = 10$, and $M \in \{2, 4, 8, 16\}$. Algorithm 5 - PAR constrained Phase quantized code (dashed-dotted lines). Algorithm 3 - PAR constrained code (o-marked curve). Notice that the curve of Algorithm 3 overlaps with that referring to Algorithm 5 for $M = 8$ and $M = 16$.

of fact, the lower bound approximation is at most 2 dB far from the true P_d curve.

In the last part of this Section, the effects of the number of quantization levels are investigate. Specifically, in Figure 3.7, the P_d versus $|\alpha|^2$ is plotted for $\bar{\nu}_d = 0.1$, $K = 10$, $\gamma = 1.3$, and several values of M ($M \in \{2, 4, 8, 16\}$). As expected, increasing the number of quantization levels, leads to better and better performances until $M \leq 8$. Then, a saturation effect is experienced and the performance obtained by the phase quantized Algorithm 5 ends up coincident with that provided by Algorithm 5, which, as already pointed out, assumes code elements with phases ranging in a continuous interval.

Finally, before concluding this section, in Table 3.1 the average CPU time required to solve the SDP problem (3.8) (and (3.23)), which is the most computational expensive step of Algorithms 3 and 5 (Algorithms 4 and 6), are provided. All the experiments were conducted on a desktop computer equipped with a Intel Core 2 Quad Q9400 CPU (2.66 GHz). The results highlight that the computational time is quite modest and acceptable for all the considered values of γ. Nevertheless, it is also worth

Table 3.1: Average CPU time in seconds required to solve problems (3.8) and (3.23).

γ	1	1.3	1.6	1.9	2.5
SDP (3.8)	0.083	0.104	0.097	0.085	0.086
SDP (3.23)	0.097	0.143	0.158	0.128	0.112

pointing out that the waveform design must not necessary be performed on-line. It can be also implemented off-line producing a waveform library [30] and then during the operation a waveform from the library is selected for that particular scenario.

3.8 Conclusions

In this Chapter, radar waveform design in the presence of colored Gaussian disturbance under a PAR and an energy constraint has been considered. First of all, the focus has been on the selection of the radar signal optimizing the SNR in correspondence of a given expected target Doppler frequency (Algorithm 3). Then, through a max-min approach, a robust version (with respect to the received Doppler) of the aforementioned technique has been devised (Algorithm 4), optimizing the worst case SNR under the same constraints as in the previous problem. Since Algorithms 3 and 4 do not impose any condition on the waveform phase, introduced their phase quantized versions (Algorithms 5 and 6 respectively) have been introduced, forcing the waveform phase to belong to a finite alphabet. Actually, this is a quite nice feature for a practical implementation of the techniques. All the problems have been formulated in terms of non-convex quadratic optimization programs with a finite (Algorithm 3 and 5) or an infinite (Algorithm 4 and 6) number of quadratic constraints. The NP-hard nature of the problems has been proved and, hence, design techniques have been introduced, relying on Semidefinite Programming (SDP) relaxation and randomization as well as on the theory of trigonometric polynomials, which provide high quality sub-optimal solutions with a polynomial time computational complexity.

At the analysis stage, the performance of the devised algorithms have been evaluated, considering both the detection probability achieved by the Neyman-Pearson detector, as well as the robustness with respect to target Doppler shifts. Additionally, the effects of the possible phase quantization have been studied, showing the trade off existing between

the number of quantization levels and some simplicity in circuitry implementation.

Possible future research tracks might concern the generalization of the waveform design problem so as to account for an additional similarity constraint with a known code sequence. This new approach will pave the way to a joint control of both the PAR and the waveform ambiguity function. Unfortunately, the additional constraint cannot be easily handled and the design of a solution method to the resulting optimization problems is still an open issue.

Chapter 4

Cognitive Design of the Receive Filter and Transmitted Phase Code in Reverberating Environment

4.1 Introduction

The problem of radar waveform diversity and receiver optimization has been addressed over and over during the last few decades, due to the increasing performance requirements in terms of target localization and tracking accuracy, range-Doppler resolution, mainlobe clutter rejection and low sidelobe signal and/or filter design. The growth in terms of technology, such as new computing architectures, high speed and Off The Shelf (OTS) processors, and digital arbitrary waveform generators, had made possible to perform very complex and effective signal processing [51, Ch. 6, 11, 25], leading the path to the recent cognitive paradigm (see [52], [53], [54], and [55]), which states indeed a new success frontier for radar signal processing. Its main innovation concerns the smart use of some a-priori information and previous radar experiences about the operating environment (as for instance location of electromagnetic interferences, reflectivity characteristic of the environment, weather conditions and discrete clutter).
Two principal research modalities, exploiting the waveform diversity to improve the radar performances, have emerged. The first is focused on

the signal-independent interference and well models, but is not limited to, radar environments where the main contribution to the disturbance is represented by thermal noise, and/or intentional interference (Jammers), and/or unintentional emissions by information sources, and/or terrain scattering due to signals from other radar platforms (hot clutter), [7, 8, 56, 57]. The latter assumes a reverberant environment, namely a signal-dependent clutter scenario, with disturbances produced by radar reflections from terrain or non-threatening targets in the surveillance volume. For a point-like target embedded in signal-dependent clutter, optimization of the transmit signal and receive filter to maximize the Signal to Interference plus Noise Ratio (SINR) has been accomplished, assuming both an energy constraint [58] and a dynamic range constraints [59], on the transmitted waveform. Implementation errors [59], amplitude and phase modulation limitations [60], and quantization error effects [61], have also been considered, modifying the procedure of [58]. In [62], a cognitive approach for the design of the transmit signal (amplitude-phase modulated pulse train) and receive filter, accounting for a similarity between the transmitted sequence and a prescribed radar code, has been devised. In [63], innovative algorithms for optimizing the mean-square error of a target backscattering estimate in the presence of signal-dependent clutter, have been derived. Either a constant-modulus or a low Peak to Average power Ratio (PAR) constraint has been enforced on the transmitted waveform. For a zero-Doppler Gaussian point target in the presence of signal-dependent Gaussian clutter, modeled as the output of a stochastic Linear-Time-Invariant (LTI) filter with a stationary Gaussian shaped impulse response, analytic approaches to optimizing the energy-constrained transmit signal spectrum while maximizing detection performance have been introduced [22].

In this Chapter, the joint optimization of the transmit signal and receive filter for a radar system which operates in a highly reverberant environment is addressed, focusing on both continuous and finite alphabet phase codes. Specifically, the assumption is that the radar system can predict the actual scattering environment, using a dynamic environmental database, including a geographical information system, meteorological data, site specific clutter maps [64], and some electromagnetic reflectivity and spectral clutter models. Thus, exploiting the aforementioned information and considering as figure of merit the Signal-to-Interference plus Noise Ratio (SINR), a suitable radar phase code and receive filter

are devised, under a similarity constraint between the sought waveform and a reference code [7], [8]. The devised constrained optimization procedure sequentially improves the SINR. Each iteration requires the solution of both a convex problem and an NP-hard optimization problem. As to the NP-hard quadratic fractional optimization problem, the relaxation and randomization approach [8] is invoked in order to find a good quality solution. The resulting computational complexity is linear with the number of iterations and trials in the randomized procedure, and polynomial with the receive filter length. The performance of the new algorithm is analyzed in a homogeneous clutter environment, showing that interesting SINR improvements can be obtained jointly optimizing the transmitter and the receiver.

The Chapter is organized as follows. In Section 4.2, we describe the system model is described, which slightly differs from the one in eq.s 1-2. In Section 4.3, the constrained optimization problems for the design of (either continuous or finite alphabet) radar phase codes and the receive filters is formulated. Additionally, two sequential optimization procedures are introduced, so as to obtain high quality solutions to these problems. In Section 4.4, the performance of the proposed algorithms are assessed. Finally, in Section 4.5, conclusions are drawn out and possible future research tracks are discussed.

4.2 System Model

The model herein considered is slightly different from the one presented in eq.s 1-2, since the clutter disturbance and the thermal noise terms will be explicitly separated. The focus is still on a monostatic radar system that transmits a coherent burst of N pulses. The waveform at the receiver end is down-converted to baseband, undergoes a pulse matched filtering operation, and then is sampled. The N-dimensional column vector $\boldsymbol{v} = [v(1), v(2), \ldots, v(N)] \in \mathbb{C}^N$ of the observations, from the range-azimuth cell under test, can be expressed as

$$\boldsymbol{v} = \alpha_T \boldsymbol{c} \odot \boldsymbol{p}(\nu_{d_T}) + \boldsymbol{i} + \boldsymbol{n}, \tag{4.1}$$

with $\boldsymbol{c} = [c(1), c(2), \ldots, c(N)]^T \in \mathbb{C}^N$ the radar code, α_T a complex parameter accounting for the target response, $\boldsymbol{p}(\nu_{d_T}) = [1, e^{j2\pi\nu_{d_T}}, \ldots, e^{j2\pi(N-1)\nu_{d_T}}]^T$, ν_{d_T} the normalized target Doppler frequency, $\boldsymbol{i} \in \mathbb{C}^N$ the vector of clutter samples, and $\boldsymbol{n} \in \mathbb{C}^N$ the vector of noise samples.

The clutter vector $\boldsymbol{i}$ is modeled as the superposition of returns from different uncorrelated scatterers, each from the $(r,i)-$th range-azimuth bin, namely:

$$\boldsymbol{i} = \sum_{r=0}^{N_c-1} \sum_{i=0}^{L-1} \alpha_{(r,i)} \boldsymbol{J}_r \left(\boldsymbol{c} \odot \boldsymbol{p}(\nu_{d_{(r,i)}}) \right), \tag{4.2}$$

where $N_c \leq N$ is the number of range rings[1] that interfere with the range-azimuth bin of interest $(0,0)$, L is the number of discrete azimuth sectors, $\alpha_{(r,i)}$ and $\nu_{d_{(r,i)}}$ are, respectively, the echo and the normalized Doppler frequency of the scatterer in the range-azimuth bin (r,i); furthermore, $\forall r \in \{0,\ldots,N-1\}$

$$\boldsymbol{J}_r(l,m) = \begin{cases} 1 & \text{if} \quad l-m=r \\ 0 & \text{if} \quad l-m \neq r \end{cases} \quad (l,m) \in \{1,\ldots,N\}^2,$$

where $\boldsymbol{J}_r = \boldsymbol{J}_{-r}^T$ denotes the shift matrix. As to the statistical characterization of the noise vector $\boldsymbol{n}$, it is still assumed that it is zero-mean and white, i.e.:

$$\mathbb{E}[\boldsymbol{n}] = 0, \qquad \mathbb{E}\left[\boldsymbol{n}\boldsymbol{n}^\dagger\right] = \sigma_n^2 \boldsymbol{I}.$$

Now, consider the statistical characterization of the clutter vector $\boldsymbol{i}$. As previously stated, the scatterers are assumed to be uncorrelated; moreover, for each scatterer, denote by $\sigma_{(r,i)}^2 = \mathbb{E}\left[|\alpha_{(r,i)}|^2\right]$, assume that the expected value of its complex amplitude is zero, i.e. $\mathbb{E}\left[\alpha_{(r,i)}\right] = 0$, and that its normalized Doppler frequency, statistically independent of $\alpha_{(r,i)}$, is uniformly distributed around a mean Doppler frequency $\bar{\nu}_{d_{(r,i)}}$, i.e. $\nu_{d_{(r,i)}} \sim \mathcal{U}\left(\bar{\nu}_{d_{(r,i)}} - \frac{\epsilon_{(r,i)}}{2}, \bar{\nu}_{d_{(r,i)}} + \frac{\epsilon_{(r,i)}}{2}\right)$. As a consequence, we have: $\mathbb{E}[\boldsymbol{i}] = 0$ and

$$\boldsymbol{\Sigma}_{\boldsymbol{i}}(\boldsymbol{c}) = \mathbb{E}\left[\boldsymbol{i}\boldsymbol{i}^\dagger\right] = \sum_{r=0}^{N_c-1} \sum_{i=0}^{L-1} \sigma_{(r,i)}^2 \boldsymbol{J}_r \boldsymbol{\Gamma}(\boldsymbol{c},(r,i)) \boldsymbol{J}_r^T, \tag{4.3}$$

where

$$\boldsymbol{\Gamma}(\boldsymbol{c},(r,i)) = \mathbf{Diag}(\boldsymbol{c}) \boldsymbol{\Phi}_{\epsilon_{(r,i)}}^{\bar{\nu}_{d_{(r,i)}}} \mathbf{Diag}(\boldsymbol{c})^\dagger,$$

and, $\forall\ (l,m) \in \{1,\ldots,N\}^2$,

$$\boldsymbol{\Phi}_{\epsilon}^{\bar{\nu}_d}(l,m) = e^{(j2\pi\bar{\nu}_d(l-m))} \frac{\sin[\pi\epsilon(l-m)]}{[\pi\epsilon(l-m)]}.$$

[1] Notice that model (4.2) refers to the general case of range ambiguous clutter. It reduces to the range unambiguous scenario letting $N_c = 1$.

A relevant scenario, which can be described and modeled according to (4.3), is now described (see also [62]). Let assume that, for any (r,i) range-azimuth bin, the Radar Cross Section (RCS) $\sigma_0^{(r,i)}$ of the scatterer is predicted through the interaction between a digital terrain map, such as the National Land Cover Data (NLCD) and RCS clutter models[2]. Whenever $\sigma_0^{(r,i)}$ has been estimated, according to the previous information, we can evaluate $\sigma^2_{(r,i)}$ as

$$\sigma^2_{(r,i)} = \sigma_0^{(r,i)} K_r |G(\theta_i)|^2,$$

where K_r is a constant accounting for the channel propagation effects, such as the free space two-way path loss and additional system losses (radar equation), θ_i is the azimuth angle of the bin (r,i), and $G(\theta)$ is the one-way antenna gain for the angle θ.

4.3 Problem Formulation and Design Issues

The present Section deals with the design of a suitable radar code and receive filter maximizing the SINR, under some constraints on the shape of the code. Specifically, assuming that the vector of observations $\boldsymbol{v}$ is filtered through $\boldsymbol{w}$, the SINR at the output of the filter[3] can be written as:

$$\text{SINR} = \frac{|\alpha_T|^2 \left| \boldsymbol{w}^\dagger \left(\boldsymbol{c} \odot \boldsymbol{p}(\nu_{d_T}) \right) \right|^2}{\boldsymbol{w}^\dagger \boldsymbol{\Sigma_i}(\boldsymbol{c}) \boldsymbol{w} + \sigma_n^2 \|\boldsymbol{w}\|^2}, \tag{4.4}$$

where $|\alpha_T|^2 \left| \boldsymbol{w}^\dagger (\boldsymbol{c} \odot \boldsymbol{p}(\nu_{d_T})) \right|^2$ is the useful energy at the output of the filter, while $\sigma_n^2 \|\boldsymbol{w}\|^2$ and $\boldsymbol{w}^\dagger \boldsymbol{\Sigma_i}(\boldsymbol{c}) \boldsymbol{w}$ represent, respectively, the noise and the clutter energy at the filter output. Notice that the clutter energy $\boldsymbol{w}^\dagger \boldsymbol{\Sigma_i}(\boldsymbol{c}) \boldsymbol{w}$ functionally depends both on the receive processing $\boldsymbol{w}$ and the transmitted waveform through $\boldsymbol{\Sigma_i}(\boldsymbol{c})$ (namely it is a quartic polynomial in variables $\boldsymbol{w}$ and $\boldsymbol{c}$). This observation represents the main difference between a signal-dependent and a signal-independent environment where the output clutter energy is only a function of $\boldsymbol{w}$, being a homogeneous quadratic form in that variable.

To develop the proposed SINR optimization algorithm, the following technical Lemma 4.3.1 (whose proof is given in [62]) has been used, so as to provide an alternative expression to the SINR:

[2] Otherwise, it could be estimated exploiting feedbacks from previous scans.

[3] Obviously, the implicit assumption is that $\boldsymbol{w} \neq \boldsymbol{0}$.

Lemma 4.3.1. *An equivalent expression of the SINR is given by:*

$$SINR = \frac{|\alpha_T|^2 \left| \boldsymbol{c}^T \left(\boldsymbol{w}^* \odot \boldsymbol{p}(\nu_{d_T}) \right) \right|^2}{\boldsymbol{c}^T \boldsymbol{\Theta_i} \left(\boldsymbol{w} \right) \boldsymbol{c}^* + \sigma_n^2 \|\boldsymbol{w}\|^2} \tag{4.5}$$

where:

$$\boldsymbol{\Theta_i} \left(\boldsymbol{w} \right) = \sum_{r=1}^{N_c-1} \sum_{i=0}^{L-1} \sigma_{(r,i)}^2 \mathbf{Diag}(\boldsymbol{J}_{-r} \boldsymbol{w}^*) \boldsymbol{\Phi}_{\epsilon_{(r,i)}}^{\bar{\nu}_{d_{(r,i)}}} \mathbf{Diag}(\boldsymbol{J}_{-r} \boldsymbol{w}) + \sum_{i=0}^{L-1} \sigma_{(0,i)}^2 \mathbf{Diag}(\boldsymbol{w}^*) \boldsymbol{\Phi}_{\epsilon_{(0,i)}}^{\bar{\nu}_{d_{(0,i)}}} \mathbf{Diag}(\boldsymbol{w}) \, .$$

As to the shape of the code, the focus is on both continuous alphabet phase codes, i.e. $|c(k)| = 1$, $k = 1, \ldots, N$, and finite alphabet phase code, namely $c(k) \in \{1, e^{j2\pi/M}, \ldots, e^{j2\pi(M-1)/M}\}$, $k = 1, \ldots, N$. Furthermore, a similarity constraint [7, 8] is enforced, namely

$$\|\boldsymbol{c} - \boldsymbol{c}_0\|_\infty \leq \delta \, , \tag{4.6}$$

where the parameter $\delta \geq 0$ governs the size of the similarity region and $\boldsymbol{c}_0$ is a prefixed phase code. By doing so, it is required the solution to be similar to a known code $\boldsymbol{c}_0$, which shares some nice properties such as reasonable range-Doppler resolution and peak sidelobe level. In other words, imposing (4.6) is tantamount to indirectly controlling the ambiguity function of the considered coded pulse train: the smaller δ the higher the degree of similarity between the ambiguity functions of the devised radar code and $\boldsymbol{c}_0$.

Summarizing, the joint design of the radar code and receive filter can be formulated in terms of the following constrained optimization problems:

- $$\mathcal{P}^c \begin{cases} \max\limits_{\boldsymbol{c},\boldsymbol{w}} & \dfrac{|\alpha_T|^2 \left| \boldsymbol{w}^\dagger \left(\boldsymbol{c} \odot \boldsymbol{p}(\nu_{d_T}) \right) \right|^2}{\boldsymbol{w}^\dagger \boldsymbol{\Sigma_i} \left(\boldsymbol{c} \right) \boldsymbol{w} + \sigma_n^2 \|\boldsymbol{w}\|^2} \\ \text{s.t.} & |c(k)| = 1, \; k = 1, \ldots, N \\ & \|\boldsymbol{c} - \boldsymbol{c}_0\|_\infty \leq \delta \end{cases} \tag{4.7}$$

  for a continuous alphabet phase code;

- $$\mathcal{P}^d \begin{cases} \max\limits_{\boldsymbol{c},\boldsymbol{w}} & \dfrac{|\alpha_T|^2 \left|\boldsymbol{w}^\dagger \left(\boldsymbol{c} \odot \boldsymbol{p}(\nu_{d_T})\right)\right|^2}{\boldsymbol{w}^\dagger \boldsymbol{\Sigma_i}\left(\boldsymbol{c}\right)\boldsymbol{w} + \sigma_n^2 \|\boldsymbol{w}\|^2} \\ \text{s.t.} & c(k) \in \{1, e^{j2\pi/M}, \ldots, e^{j2\pi(M-1)/M}\},\ k = 1, \ldots, N, \\ & \|\boldsymbol{c} - \boldsymbol{c}_0\|_\infty \leq \delta \end{cases} \tag{4.8}$$

  for a discrete alphabet phase code.

Problems $\mathcal{P}^c$ and $\mathcal{P}^d$ are non-convex optimization problems, since the objective function is a non-convex function and the constraints $|c(k)|^2 = 1$, $k = 1, \ldots, N$, and $c(k) \in \left\{1, e^{j2\pi/M}, \ldots, \ e^{j2\pi(M-1)/M}\right\}$, $k = 1, \ldots, N$, define non-convex sets. The technique adopted to find a good quality solution for $\mathcal{P}^c$ and $\mathcal{P}^d$ is based on a sequential optimization procedure. The idea is to iteratively improve the SINR. Specifically, given $\boldsymbol{w}^{(n-1)}$, it will be searched an admissible radar code $\boldsymbol{c}^{(n)}$ at step n improving the SINR corresponding to the receive filter $\boldsymbol{w}^{(n-1)}$ and the transmitted signal $\boldsymbol{c}^{(n-1)}$. Whenever $\boldsymbol{c}^{(n)}$ is found, the signal will be fixed and a new search, now for the adaptive filter $\boldsymbol{w}^{(n)}$ improving the SINR corresponding to the radar code $\boldsymbol{c}^{(n)}$ and the receive filter $\boldsymbol{w}^{(n-1)}$. will start, and so on. Otherwise stated, $\boldsymbol{w}^{(n)}$ and $\boldsymbol{c}^{(n)}$ are used as starting point at step $n+1$. To trigger the procedure, the optimal receive filter $\boldsymbol{w}^{(0)}$ to an admissible code $\boldsymbol{c}^{(0)}$ is considered.
From an analytical point of view, $\boldsymbol{w}^{(n)}$ is an optimal solution to the optimization problem:

$$\mathcal{P}_{\boldsymbol{w}^{(n)}} \begin{cases} \max\limits_{\boldsymbol{w}} & \dfrac{|\alpha_T|^2 \left|\boldsymbol{w}^\dagger \left(\boldsymbol{c}^{(n)} \odot \boldsymbol{p}(\nu_{d_T})\right)\right|^2}{\boldsymbol{w}^\dagger \boldsymbol{\Sigma_i}\left(\boldsymbol{c}^{(n)}\right)\boldsymbol{w} + \sigma_n^2 \|\boldsymbol{w}\|^2} \end{cases} . \tag{4.9}$$

As shown in [62], $\mathcal{P}_{\boldsymbol{w}^{(n)}}$ is solvable and a closed form optimal solution $\boldsymbol{w}^{(n)}$ can be found for any feasible $\boldsymbol{c}^{(n)}$. Specifically, an optimal solution to $\mathcal{P}_{\boldsymbol{w}^{(n)}}$ is given by:

$$\boldsymbol{w}^{(n)} = \frac{\left(\boldsymbol{\Sigma_i}\left(\boldsymbol{c}^{(n)}\right) + \sigma_n^2 \boldsymbol{I}\right)^{-1} \left(\boldsymbol{c}^{(n)} \odot \boldsymbol{p}(\nu_{d_T})\right)}{\left\| \left(\boldsymbol{\Sigma_i}\left(\boldsymbol{c}^{(n)}\right) + \sigma_n^2 \boldsymbol{I}\right)^{-1/2} \left(\boldsymbol{c}^{(n)} \odot \boldsymbol{p}(\nu_{d_T})\right) \right\|^2}, \tag{4.10}$$

from which it is evident the influence of $\boldsymbol{c}^{(n)}$ and the steering vector

$\boldsymbol{p}(\nu_{d_T})$ on $\boldsymbol{w}^{(n)}$. Furthermore, $\boldsymbol{c}^{(n)}$ is given by:

$$\boldsymbol{c}^{(n)} = \underset{\boldsymbol{c}\in\left\{\boldsymbol{c}^{(n-1)},\boldsymbol{c}^{(\star)}\right\}}{\arg\max} \frac{|\alpha_T|^2\left|\boldsymbol{w}^{(n-1)^\dagger}\left(\boldsymbol{c}\odot\boldsymbol{p}(\nu_{d_T})\right)\right|^2}{\boldsymbol{w}^{(n-1)^\dagger}\boldsymbol{\Sigma_i}\left(\boldsymbol{c}\right)\boldsymbol{w}^{(n-1)}+\sigma_n^2\|\boldsymbol{w}^{(n-1)}\|^2}$$

where $\boldsymbol{c}^{(\star)}$ is a good solution of problem $\mathcal{P}_{\boldsymbol{c}}^{c(n)}$ if the focus is on $\mathcal{P}^c$, and a good solution of problem $\mathcal{P}_{\boldsymbol{c}}^{d(n)}$ if the focus is on $\mathcal{P}^d$, respectively given by:

- $$\mathcal{P}_{\boldsymbol{c}}^{c(n)} \begin{cases} \max\limits_{\boldsymbol{c}} & \dfrac{|\alpha_T|^2\left|\boldsymbol{w}^{(n-1)^\dagger}\left(\boldsymbol{c}\odot\boldsymbol{p}(\nu_{d_T})\right)\right|^2}{\boldsymbol{w}^{(n-1)^\dagger}\boldsymbol{\Sigma_i}\left(\boldsymbol{c}\right)\boldsymbol{w}^{(n-1)}+\sigma_n^2\|\boldsymbol{w}^{(n-1)}\|^2} \\ \text{s.t.} & |c(k)|=1,\ k=1,\ldots,N, \\ & \|\boldsymbol{c}-\boldsymbol{c}_0\|_\infty \leq \delta \end{cases} ; \quad (4.11)$$

- $$\mathcal{P}_{\boldsymbol{c}}^{d(n)} \begin{cases} \max\limits_{\boldsymbol{c}} & \dfrac{|\alpha_T|^2\left|\boldsymbol{w}^{(n-1)^\dagger}\left(\boldsymbol{c}\odot\boldsymbol{p}(\nu_{d_T})\right)\right|^2}{\boldsymbol{w}^{(n-1)^\dagger}\boldsymbol{\Sigma_i}\left(\boldsymbol{c}\right)\boldsymbol{w}^{(n-1)}+\sigma_n^2\|\boldsymbol{w}^{(n-1)}\|^2} \\ \text{s.t.} & c(k)\in\{1,e^{j2\pi/M},\ldots,e^{j2\pi(M-1)/M}\}, \\ & k=1,\ldots,N, \\ & \|\boldsymbol{c}-\boldsymbol{c}_0\|_\infty \leq \delta \end{cases} . \quad (4.12)$$

Making use of [62, Proposition 2.1], the following Proposition 4.3.2 holds true:

Proposition 4.3.2. *Let $\left\{\left(\boldsymbol{c}^{(n)},\boldsymbol{w}^{(n)}\right)\right\}$ be a sequence of points obtained through the proposed sequential optimization procedure, either for the continuous or the discrete alphabet cases; let $SINR^{(n)}$ be the SINR value corresponding to the point $\left(\boldsymbol{c}^{(n)},\boldsymbol{w}^{(n)}\right)$ at the $n-th$ iteration. Then:*

- *the sequence $SINR^{(n)}$ is a monotonic increasing sequence;*
- *the sequence $SINR^{(n)}$ converges to a finite value $SINR^\star$;*
- *starting from the sequence $\left\{\left(\boldsymbol{c}^{(n)},\boldsymbol{w}^{(n)}\right)\right\}$, it is possible to construct another sequence $\left\{\left(\tilde{\boldsymbol{c}}^{(n')},\tilde{\boldsymbol{w}}^{(n')}\right)\right\}$, that converges to a feasible point $(\tilde{\boldsymbol{c}}^\star,\tilde{\boldsymbol{w}}^\star)$ of problems $\mathcal{P}^c$ or $\mathcal{P}^d$, such that the SINR evaluated in $(\tilde{\boldsymbol{c}}^\star,\tilde{\boldsymbol{w}}^\star)$ is equal to $SINR^\star$.*

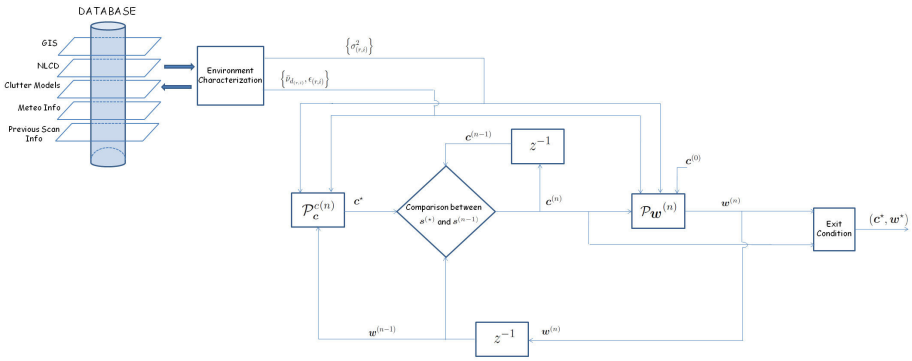

Figure 4.1: Block diagram of the proposed transmit-receive optimization procedure, for both the continuous phase code case and the discrete phase code case.

Observe that, from a practical point of view, the proposed optimization procedure requires a condition to stop the iterations; to this end, an iteration gain constraint can be forced, namely $|\mathrm{SINR}^{(n)} - \mathrm{SINR}^{(n-1)}| \leq \zeta$, where ζ is the desired gain. In Figure 4.1 a pictorial representation of the proposed joint optimization procedure of the receive filter and the transmit phase code is given (in particular, the symbol $\mathcal{P}_{\boldsymbol{c}}^{(n)}$ refers to either problem $\mathcal{P}_{\boldsymbol{c}}^{c(n)}$ for the continuous phase code case or to problem $\mathcal{P}_{\boldsymbol{c}}^{d(n)}$ for the discrete phase code case). The next Subsections will be devoted to the study of the optimization problems $\mathcal{P}_{\boldsymbol{c}}^{c(n)}$ and $\mathcal{P}_{\boldsymbol{c}}^{d(n)}$ required for implementing the proposed sequential optimization procedures.

4.3.1 Radar Code Optimization: Solution of the Problem 4.11

An algorithm to find in polynomial time a good quality solution to the NP-hard problem $\mathcal{P}_{\boldsymbol{c}}^{c(n)}$ is now described. Using Lemma 4.3.1, $\mathcal{P}_{\boldsymbol{c}}^{c(n)}$ can be equivalently recast as the following problem $\mathcal{P}_1$:

$$\mathcal{P}_1 \begin{cases} \max\limits_{\boldsymbol{c}} & \dfrac{\left|\boldsymbol{c}^T\left(\boldsymbol{w}^{(n-1)*} \odot \boldsymbol{p}(\nu_{d_T})\right)\right|^2}{\boldsymbol{c}^T\boldsymbol{\Theta}_{\boldsymbol{i}}\left(\boldsymbol{w}^{(n-1)}\right)\boldsymbol{c}^* + \sigma_n^2\|\boldsymbol{w}^{(n-1)}\|^2} \\ \text{s.t.} & |c(k)| = 1,\ k = 1,\ldots,N \\ & \|\boldsymbol{c} - \boldsymbol{c}_0\|_\infty \leq \delta \end{cases}, \tag{4.13}$$

This is a non-convex fractional quadratic problem. Notice that, since $|c(k)| = |c_0(k)| = 1$, $k = 1, \ldots, N$, the similarity constraint

$$\max_{k\in[1,\ldots,N]} |c(k) - c_0(k)| \leq \delta$$

can be equivalently written as $\Re\left[c^*(k)c_0(k)\right] \geq 1-\delta^2/2$ for $k = 1, \ldots, N$, which is tantamount to imposing $\arg\left(c(k)\right) \in [\gamma_k, \gamma_k + \delta_c]$, where $\gamma_k = \arg\left(c_0(k)\right) - \arccos(1 - \delta^2/2)$ and $\delta_c = 2\arccos\left(1 - \delta^2/2\right)$ for $k = 1, \ldots, N$, [8]. Thus, problem (4.13) is equivalent to:

$$\mathcal{P}_1' \begin{cases} \max\limits_{\boldsymbol{c}} & \dfrac{\left|\boldsymbol{c}^T\left(\boldsymbol{w}^{(n-1)^*} \odot \boldsymbol{p}(\nu_{d_T})\right)\right|^2}{\boldsymbol{c}^T\boldsymbol{\Theta_i}\left(\boldsymbol{w}^{(n-1)}\right)\boldsymbol{c}^* + \sigma_n^2\|\boldsymbol{w}^{(n-1)}\|^2} \\ \text{s.t.} & |c(k)| = 1,\ k = 1, \ldots, N \\ & \arg\left(s(k)\right) \in [\gamma_k, \gamma_k + \delta_c],\ k = 1, \ldots, N \end{cases} . \tag{4.14}$$

Observe that problem $\mathcal{P}_1'$, even in the simpler formulation corresponding to $\epsilon = 2$, is generally NP-hard, consequently one cannot find polynomial time algorithms for computing its optimal solutions. Hence, the focus is on approximation techniques, thus a relaxation and randomization based algorithm is proposed, which provides a randomized feasible solution to (4.14). To this end, assume that

$$\boldsymbol{S} = \left(\boldsymbol{w}^{(n-1)} \odot \boldsymbol{p}(\nu_{d_T})^*\right)\left(\boldsymbol{w}^{(n-1)} \odot \boldsymbol{p}(\nu_{d_T})^*\right)^\dagger, \tag{4.15}$$

and

$$\boldsymbol{M} = \boldsymbol{\Theta_i}\left(\boldsymbol{w}^{(n-1)}\right)^* + \frac{\sigma_n^2}{N}\|\boldsymbol{w}^{(n-1)}\|^2\boldsymbol{I}. \tag{4.16}$$

The relaxed version of problem $\mathcal{P}_1'$, obtained neglecting the similarity constraint, namely the conditions $\arg\left(s(k)\right) \in [\gamma_k, \gamma_k + \delta_c]$, $k = 1, \ldots, N$, is given by the following fractional quadratic problem $\mathcal{P}_1''$;

$$\mathcal{P}_1'' \begin{cases} \max\limits_{\boldsymbol{c}} & \dfrac{\left|\boldsymbol{c}^T\left(\boldsymbol{w}^{(n-1)^*} \odot \boldsymbol{p}(\nu_{d_T})\right)\right|^2}{\boldsymbol{c}^T\boldsymbol{\Theta_i}\left(\boldsymbol{w}^{(n-1)}\right)\boldsymbol{c}^* + \sigma_n^2\|\boldsymbol{w}^{(n-1)}\|^2} \\ \text{s.t.} & |c(k)| = 1,\ k = 1, \ldots, N \end{cases} , \tag{4.17}$$

which is equivalent to

$$\mathcal{P}_1''' \begin{cases} \max\limits_{\boldsymbol{X},\boldsymbol{c}} & \dfrac{\text{tr}\left(\boldsymbol{S}\boldsymbol{X}\right)}{\text{tr}\left(\boldsymbol{M}\boldsymbol{X}\right)} \\ \text{s.t.} & X(k,k) = 1,\ k = 1, \ldots, N \\ & \boldsymbol{X} = \boldsymbol{c}\boldsymbol{c}^\dagger,\ \ \boldsymbol{c} \in \mathbb{C}^N \end{cases} . \tag{4.18}$$

The SDP relaxation [26] of problem $\mathcal{P}_1'''$, obtained dropping the rank-one constraint $\boldsymbol{X} = \boldsymbol{c}\boldsymbol{c}^\dagger$, is:

$$\begin{cases} \max\limits_{\boldsymbol{X}} & \dfrac{\text{tr}\,(\boldsymbol{S}\boldsymbol{X})}{\text{tr}\,(\boldsymbol{M}\boldsymbol{X})} \\ \text{s.t.} & X(k,k) = 1,\ k = 1, \ldots, N \\ & \boldsymbol{X} \succeq \boldsymbol{0} \end{cases} . \tag{4.19}$$

In order to solve the fractional problem (4.19), following the guidelines of [65], it suffices to solve the equivalent SDP problem:

$$(\text{SDP}) \quad \begin{cases} \max\limits_{\boldsymbol{X},\, u} & \text{tr}\,(\boldsymbol{S}\boldsymbol{X}) \\ \text{s.t.} & \text{tr}\,(\boldsymbol{M}\boldsymbol{X}) = 1 \\ & X(k,k) = u \\ & \boldsymbol{X} \succeq \boldsymbol{0},\ u > 0 \end{cases} . \tag{4.20}$$

Indeed, both problems (4.19) and (4.20) are solvable and have equal optimal value; in fact, if $\left(\hat{\boldsymbol{X}}, \hat{u}\right)$ is an optimal solution of (4.20), then it can be shown straightforward that $\hat{\boldsymbol{X}}/\hat{u}$ is an optimal solution of (4.19); also, if $\hat{\boldsymbol{X}}$ solves (4.19), then $\left(\hat{\boldsymbol{X}}/\text{tr}\,(\boldsymbol{M}\hat{\boldsymbol{X}}), 1/\text{tr}\,(\boldsymbol{M}\hat{\boldsymbol{X}})\right)$ solves (4.20). Thus, following the same approach as in [8, pp. 8-9], a randomized feasible solution $\boldsymbol{c}^{(\star)}$ to problem $\mathcal{P}_{\boldsymbol{c}}^{c(n)}$ can be computed using Algorithm 7, where H indicates the number of randomizations involved in the procedure.

Notice that the H randomizations involved into steps 3-6 are meant to improve the approximation quality; in fact the randomized feasible solution yielding the largest objective value will be chosen as the approximate solution. As to the computational complexity connected with the implementation of the algorithm, the solution of the SDP relaxation requires $O(N^{3.5})$ floating point operations (flops)[4] whereas each randomization involves $O(N^2)$ flops [35]. It follows that, for a modest number of randomizations, the most relevant contribution to the computational complexity is connected with the SDP solution.

4.3.2 Radar Code optimization: Solution of the Problem 4.12

At the current state of the art, most radar systems use phase coded waveforms, where the phases are taken from a finite and regularly spaced

[4]Herein, the Landau notation $O(n)$ is used; hence, an algorithm is $O(n)$ if its implementation requires a number of flops proportional to n [66].

Algorithm 7 Radar Phase Code Optimization

Require: $\boldsymbol{M}, \boldsymbol{S}, H, \{\gamma_i\}, \delta_c$.
Ensure: A randomized approximate solution $\boldsymbol{c}^{(\star)}$ to $\mathcal{P}_{\boldsymbol{c}}^{c(n)}$;

1: Let $(\boldsymbol{X}^\star, u^\star)$ be an optimal solution to problem (4.20).
2: Denote by $\hat{\boldsymbol{X}} = \boldsymbol{X}^\star / u^\star$.
3: Generate random vectors $(\boldsymbol{\xi})_h \in \mathbb{C}^N$, $h = 1, \ldots, H$, from the complex normal distribution $\mathcal{N}_{\mathbb{C}}(0, \boldsymbol{Y})$ where $\boldsymbol{Y} = \hat{\boldsymbol{X}} \odot \boldsymbol{y}_c \boldsymbol{y}_c^\dagger$, where $\boldsymbol{y}_c = [e^{-j\gamma_1}, \ldots, e^{-j\gamma_N}]^T$.
4: Let $(s(k))_h = y_c^*(k)\sigma((\xi(k))_h)$, $k = 1, \ldots, N$, $h = 1, \ldots, H$, where $\sigma(x) = e^{j\frac{\arg(x)}{2\pi}\delta_c}, x \in \mathbb{C}$.
5: Compute

$$t(h) = \frac{\boldsymbol{c}_h^\dagger \boldsymbol{S} \boldsymbol{c}_h}{\boldsymbol{c}_h^\dagger \boldsymbol{M} \boldsymbol{c}_h}, \quad h = 1 \ldots, H.$$

6: Pick the maximal value over $\{t(1), \ldots, t(H)\}$, say $t(1)$, and output $\boldsymbol{c}^{(\star)} = \boldsymbol{c}_1$.

alphabet. As a consequence, in this Subsection, an algorithm to find in polynomial time good solutions to the NP-hard problem $\mathcal{P}_{\boldsymbol{c}}^{d(n)}$ is described.
Firstly, assume that $c_0(k) \in \{1, e^{j2\pi\frac{1}{M}}, \ldots, e^{j2\pi\frac{M-1}{M}}\}, k = 1, \ldots, N$, and[5] $M \geq 2$. Then, using Lemma 4.3.1, $\mathcal{P}_{\boldsymbol{c}}^{d(n)}$ can be equivalently rewritten in terms of the following problem $\mathcal{P}_2$:

$$\mathcal{P}_2 \left\{ \begin{array}{ll} \max\limits_{\boldsymbol{c}} & \dfrac{\left| \boldsymbol{c}^T \left(\boldsymbol{w}^{(n-1)^*} \odot \boldsymbol{p}(\nu_{d_T}) \right) \right|^2}{\boldsymbol{c}^T \boldsymbol{\Theta_i} \left(\boldsymbol{w}^{(n-1)} \right) \boldsymbol{c}^* + \sigma_n^2 \|\boldsymbol{w}^{(n-1)}\|^2} \\ \text{s.t.} & c(k) \in \{1, e^{j2\pi\frac{1}{M}}, \ldots, e^{j2\pi\frac{M-1}{M}}\}, \ k = 1, \ldots, N \\ & \|\boldsymbol{c} - \boldsymbol{c}_0\|_\infty \leq \delta \end{array} \right. . \quad (4.21)$$

This is a non-convex fractional quadratic problem. Notice that, accounting for $\{c(k), c_0(k)\} \in \left\{1, e^{j2\pi\frac{1}{M}}, \ldots, \ e^{j2\pi\frac{M-1}{M}}\right\}^2$, $k = 1, \ldots, N$, the constraint $\max\limits_{k \in [1,\ldots,N]} |c(k) - c_0(k)| \leq \delta$, $k = 1, \ldots, N$, can be equivalently written as $\Re\left[c^*(k)c_0(k)\right] \geq 1 - \delta^2/2$ for $k = 1, \ldots, N$, which in turn

[5] Notice that, for $M = 2$ and $\delta < 2$, the optimal solution to problem (4.21) is the trivial one, i.e. $\boldsymbol{c}^{(\star)} \triangleq \boldsymbol{c}_0$.

amounts to enforcing

$$c(k) \in \{e^{j2\pi\frac{\beta_k}{M}}, e^{j2\pi\frac{\beta_k+1}{M}}, \ldots, e^{j2\pi\frac{\beta_k+\delta_d-1}{M}}\},$$

where

$$\beta_k = [M \arg(s_0(k))/(2\pi)] - \lfloor [M \arccos(1-\delta^2/2)]/(2\pi) \rfloor$$

depends on $c_0(k)$ and δ,

$$\delta_d = \begin{cases} 1 + 2\lfloor \frac{M \arccos(1-\delta^2/2)}{2\pi} \rfloor & \delta \in [0,2) \\ M & \delta = 2 \end{cases}$$

depends only on δ [8].

Thus, problem (4.21) is equivalent to:

$$\mathcal{P}_2' \begin{cases} \max\limits_{\boldsymbol{c}} & \dfrac{\left|\boldsymbol{c}^T \left(\boldsymbol{w}^{(n-1)^*} \odot \boldsymbol{p}(\nu_{d_T})\right)\right|^2}{\boldsymbol{c}^T \boldsymbol{\Theta_i} \left(\boldsymbol{w}^{(n-1)}\right) \boldsymbol{c}^* + \sigma_n^2 \|\boldsymbol{w}^{(n-1)}\|^2} \\ \text{s.t.} & \arg\left(c(k)\right) \in \frac{2\pi}{M}\left[\beta_k, \beta_k + 1, \ldots, \beta_k + \delta_d - 1\right], \\ & |c(k)| = 1,\ k = 1, \ldots, N. \end{cases} . \quad (4.22)$$

Observe that problem $\mathcal{P}_2'$, even in the simpler formulation corresponding to $\epsilon = 2$, is generally NP-hard, consequently one cannot find polynomial time algorithms for computing its optimal solutions. As a consequence, in the following, the focus is on approximation techniques, and a relaxation and randomization based algorithm is proposed, which provides a randomized feasible solution of (4.22). Thus, using $\boldsymbol{S}$ and $\boldsymbol{M}$ defined respectively in (4.15) and (4.16), resorting to the same relaxation procedure as in (4.17)-(4.20), and following the same steps as in [8, pp. 13-14], a randomized feasible solution $\boldsymbol{c}^{(\star)}$ to problem $\mathcal{P}_{\boldsymbol{c}}^{d(n)}$ can be computed using Algorithm 8.

As for Algorithm 7, the H randomizations involved into steps 3-6 are meant to improve the approximation quality; moreover, the computational complexity is mostly related to the solution of the SDP problem ($O(N^{3.5})$ flops). Finally, also with reference to the finite alphabet case, a modest number of randomizations is sufficient to ensure satisfactory performances.

Algorithm 8 Radar Quantized Phase Code Optimization

Require: $\boldsymbol{M}$, $\boldsymbol{S}$, H, $\{\beta_i\}$, M, δ_d.

Ensure: A randomized approximate solution $\boldsymbol{c}^{(\star)}$ of $\mathcal{P}_{\boldsymbol{c}}^{d(n)}$;

1: Let $(\boldsymbol{X}^\star, u^\star)$ be an optimal solution to problem (4.20).

2: Denote by $\hat{\boldsymbol{X}} = \boldsymbol{X}^\star / u^\star$.

3: Generate a random vector $(\boldsymbol{\xi})_h \in \mathbb{C}^N$, $h = 1, \ldots, H$, from the complex normal distribution $\mathcal{N}_{\mathbb{C}}(0, \boldsymbol{W})$ where $\boldsymbol{W} = \hat{\boldsymbol{X}} \odot \boldsymbol{y}_d \boldsymbol{y}_d^\dagger$, with $\boldsymbol{y}_d = [e^{-j\frac{2\pi}{M}\beta_1}, \ldots, e^{-j\frac{2\pi}{M}\beta_N}]^T$.

4: Let $(s(k))_h = y_d^*(k)\mu((\xi(k))_h)$, $k = 1, \ldots, N$, $h = 1, \ldots, H$, where

$$\mu(x) = \begin{cases} 1, & \text{if } \arg(x) \in [0, 2\pi\frac{1}{\delta_d}); \\ e^{j2\pi\frac{1}{M}}, & \text{if } \arg(x) \in [2\pi\frac{1}{\delta_d}, 2\pi\frac{2}{\delta_d}); \\ \vdots & \\ e^{j2\pi\frac{\delta_d - 1}{M}}, & \text{if } \arg(x) \in [2\pi\frac{\delta_d - 1}{\delta_d}, 2\pi). \end{cases}$$

5: Compute

$$t(h) = \frac{\boldsymbol{c}_h^\dagger \boldsymbol{S} \boldsymbol{c}_h}{\boldsymbol{c}_h^\dagger \boldsymbol{M} \boldsymbol{c}_h}, \quad h = 1 \ldots, H.$$

6: Pick the maximal value over $\{t(1), \ldots, t(H)\}$, say $t(1)$, and output $\boldsymbol{c}^{(\star)} = \boldsymbol{c}_1$.

4.3.3 Transmit-Receive System Design: Optimization Procedure

In this Subsection, the proposed sequential optimization procedures for the receive filter and the radar code are summarized and schematized respectively as Algorithm 9 for the continuous alphabet case and Algorithm 10 for the finite alphabet case. To trigger the recursion, an initial radar code $\boldsymbol{c}^{(0)}$, from which we obtain the optimal receive filter $\boldsymbol{w}^{(0)}$, is required; a natural choice is obviously $\boldsymbol{c}^{(0)} = \boldsymbol{c}_0$.

The computational complexity, connected with the implementation of both Algorithm 9 and Algorithm 10, depends on the number of iterations $\overline{N}$ as well as on and the complexity involved in each iteration. Precisely, the overall complexity is linear with respect to $\overline{N}$, while each iteration includes the computation of the inverse of $\boldsymbol{\Sigma_i}(\boldsymbol{c}_0) + \sigma_n^2 \boldsymbol{I}$ and

Algorithm 9 Transmit-Receive System Design for Continuous Alphabet Phase Codes

Require: $\left\{\sigma_{(r,i)}\right\}, \left\{\bar{\nu}_{d_{(r,i)}}, \epsilon_{(r,i)}\right\}, \sigma_n^2, \boldsymbol{c}_0, \nu_{d_T}, H, \delta, \zeta$.

Ensure: A solution $(\boldsymbol{c}^\star, \boldsymbol{w}^\star)$ of $\mathcal{P}^c$.

1: Set $n = 0$, $\boldsymbol{c}^{(n)} = \boldsymbol{c}_0$,

$$\boldsymbol{w}^{(n)} := \frac{\left(\boldsymbol{\Sigma_i}\left(\boldsymbol{c}_0\right) + \sigma_n^2 \boldsymbol{I}\right)^{-1}\left(\boldsymbol{c}_0 \odot \boldsymbol{p}(\nu_{d_T})\right)}{\left\|\left(\boldsymbol{\Sigma_i}\left(\boldsymbol{c}_0\right) + \sigma_n^2 \boldsymbol{I}\right)^{-1/2}\left(\boldsymbol{c}_0 \odot \boldsymbol{p}(\nu_{d_T})\right)\right\|^2},$$

and $\mathrm{SINR}^{(n)} = \mathrm{SINR}$.

2: **do**

3: $n := n + 1$;

4: Construct the matrices $\boldsymbol{S} = \left(\boldsymbol{w}^{(n-1)} \odot \boldsymbol{p}(\nu_{d_T})^*\right)\left(\boldsymbol{w}^{(n-1)} \odot \boldsymbol{p}(\nu_{d_T})^*\right)^\dagger$ and $\boldsymbol{M} = \boldsymbol{\Theta_i}\left(\boldsymbol{w}^{(n-1)}\right)^* + \sigma_n^2 \|\boldsymbol{w}^{(n-1)}\|^2 \boldsymbol{I}$, and the parameters $\{\gamma_i\}$, δ_c.

5: Find a good quality solution $\boldsymbol{c}^{(\star)}$ to problem $\mathcal{P}_{\boldsymbol{c}}^{c(n)}$, through the use of Algorithm 7.

6: Set

$$\boldsymbol{c}^{(n)} = \underset{\boldsymbol{c} \in \left\{\boldsymbol{c}^{(n-1)}, \boldsymbol{c}^{(\star)}\right\}}{\arg\max} \frac{|\alpha_T|^2 \left|\boldsymbol{w}^{(n-1)^\dagger}\left(\boldsymbol{c} \odot \boldsymbol{p}(\nu_{d_T})\right)\right|^2}{\boldsymbol{w}^{(n-1)^\dagger} \boldsymbol{\Sigma_i}\left(\boldsymbol{c}\right) \boldsymbol{w}^{(n-1)} + \sigma_n^2 \|\boldsymbol{w}^{(n-1)}\|^2}.$$

7: Construct the matrix $\boldsymbol{\Sigma_i}\left(\boldsymbol{c}^{(n)}\right)$.

8: Solve problem $\mathcal{P}_{\boldsymbol{w}}{}^{(n)}$ finding an optimal receive filter

$$\boldsymbol{w}^{(n)} := \frac{\left(\boldsymbol{\Sigma_i}\left(\boldsymbol{c}^{(n)}\right) + \sigma_n^2 \boldsymbol{I}\right)^{-1}\left(\boldsymbol{c}^{(n)} \odot \boldsymbol{p}(\nu_{d_T})\right)}{\left\|\left(\boldsymbol{\Sigma_i}\left(\boldsymbol{c}^{(n)}\right) + \sigma_n^2 \boldsymbol{I}\right)^{-1/2}\left(\boldsymbol{c}^{(n)} \odot \boldsymbol{p}(\nu_{d_T})\right)\right\|^2},$$

and the value of the SINR for the pair $\left(\boldsymbol{c}^{(n)}, \boldsymbol{w}^{(n)}\right)$.

9: Let $\mathrm{SINR}^{(n)} = \mathrm{SINR}$.

10: **until** $|\mathrm{SINR}^{(n)} - \mathrm{SINR}^{(n-1)}| \leq \zeta$.

11: Output $\boldsymbol{c}^\star = \boldsymbol{c}^{(n)}$ and $\boldsymbol{w}^\star = \boldsymbol{w}^{(n)}$.

Algorithm 10 Transmit-Receive System Design for Finite Alphabet Phase Codes

Require: $\{\sigma_{(r,i)}\}$,$\left\{\bar{\nu}_{d_{(r,i)}}, \epsilon_{(r,i)}\right\}$,$\sigma_n^2$,$\boldsymbol{c}_0$,$\nu_{d_T}$,$H$,$\delta$,$\zeta$,$M$.

Ensure: A solution $(\boldsymbol{c}^\star, \boldsymbol{w}^\star)$ of $\mathcal{P}^d$.

1: Set $n = 0$, $\boldsymbol{c}^{(n)} = \boldsymbol{c}_0$,

$$\boldsymbol{w}^{(n)} := \frac{\left(\boldsymbol{\Sigma_i}\left(\boldsymbol{c}_0\right) + \sigma_n^2\boldsymbol{I}\right)^{-1}\left(\boldsymbol{c}_0 \odot \boldsymbol{p}(\nu_{d_T})\right)}{\left\|\left(\boldsymbol{\Sigma_i}\left(\boldsymbol{c}_0\right) + \sigma_n^2\boldsymbol{I}\right)^{-1/2}\left(\boldsymbol{c}_0 \odot \boldsymbol{p}(\nu_{d_T})\right)\right\|^2},$$

and $\mathrm{SINR}^{(n)} = \mathrm{SINR}$.

2: **do**

3: $n := n + 1$;

4: Construct the matrices $\boldsymbol{S} = \left(\boldsymbol{w}^{(n-1)} \odot \boldsymbol{p}(\nu_{d_T})^*\right)\left(\boldsymbol{w}^{(n-1)} \odot \boldsymbol{p}(\nu_{d_T})^*\right)^\dagger$ and $\boldsymbol{M} = \boldsymbol{\Theta_i}\left(\boldsymbol{w}^{(n-1)}\right)^* + \sigma_n^2\|\boldsymbol{w}^{(n-1)}\|^2\boldsymbol{I}$, and the parameters $\{\beta_i\}$, δ_d.

5: Find a good solution of problem $\mathcal{P}_{\boldsymbol{c}}^{d(n)}$, through the use of Algorithm 8.

6: Set

$$\boldsymbol{c}^{(n)} = \underset{\boldsymbol{c}\in\left\{\boldsymbol{c}^{(n-1)},\boldsymbol{c}^{(\star)}\right\}}{\arg\max} \frac{|\alpha_T|^2\left|\boldsymbol{w}^{(n-1)^\dagger}\left(\boldsymbol{c} \odot \boldsymbol{p}(\nu_{d_T})\right)\right|^2}{\boldsymbol{w}^{(n-1)^\dagger}\boldsymbol{\Sigma_i}\left(\boldsymbol{c}\right)\boldsymbol{w}^{(n-1)} + \sigma_n^2\|\boldsymbol{w}^{(n-1)}\|^2}.$$

7: Construct the matrix $\boldsymbol{\Sigma_i}\left(\boldsymbol{c}^{(n)}\right)$.

8: Solve problem $\mathcal{P}_{\boldsymbol{w}}{}^{(n)}$ finding an optimal receive filter

$$\boldsymbol{w}^{(n)} := \frac{\left(\boldsymbol{\Sigma_i}\left(\boldsymbol{c}^{(n)}\right) + \sigma_n^2\boldsymbol{I}\right)^{-1}\left(\boldsymbol{c}^{(n)} \odot \boldsymbol{p}(\nu_{d_T})\right)}{\left\|\left(\boldsymbol{\Sigma_i}\left(\boldsymbol{c}^{(n)}\right) + \sigma_n^2\boldsymbol{I}\right)^{-1/2}\left(\boldsymbol{c}^{(n)} \odot \boldsymbol{p}(\nu_{d_T})\right)\right\|^2},$$

and the value of the SINR for the pair $\left(\boldsymbol{c}^{(n)}, \boldsymbol{w}^{(n)}\right)$.

9: Let $\mathrm{SINR}^{(n)} = \mathrm{SINR}$.

10: **until** $|\mathrm{SINR}^{(n)} - \mathrm{SINR}^{(n-1)}| \leq \zeta$.

11: Output $\boldsymbol{c}^\star = \boldsymbol{c}^{(n)}$ and $\boldsymbol{w}^\star = \boldsymbol{w}^{(n)}$.

the complexity effort of Algorithm 7 and Algorithm 8, respectively. The former is in the order of $O(N^3)$ [66]. The latter, for a modest number of randomizations, is connected with the SDP solution, i.e. $O(N^{3.5})$ [62].

4.4 Performance Analysis

In this Section, the performance analysis of the proposed algorithm for the joint optimization of the radar code and the receive filter s presented. An L-band radar is considered, whose operating frequency is $f_0 = 1.4$ GHz, and exploiting a broadside array with $N_a = 21$ elements pointing in the range-azimuth bin of interest $(0, 0)$. Specifically, a uniformly weighted linear array with uniform spacing equal to $d = \lambda/2$ is considered. Consequently, the radiation pattern is given by:

$$G(\theta) = \begin{cases} \dfrac{1}{N_a} \dfrac{\sin\left(N_a \dfrac{\pi}{2}\cos(\theta)\right)}{\sin\left(\dfrac{\pi}{2}\cos(\theta)\right)} & \text{if} \quad 0 \le \theta \le \pi \\ 10^{-3} & \text{if} \quad \pi \le \theta \le 2\pi \end{cases} .$$

The focus is on a scenario with a homogeneous range-azimuth clutter where the number of range rings that interfere with the range-azimuth bin of interest $(0, 0)$ is $N_c = 2$ and the number of azimuth cells in each ring is $L = 100$. Moreover, the pulse train length is set to $N = 20$ and, as similarity code $\boldsymbol{c}_0$, the N-dimensional generalized Barker code and its M-quantized version[6] are set for Algorithm 9 and Algorithm Cogn:Alg4, respectively. With reference to the continuous phase case, it is worth to remark that the choice for this similarity code is mainly due to its autocorrelation properties, namely its minimal peak-to-sidelobe ratio excluding the outermost sidelobe. The description of generalized Barker codes can be found in [67] and [68], also for other values of N. The exit

[6] Specifically, given the code $\boldsymbol{c}$, its M-quantized version $\boldsymbol{c}^q$ is constructed as $c^q(k) = \bar{\mu}(c(k))$, $k = 1, \ldots, N$, where the non-linearity $\bar{\mu}(x)$ is defined by

$$\bar{\mu}(x) = \begin{cases} 1, & \text{if } \arg(x) \in [0, 2\pi\frac{1}{M}) \\ e^{j2\pi\frac{1}{M}}, & \text{if } \arg(x) \in [2\pi\frac{1}{M}, 2\pi\frac{2}{M}) \\ \vdots & \\ e^{j2\pi\frac{M-1}{M}}, & \text{if } \arg(x) \in [2\pi\frac{M-1}{M}, 2\pi) \end{cases} .$$

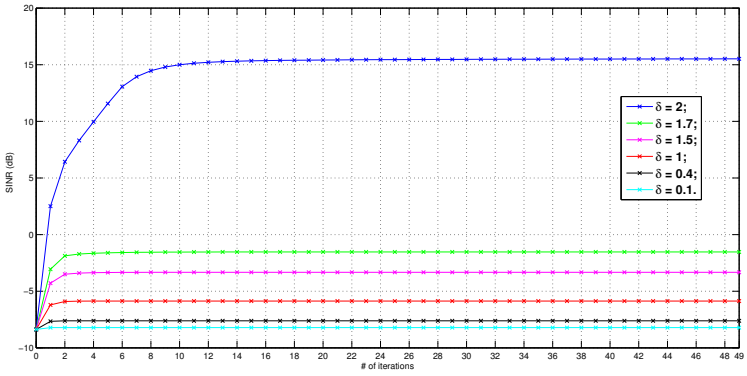

Figure 4.2: Algorithm 3 - SINR behavior for $\delta = [0.1, 0.4, 1, 1.5, 1.7, 2]$.

condition implemented to stop the procedure assumes $\zeta = 10^{-5}$, namely:

$$|\mathrm{SINR}^{(n)} - \mathrm{SINR}^{(n-1)}| \leq 10^{-5}.$$

The randomizations for both Algorithms 7 and 8 have been set to $H = 100$.

As to the parameters of the uniform clutter, the assumption is that $\frac{\sigma_0}{\sigma_n^2} K_r = \mathrm{CNR}\, K_r = 30$ dB, a mean Doppler frequency $\bar{\nu}_d = 0$, and Doppler uncertainty $\frac{\epsilon}{2} = 0.35$ for each range-azimuth bin. Additionally, a target with Signal to Noise Ratio $\frac{|\alpha_T|^2}{\sigma_n^2} = \mathrm{SNR} = 10$ dB and normalized Doppler frequency $\nu_{d_T} = -0.4$ is supposed to be on the scene.

The analysis is conducted in terms of the attainable SINR, in correspondence of the devised transmit code and receive filter, as well as the shape of the related auto- and cross-ambiguity functions[7].

In Figure 4.2, the SINR behavior, averaged over 100 independent trials of Algorithm 9, is plotted versus the number of iterations, for different values of the similarity parameter δ. As expected, increasing δ, the optimal value of the SINR improves since the feasible set of the optimization problem becomes larger and larger. Actually, performance gains up to 22 dB, with respect to step zero of the procedure, corresponding to the traditional adaptation on receive side only, can be observed for $\delta = 2$. Of

[7] The MATLAB© toolbox SeDuMi [28] for solving the SDP relaxation, and the MATLAB© toolbox of [70] for plotting the ambiguity functions of the coded pulse trains, have been exploited.

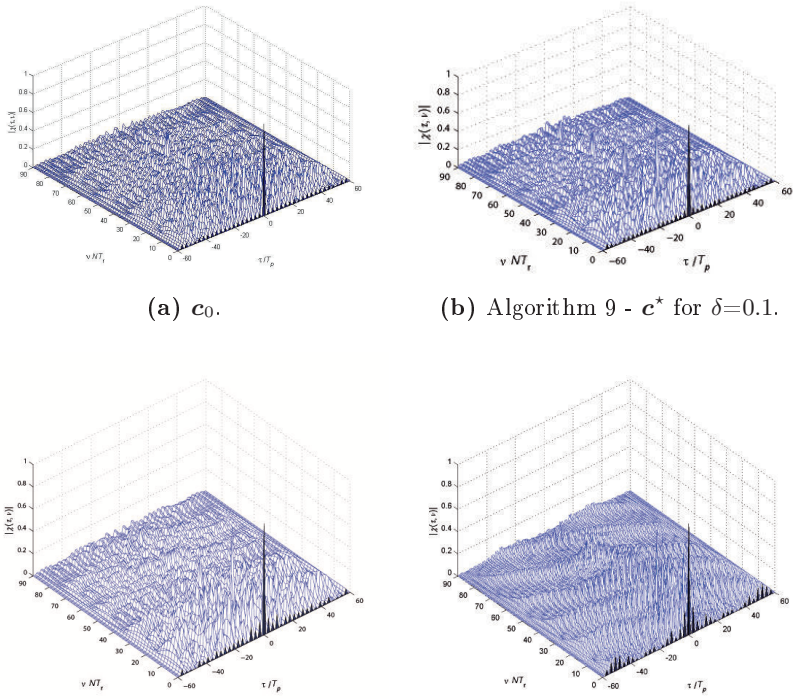

(a) $\boldsymbol{c}_0$. **(b)** Algorithm 9 - $\boldsymbol{c}^\star$ for δ=0.1.

(c) Algorithm 9 - $\boldsymbol{c}^\star$ for δ=1. **(d)** Algorithm 9 - $\boldsymbol{c}^\star$ for δ=2.

Figure 4.3: Algorithm 9 - Ambiguity Function modulus of the radar codes, assuming $T_r = 3T_p$.

course, this is just a potential value and in real conditions smaller gains could be experienced due to some inaccuracies in the available information. Also, observe that the number of iterations, required to achieve convergence, increases as well.

In Figures 4.3, the ambiguity function[8] of a synthesized code $\boldsymbol{c}^\star$, together with that of the reference code $\boldsymbol{c}_0$, is plotted for two different sizes of the similarity region. Indeed, an opposite behavior with respect to Figure 4.2 can be observed. Precisely, increasing δ, the set of feasible points becomes larger and larger, and better and better SINR performances are swapped for worse and worse ambiguity behaviors. Notice that the ambiguity function allows to visually represent the similarity between

[8] A coherent pulse train with ideal rectangular pulses of width T_p and pulse repetition time T_r is considered.

the reference code and the devised one. Moreover, it has also a certain relevance for the following reason: in order to update the site specific clutter maps, as well as to dynamically estimate other clutter parameters and account for a full cognitive implementation, a parallel receiving processing branch, exploiting a conventional pulse train matched filter, could be adopted. It is thus of paramount importance the availability of a signal sharing good range-Doppler resolution and ambiguity properties. By doing so, effective real-time estimates of the clutter parameters with a low computational cost can be obtained.

In Figures 4.4, the frequency behavior of the radar code and the receive filter, corresponding to $\delta = 2$, and for different values of the iteration number ($n = [0, 5, 20, 50]$), is analyzed.

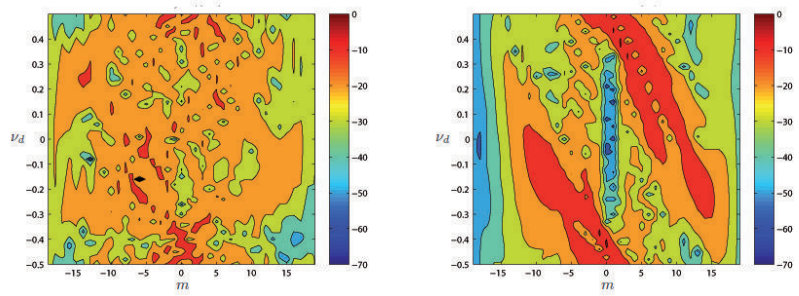

(a) $\left(\boldsymbol{c}^{(0)}, \boldsymbol{w}^{(0)}\right)$.

(b) $\left(\boldsymbol{c}^{(5)}, \boldsymbol{w}^{(5)}\right)$.

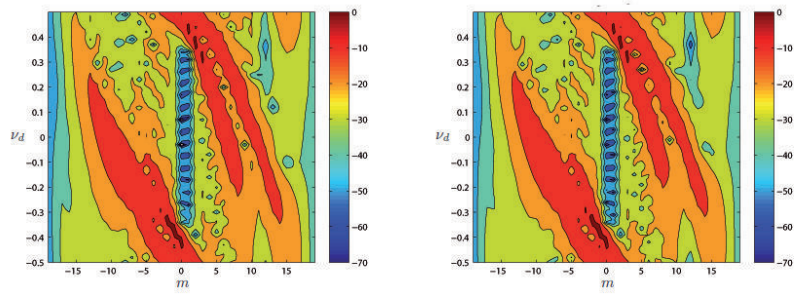

(c) $\left(\boldsymbol{c}^{(19)}, \boldsymbol{w}^{(19)}\right)$.

(d) $\left(\boldsymbol{c}^{(50)}, \boldsymbol{w}^{(50)}\right)$.

Figure 4.4: Algorithm 9 - Cross-Ambiguity Function, in dB, of the radar code and receive filter.

Precisely, the contour map of the (slow-time) cross-ambiguity function is plotted,

$$\mathrm{g}^{(n)}\left(m, \nu_d\right) = \left| \boldsymbol{w}^{(n)\dagger} \left(\boldsymbol{J}_m \left(\boldsymbol{c}^{(n)} \odot \boldsymbol{p}\left(\nu_d\right) \right) \right) \right|^2 \tag{4.23}$$

where m is the delay-lag and ν_d is the Doppler frequency of the incoming signal, which also allows to visualize the systems response to ambiguous ranges. For a given value of m, it gives the Doppler response to a clutter patch located m PRI away from the one of interest. As forced by the design procedure, the cross-ambiguity function is equal to one at $(m, \nu_d) = (0, -0.4)$, which is the range-Doppler position of the nominal target. Moreover, lower and lower values of $\mathrm{g}^{(n)}\left(m, \nu_d\right)$ can be observed in the strip $0 \leq m \leq 2$, $-0,35 \leq \nu_d \leq 0.35$ as the iteration step n grows up. Interestingly, this performance trend reflects the capability of the

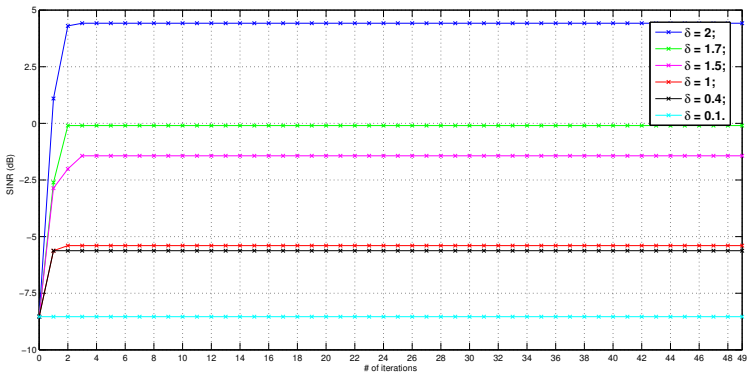

Figure 4.5: Algorithm 10 - SINR behavior for $\delta = [0.1, 0.4, 1, 1.5, 1.7, 2]$, $M = 16$.

proposed joint transmit-receive optimization procedure to sequentially refine the shape of the cross-ambiguity function in order to get better and better clutter suppression levels.

In Figure 4.5, the SINR behavior, averaged over 100 independent trials of Algorithm 10, is plotted versus the number of iterations, for different values of the similarity parameter δ, and for $M = 16$. The same considerations as for the analysis conducted in Figure 4.2 hold true; indeed, increasing δ, better and better SINR values are experienced, due to the enlargement of the feasible set. Performance gains up to approximatively 12 dB, with respect to step zero of our procedure can be observed for $\delta = 2$.

In Figures 4.6, the ambiguity function of a synthesized code $\boldsymbol{c}^{\star}$, together with that of the reference quantized code $\boldsymbol{c}_0^q$, is plotted for three different sizes of the similarity region, assuming $M = 16$. Again, an opposite trend with respect to Figure 4.5 is observed, which reflects how δ rules the trade-off between SINR performance and ambiguity behavior. Precisely, increasing δ, the set of feasible points becomes larger and larger, and better and better SINR performances are swapped for worse and worse ambiguity shapes.

In Figure 4.7, the impact of the number of quantization level on the devised code is considered, for a fixed similarity parameter $\delta = 2$. As expected, the achieved average SINR increases as the number of levels involved into the quantization procedure increases. Indeed, the greater the cardinality of the alphabet, the higher the degrees of freedom available in the choice of the radar code.

4.5 Conclusions

In this Chapter, the problem of cognitive constant envelope transmit signal and receive filter joint optimization in a signal-dependent clutter environment has been considered. Iterative algorithms have been devised, trying to optimize the SINR while accounting for a similarity constraint on the transmitted sequence. At each step, the proposed procedures require the solution of both convex and NP-hard problems. In order to find a good quality solution to the latter, relaxation and randomization techniques have been invoked. At the analysis stage,the performance of the proposed algorithms have been assessed in terms of average SINR (versus the number of iterations), ambiguity function of the resulting phase code, and cross-ambiguity function of the transmit signal and receive filter pair. Furthermore, with reference to the finite alphabet case, the impact of the quantization level on the system performance have been analyzed. The results have highlighted that, in the presence of a perfect a-priori knowledge, with a modest number of trials, significant SINR gains (up to 22 dB foe the continuous alphabet case, or 12 dB with $M = 16$ for the quantized alphabet case, respectively) can be obtained jointly optimizing the transmitter and receiver. Possible future research tracks might concern the study of further constraints on the receive filter, so as to keep under control other key parameters such as the Integrated-to-Sidelobe Level or the Peak-to-Sidelobe Level. finally, it is of primary concern to study the impact of an imperfect a-priori knowledge, due to different error sources, on the potential performance gain.

4.6 Acknowledgment

The author of the present Chapter thanks the Air Force Office of Scientific Research, Air Force Material Command, USAF, under grant

number FA8655-09-1-3006. The US Government is authorised to reproduce and distribute reprints for Government purpose notwithstanding any copyright notation thereon. The views and conclusions contained herein are those of the authors and should not be interpreted as necessarily representing the official policies or endorsements, either expressed or implied, of the Air Force Office of Scientific Research or the US Government.

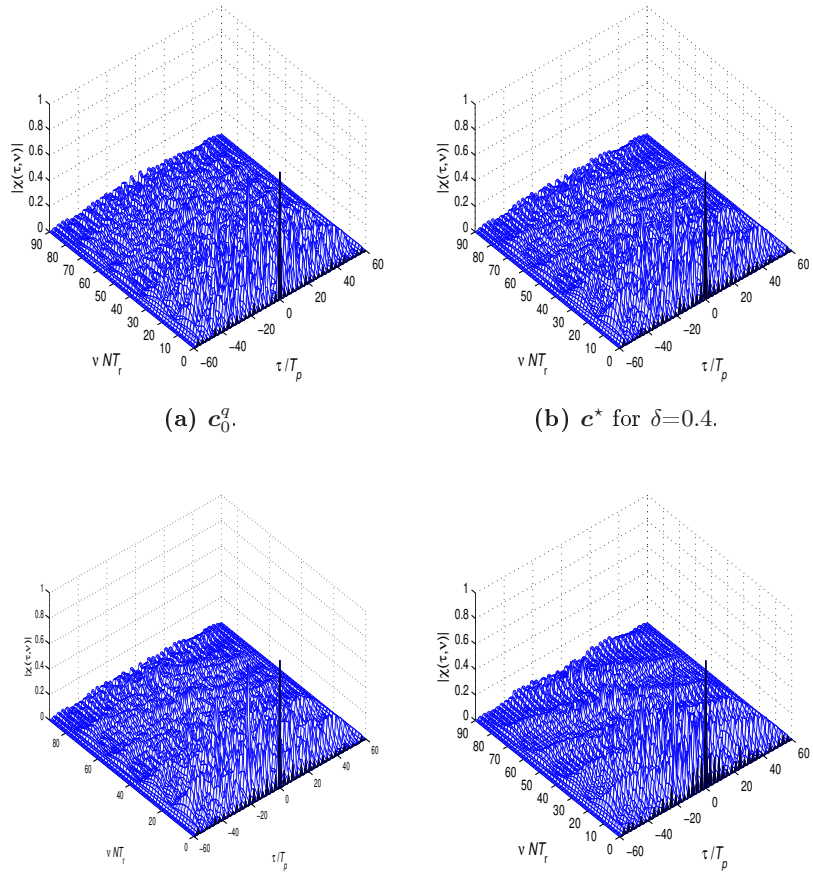

(a) $\boldsymbol{c}_0^q$.

(b) $\boldsymbol{c}^\star$ for δ=0.4.

(c) $\boldsymbol{c}^\star$ for δ=1.

(d) $\boldsymbol{c}^\star$ for δ=2.

Figure 4.6: Algorithm 10 - Ambiguity Function modulus of the radar codes, assuming $M = 16$ and $T_r = 3T_p$.

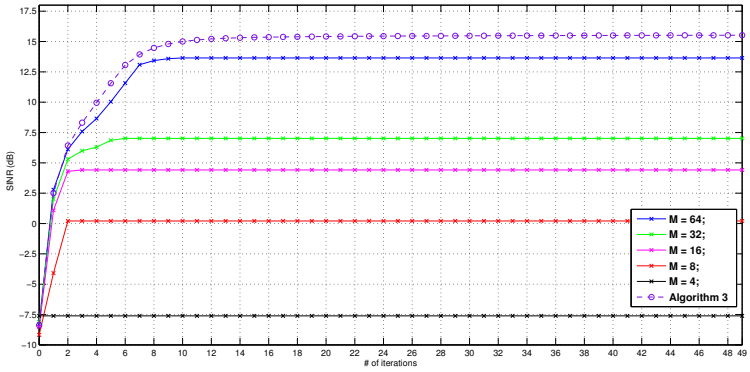

Figure 4.7: Algorithm 10 - $\mathrm{SINR}^{(n)}$ behavior for $\delta = 2$, $M = [4, 8, 16, 32, 64]$; Algorithm 9 (o-marked violet dashed line).

Appendix A

Multi-Objective Optimization Problems

A multi-objective optimization problem[1] presents a vector-valued objective function and can be written in the form

$$\begin{array}{ll} \min\limits_{\boldsymbol{x}} & \boldsymbol{f}_0(\boldsymbol{x}) \\ \text{s.t.} & f_i(\boldsymbol{x}) \leq 0, \qquad \forall i = 1, \ldots, m, \\ & h_i(\boldsymbol{x}) = 0, \qquad \forall i = 1, \ldots, p \end{array} \tag{A.1}$$

where $\boldsymbol{x} \in \mathbb{R}^n$ is the optimization variable, $f_i(\boldsymbol{x})$, $i = 1, \ldots, m$ and $h_i(\boldsymbol{x})$, $i = 1, \ldots, p$ denote respectively the i-th inequality constraint and the i-th equality constraint function, $\boldsymbol{f}_0(\boldsymbol{x}) \ : \ \boldsymbol{x} \in \mathbb{R}^n \rightarrow \mathbb{R}^q$ is the vector-valued objective function whose q components $F_1(\boldsymbol{x}), \ldots, F_q(\boldsymbol{x})$ can be interpreted as q different scalar objectives, each of which we would like to minimize[2].

If $\boldsymbol{x}$ and $\boldsymbol{y}$ are both feasible, we say that $\boldsymbol{x}$ *is at least as good as* $\boldsymbol{y}$ according the i-th objective if $F_i(\boldsymbol{x}) \leq F_i(\boldsymbol{y})$, while $\boldsymbol{x}$ *is better than* $\boldsymbol{y}$ (or $\boldsymbol{x}$ beats $\boldsymbol{y}$) according the i-th objective if $F_i(\boldsymbol{x}) < F_i(\boldsymbol{y})$; so, if $F_i(\boldsymbol{x}) \leq F_i(\boldsymbol{y})$ for $i = 1, \ldots, q$ and, for al least one j, $F_j(\boldsymbol{x}) < F_j(\boldsymbol{y})$, we say that $\boldsymbol{x}$ *dominates* $\boldsymbol{y}$.
A point $\boldsymbol{x}^\star$ is defined optimal only if it complies with

$$F_i(\boldsymbol{x}^\star) \leq F_i(\boldsymbol{y}), \qquad i = 1, \ldots, q$$

[1] The material in this sub-section is taken from [11, pp. 174-187].
[2] The material of this Appendix is taken from [11, pp. 174-187]

for every feasible $\boldsymbol{y}$; otherwise stated, $\boldsymbol{x}^\star$ has to be simultaneously optimal for each of the scalar problems

$$\begin{array}{ll} \min\limits_{\boldsymbol{x}} & F_j(\boldsymbol{x}) \\ \text{s.t.} & f_i(\boldsymbol{x}) \leq 0 \qquad \forall i = 1, \ldots, m, \\ & h_i(\boldsymbol{x}) = 0, \qquad \forall i = 1, \ldots, p \end{array}$$

for $j = 1, \ldots, q$. In the presence of an optimal point, the objectives are said *noncompeting*, since no compromises have to be made among them: each objective is as small as it could be made, even if the others were ignored.
However, the set of achievable values for problem (A.1) does not always present a minimum element, and thus the problem itself has not an optimal point and an optimal value. In these cases, one focuses on the *minimal* elements [11, pp. 45] of the set, namely on the so-called Pareto-optimal points.

A feasible point $\boldsymbol{x}^\star$ is referred to as Pareto-optimal only if $\boldsymbol{f}_0(\boldsymbol{x}^\star)$ is a minimal element of the set of achievable values $\mathcal{O}$ (the set of objective values of feasible points[3]); in this case, $\boldsymbol{f}_0(\boldsymbol{x}^\star)$ is a Pareto-optimal value for (A.1). Considering the q scalar components of the objective function $\boldsymbol{f}_0(\boldsymbol{x})$, $\boldsymbol{x}^\star$ can be considered Pareto-optimal only if it is feasible and no better feasible point exists. Precisely, if $\boldsymbol{y}$ is a feasible point and $F_i(\boldsymbol{y}) \leq F_i(\boldsymbol{x}^\star)$ for $i = 1, \ldots, q$, then necessarily $F_i(\boldsymbol{x}^\star) = F_i(\boldsymbol{y})$ for $i = 1, \ldots, q$. This also implies that: if a feasible point is not Pareto-optimal, than there is at least another feasible point that is better. Hence, the search for "*good*" points can be limited to Pareto-optimal ones.
A standard technique to find Pareto-optimal points is the *scalarization*, where the vectorial problem (A.1) is reduced to the scalar one

$$\begin{array}{ll} \min\limits_{\boldsymbol{x}} & \boldsymbol{\lambda}^T \boldsymbol{f}_0(\boldsymbol{x}) \\ \text{s.t.} & f_i(\boldsymbol{x}) \leq 0 \\ & h_i(\boldsymbol{x}) = 0 \end{array} \tag{A.2}$$

once it has been defined the vector of weights $\boldsymbol{\lambda} \succ 0$, namely a vector with positive components. In fact, it can be shown [11, pp. 178] that if $\boldsymbol{x}^\star$ is an optimal point for problem (A.2), than it is also a Pareto-optimal point for the problem (A.1). Nevertheless it is worth pointing out that, for

[3] $\mathcal{O} = \{\boldsymbol{f}_0(\boldsymbol{x}^\star) \,:\, \exists \boldsymbol{x} \in \mathcal{D},\ f_i(\boldsymbol{x}) \leq 0,\ i = 1, \ldots, m,\ h_i(\boldsymbol{x}) = 0,\ i = 1, \ldots, p\}$, where $\mathcal{D}$ is the domain of the optimization problem.

non-convex multi-objective optimization problems, it is possible through scalarization to obtain a sub-set, but not all, the Pareto-optimal points.

The choice of the parameter $\boldsymbol{\lambda}$ plays a primary role in the determination of the Pareto points, defining the *weight* given to each of the scalar components. Specifically, it quantifies our desire to make $F_i(\boldsymbol{x})$ small.

Appendix B

Proof of Lemma 2.3.2

We first claim that problem (2.9) is feasible. It is seen that $(\boldsymbol{c}_0,\, t^\star)$ with

$$t^\star = \min_{\nu_d \in [0,1]} \boldsymbol{p}^\dagger (\boldsymbol{M}^{-1} \odot (\boldsymbol{c}_0 \boldsymbol{c}_0^\dagger)^*) \boldsymbol{p},$$

is feasible for problem (2.3), and thus $(\boldsymbol{c}_0 \boldsymbol{c}_0^\dagger,\, t^\star)$ is feasible for SDP problem (2.6). It follows by Lemma 2.3.1 that there is a matrix $\boldsymbol{X} \succeq \boldsymbol{0}$ such that $(\boldsymbol{c}_0 \boldsymbol{c}_0^\dagger,\, \boldsymbol{X},\, t^\star)$ is feasible for (2.9).

Now, we wish to show that problem (2.9) is solvable. To this end, we are about to prove that the dual problem of (2.9) is strictly feasible and bounded above. Let us compute the dual of SDP problem (2.9).

Recall that $\boldsymbol{W} = [\boldsymbol{w}_0, \ldots, \boldsymbol{w}_{N-1}] \in C^{M \times N}$, $\boldsymbol{w}_k = \left[1, e^{-jk\theta}, \ldots, e^{-j(M-1)k\theta}\right]^T$, $k = 0, \ldots, N-1$, $\theta = 2\pi/M$, $M = 2N-1$. Then, we can rewrite $\boldsymbol{W}$ as

$$\boldsymbol{W} = \begin{bmatrix} \boldsymbol{v}_0^\dagger \\ \boldsymbol{v}_1^\dagger \\ \vdots \\ \boldsymbol{v}_{M-1}^\dagger \end{bmatrix}, \boldsymbol{v}_m = \begin{bmatrix} 1 \\ e^{jm\theta} \\ \vdots \\ e^{j(N-1)m\theta} \end{bmatrix}, m = 0, \ldots, M-1. \tag{B.1}$$

Thus, $\boldsymbol{W}^\dagger \mathbf{diag}(\boldsymbol{W}\boldsymbol{X}\boldsymbol{W}^\dagger) = \sum_{m=1}^{M-1} (\boldsymbol{v}_m^\dagger \boldsymbol{X} \boldsymbol{v}_m) \boldsymbol{v}_m$. From the equality constraint $t\boldsymbol{e}_1 = \boldsymbol{x} - \boldsymbol{W}^\dagger \mathbf{diag}(\boldsymbol{W}\boldsymbol{X}\boldsymbol{W}^\dagger)$, we have

$$t = \frac{1}{N} \sum_{i=1}^{N} (\boldsymbol{M}^{-1} \odot \boldsymbol{C}^*)(i,i) - \sum_{m=0}^{M-1} \boldsymbol{v}_m^\dagger \boldsymbol{X} \boldsymbol{v}_m, \tag{B.2}$$

and

$$\frac{1}{N}\sum_{i=1}^{N-k}(\boldsymbol{M}^{-1}\odot\boldsymbol{C}^{*})(i+k,i)=\sum_{m=0}^{M-1}\boldsymbol{v}_m^{\dagger}\boldsymbol{X}\boldsymbol{v}_m e^{jkm\theta},\ k=1,\ldots,N-1. \tag{B.3}$$

It is clear that (B.2) can be further rewritten into

$$t=\mathrm{tr}\,(\boldsymbol{A}_0\boldsymbol{C})-\mathrm{tr}\,(\boldsymbol{B}_0\boldsymbol{X}), \tag{B.4}$$

where

$$\boldsymbol{A}_0=\frac{1}{N}\boldsymbol{I}\odot\boldsymbol{M}^{-1}\,,\qquad \boldsymbol{B}_0=\sum_{m=0}^{M-1}\boldsymbol{v}_m\boldsymbol{v}_m^{\dagger}, \tag{B.5}$$

that is, $\boldsymbol{A}_0$ is the diagonal matrix with diagonal elements being $\frac{1}{N}\boldsymbol{M}^{-1}$'s diagonal elements. Observe that (B.3) has $2(N-1)$ equalities (counting the real part and imaginary part):

$$\mathrm{tr}\,(\boldsymbol{A}_{k,1}\boldsymbol{C})=\mathrm{tr}\,(\boldsymbol{B}_{k,1}\boldsymbol{X}),\ \ \mathrm{tr}\,(\boldsymbol{A}_{k,2}\boldsymbol{C})=\mathrm{tr}\,(\boldsymbol{B}_{k,2}\boldsymbol{X}),\ k=1,\ldots,N-1, \tag{B.6}$$

where

$$\boldsymbol{B}_{k,1}=\sum_{m=0}^{M-1}\boldsymbol{v}_m\boldsymbol{v}_m^{\dagger}\cos(km\theta),\ \ \boldsymbol{B}_{k,2}=\sum_{m=0}^{M-1}\boldsymbol{v}_m\boldsymbol{v}_m^{\dagger}\sin(km\theta),\quad k=1,\ldots,N-1, \tag{B.7}$$

and

$$\boldsymbol{A}_{k,1}=\frac{1}{2}\boldsymbol{M}_k,\qquad \boldsymbol{A}_{k,2}=\frac{1}{2}(\boldsymbol{M}_k\odot\boldsymbol{E}),\qquad k=1,\ldots,N-1. \tag{B.8}$$

The $N\times N$ Hermitian matrices $\boldsymbol{M}_k$ are defined by

$$\boldsymbol{M}_k(i+k,i)=\boldsymbol{M}^{-1}(i+k,i),\qquad i=1,\ldots,N-k\,; \tag{B.9}$$

the diagonal elements and the other lower triangular elements of $\boldsymbol{M}_k$ equal to zero. The $N\times N$ Hermitian matrix $\boldsymbol{E}$ is defined by

$$\begin{cases}\boldsymbol{E}(i,i)=1, & i=1,\ldots,N,\\ \boldsymbol{E}(i,l)=-j, & \forall i>l.\end{cases} \tag{B.10}$$

By considering (B.2)-(B.4), (B.6), we can rewrite problem (2.9) equivalently into the following form

$$\begin{array}{ll} \max\limits_{\boldsymbol{X},\boldsymbol{C}} & \mathrm{tr}\,(\boldsymbol{A}_0\boldsymbol{C}) - \mathrm{tr}\,(\boldsymbol{B}_0\boldsymbol{X}) \\ \text{s.t.} & \mathrm{tr}\,(\boldsymbol{A}_{k,1}\boldsymbol{C}) - \mathrm{tr}\,(\boldsymbol{B}_{k,1}\boldsymbol{X}) = 0, \;\; k = 1,\ldots,N-1, \\ & \mathrm{tr}\,(\boldsymbol{A}_{k,2}\boldsymbol{C}) - \mathrm{tr}\,(\boldsymbol{B}_{k,2}\boldsymbol{X}) = 0, \;\; k = 1,\ldots,N-1, \\ & \mathrm{tr}\,(\boldsymbol{c}_0\boldsymbol{c}_0^\dagger\boldsymbol{C}) \geq \delta_\epsilon, \\ & \mathrm{tr}\,(\boldsymbol{C}) = 1, \\ & \boldsymbol{C} \succeq \boldsymbol{0}, \\ & \boldsymbol{X} \succeq \boldsymbol{0}. \end{array} \tag{B.11}$$

Therefore, the dual problem of (B.11) is

$$\begin{array}{ll} \min\limits_{y,z,\{x_1(k)\},\{x_2(k)\}} & y\delta_\epsilon + z \\ \text{s.t.} & z\boldsymbol{I} + y\boldsymbol{c}_0\boldsymbol{c}_0^\dagger + \sum_{k=1}^{N-1}(x_1(k)\boldsymbol{A}_{k,1} + x_2(k)\boldsymbol{A}_{k,2}) \succeq \boldsymbol{A}_0, \\ & \sum_{k=1}^{N-1}(x_1(k)\boldsymbol{B}_{k,1} + x_2(k)\boldsymbol{B}_{k,2}) \preceq \boldsymbol{B}_0, \\ & y \leq 0,\, z \in \mathbb{R},\, x_1(k) \in \mathbb{R},\, x_2(k) \in \mathbb{R}, \\ & \forall k = 1,\ldots,N-1\,, \end{array} \tag{B.12}$$

with $\mathbb{R}$ the set of real numbers.

Since problem (2.9) is feasible, then (B.11) is feasible. It follows by weak duality theorem that problem (B.12) is bounded below. It can be also proved that problem (B.12) is strictly feasible. In fact, let z be a sufficiently large positive number, y a negative number sufficiently close to zero, $x_1(k)$, $x_2(k)$ equal to zero, then $(z, y, x_1(1), x_2(1), \ldots, x_1(N-1), x_2(N-1))$ is a strictly feasible solution of (B.12). Therefore, from Theorem 1.7.1 of [26] (Conic Duality Theorem), we can conclude that problem (2.9) is solvable because the dual is bounded below and strictly feasible.

Appendix C

Proof of Proposition 3.3.1

It is clear that problem (3.6) is equivalent to the problem:

$$\begin{array}{ll} \max\limits_{\boldsymbol{z}} & \boldsymbol{z}^\dagger \boldsymbol{R}\boldsymbol{z} \\ \text{s.t.} & |z(i)|^2 \le 1,\, i=1,\ldots,N \\ & \|\boldsymbol{z}\|^2 = N/\gamma. \end{array} \tag{C.1}$$

Let $N = 3P+1$, $\gamma = 1+\frac{P}{2P+1}$, $\boldsymbol{z} = [\boldsymbol{x}^T, \boldsymbol{y}^T]^T$, where $\boldsymbol{x} = [z(0), z(1), \ldots, z(P), z(P+1), \ldots, z(2P)]^T$ and $\boldsymbol{y} = [z(2P+1), \ldots, z(3P)]^T$; let $\boldsymbol{b}_0 = [\frac{-j}{2}\boldsymbol{e}^T\boldsymbol{a}, \boldsymbol{a}^T, \boldsymbol{0}_P^T, \boldsymbol{0}_P^T]^T$, $\boldsymbol{b}_i = [-j, \boldsymbol{e}_i^T, -\boldsymbol{e}_i^T, \boldsymbol{0}_P^T]^T$, $i = 1, \ldots, P$, where $\boldsymbol{a} \in \mathbb{R}^P$ is a given vector with integer-valued components and $\boldsymbol{e} \in \mathbb{R}^P$ is the all-one vector. Let λ be any number not less than the maximal eigenvalue of $\sum_{i=0}^P \boldsymbol{b}_i\boldsymbol{b}_i^\dagger$, and $\boldsymbol{R}$ be

$$\left[\begin{array}{cc} \lambda \boldsymbol{I}_{2P+1} & \boldsymbol{0} \\ \boldsymbol{0} & \boldsymbol{0}_{P\times P} \end{array}\right] - \sum_{i=0}^P \boldsymbol{b}_i\boldsymbol{b}_i^\dagger. \tag{C.2}$$

This previous assumption ensures $\boldsymbol{R} \succeq \boldsymbol{0}$. Therefore, it follows that

$$\boldsymbol{z}^\dagger\boldsymbol{R}\boldsymbol{z} = \lambda\|\boldsymbol{x}\|^2 - \sum_{i=0}^P |\boldsymbol{z}^\dagger\boldsymbol{b}_i|^2 \le \lambda N/\gamma = \lambda(2P+1) \tag{C.3}$$

and the equality holds for any feasible point $\boldsymbol{z}$ for (C.1), if and only if $|z(i)| = 1$, $i = 0, \ldots, 2P$, and $\boldsymbol{b}_i^\dagger\boldsymbol{z} = 0$, $i = 0, \ldots, P$. That is, all $z(i)$, $i = 0, \ldots, 2P$, are of unit modulus and

$$\frac{j}{2}\boldsymbol{e}^T\boldsymbol{a}z(0) + \sum_{i=1}^P a(i)z(i) = 0,\; jz(0) + z(i) - z(P+i) = 0,\; k = 1, \ldots, P,$$

which, due to nonzero z_0, are equivalent to

$$\frac{j}{2}\boldsymbol{e}^T\boldsymbol{a} + \sum_{i=1}^{P} a(i)(z(i)/z(0)) = 0, \quad j + z(i)/(z(0)) - z(P+i)/(z(0)) = 0, \\ i = 1, \ldots, P, \tag{C.4}$$

Set $z(i)/z(0) = e^{j\theta_i}$, $i = 1, \ldots, 2P$, and the last P equations of (C.4) become

$$\cos\theta_i - \cos\theta_{P+i} = 0,\ 1 + \sin\theta_i - \sin\theta_{P+i} = 0,\ i = 1, \ldots, P,$$

which imply that $\theta_i = -\theta_{P+i} \in \{-\frac{\pi}{6}, -\frac{5}{6}\pi\}$, and the first equation of (C.4) becomes

$$\frac{1}{2}\boldsymbol{e}^T\boldsymbol{a} + \sum_{i=1}^{P} a(i)\sin\theta_i = 0,\ \sum_{i=1}^{P} a(i)\cos\theta_i = 0,$$

which further amounts to

$$\sum_{i=1}^{P} a(i)\cos\theta_i = 0,\ \theta_i \in \{-\frac{\pi}{6}, -\frac{5}{6}\pi\},\ i = 1, \ldots, P.$$

This is clearly equivalent to the partition problem described in [48, pages 47 and 60], namely finding a binary vector $\boldsymbol{x}$ such that

$$\sum_{i=1}^{P} a(i)x(i) = 0,\ x(i) \in \{\pm 1\},\ i = 1, \ldots, P. \tag{C.5}$$

Summarizing, the conclusion is that finding a feasible solution such that (C.3) is valid with equality, is equivalent to finding a solution $\boldsymbol{x} \in \mathbb{R}^P$ of (C.5).

Appendix D

Proof of Proposition 3.3.2

(i) It follows from (3.13) that $\boldsymbol{I} - \boldsymbol{D}^{-}\boldsymbol{D} \succeq \boldsymbol{0}$. Thus $\tilde{\boldsymbol{C}}^{\star} = \boldsymbol{C}^{\star} + (\boldsymbol{I} - \boldsymbol{D}^{-}\boldsymbol{D}) \succeq \boldsymbol{0}$, which implies $\boldsymbol{D}^{-}\tilde{\boldsymbol{C}}^{\star}\boldsymbol{D}^{-} \succeq \boldsymbol{0}$.

(ii) It is seen immediately from (3.10)-(3.12) and (3.15).

Appendix E

Proof of Proposition 3.3.4

Notice that $\boldsymbol{D}^{-}\boldsymbol{D} = \boldsymbol{D}\boldsymbol{D}^{-}$, namely $\boldsymbol{D}$ and $\boldsymbol{D}^{-}$ commute. Since $\boldsymbol{C}^{\star}$ is positive semidefinite, then

$$\boldsymbol{D}\boldsymbol{D}^{-}\boldsymbol{C}^{\star}\boldsymbol{D}^{-}\boldsymbol{D} = \boldsymbol{C}^{\star},$$

where the property that, if a positive semidefinite matrix has a diagonal element 0, then the corresponding row and column contains all zero elements, has been used. Observe that $(\boldsymbol{I} - \boldsymbol{D}^{-}\boldsymbol{D})\boldsymbol{D}^{-}\boldsymbol{D} = \boldsymbol{0}$. Then, it follows that

$$\boldsymbol{D}\boldsymbol{D}^{-}\tilde{\boldsymbol{C}}^{\star}\boldsymbol{D}^{-}\boldsymbol{D} = \boldsymbol{D}\boldsymbol{D}^{-}(\boldsymbol{C}^{\star} + (\boldsymbol{I} - \boldsymbol{D}^{-}\boldsymbol{D}))\boldsymbol{D}^{-}\boldsymbol{D} = \boldsymbol{C}^{\star}.$$

Appendix F

Proof of Proposition 3.3.5

Let $y(i) = e^{j \arg(\xi(i))}$, $i = 1, \ldots, N$, where $\xi(i)$ is generated by step 3 of Algorithm 3. Thus $\boldsymbol{c} = \boldsymbol{D}\boldsymbol{y}$. It follows from Lemma 3.3.3 that the expectation of $\boldsymbol{y}\boldsymbol{y}^\dagger$ is

$$E[\boldsymbol{y}\boldsymbol{y}^\dagger] = F(\boldsymbol{D}^-\tilde{\boldsymbol{C}}^\star\boldsymbol{D}^-) \succeq \frac{\pi}{4}\boldsymbol{D}^-\tilde{\boldsymbol{C}}^\star\boldsymbol{D}^-.$$

Therefore, it follows that

$$\begin{aligned}
E[\boldsymbol{c}^\dagger\boldsymbol{R}\boldsymbol{c}] &= E[\boldsymbol{y}^\dagger\boldsymbol{D}\boldsymbol{R}\boldsymbol{D}\boldsymbol{y}] \\
&= \mathrm{tr}\,(\boldsymbol{D}\boldsymbol{R}\boldsymbol{D}E[\boldsymbol{y}\boldsymbol{y}^\dagger]) \\
&\geq \frac{\pi}{4}\mathrm{tr}\,(\boldsymbol{D}\boldsymbol{R}\boldsymbol{D}\boldsymbol{D}^-\tilde{\boldsymbol{C}}^\star\boldsymbol{D}^-) \\
&= \frac{\pi}{4}\mathrm{tr}\,(\boldsymbol{R}\boldsymbol{D}\boldsymbol{D}^-\tilde{\boldsymbol{C}}^\star\boldsymbol{D}^-\boldsymbol{D}) \\
&= \frac{\pi}{4}\mathrm{tr}\,(\boldsymbol{R}\boldsymbol{C}^\star) \\
&\geq \frac{\pi}{4}v((3.6))
\end{aligned}$$

where the first inequality is due to the fact that $\boldsymbol{D}\boldsymbol{R}\boldsymbol{D} \succeq \boldsymbol{0}$ and, in the last equality, Proposition 3.3.4 has been applied.

Appendix G

Proof of Proposition 3.4.2

This appendix deals with the dual problem of (3.23), showing that it is strictly feasible and bounded above, which by the strong duality [26, Theorem 1.7.1], means that (3.23) is solvable.

Recall that $\boldsymbol{W} = [\boldsymbol{w}_0, \ldots, \boldsymbol{w}_{N-1}] \in \mathbb{C}^{L\times N}$, $\boldsymbol{w}_k = [1, e^{-jk\theta}, \ldots, e^{-j(L-1)k\theta}]^T$, $k = 0, \ldots, N-1$, $\theta = 2\pi/L$, $L = 2N-1$. Then, $\boldsymbol{W}$ can be rewritten as

$$\boldsymbol{W} = \begin{bmatrix} \boldsymbol{v}_0^\dagger \\ \boldsymbol{v}_1^\dagger \\ \vdots \\ \boldsymbol{v}_{L-1}^\dagger \end{bmatrix}, \boldsymbol{v}_m = \begin{bmatrix} 1 \\ e^{jm\theta} \\ \vdots \\ e^{j(N-1)m\theta} \end{bmatrix}, m = 0, \ldots, L-1. \tag{G.1}$$

Thus, $\boldsymbol{W}^\dagger \mathbf{diag}(\boldsymbol{W}\boldsymbol{X}\boldsymbol{W}^\dagger) = \sum_{m=0}^{L-1}(\boldsymbol{v}_m^\dagger \boldsymbol{X}\boldsymbol{v}_m)\boldsymbol{v}_m$. From the equality constraint $t\boldsymbol{e}_1 = \boldsymbol{x} - \boldsymbol{W}^\dagger \mathbf{diag}(\boldsymbol{W}\boldsymbol{X}\boldsymbol{W}^\dagger)$, we have

$$t = \sum_{i=1}^{N}(\boldsymbol{M}\odot\boldsymbol{C}^*)(i,i) - \sum_{m=0}^{L-1}\boldsymbol{v}_m^\dagger \boldsymbol{X}\boldsymbol{v}_m, \tag{G.2}$$

and

$$\sum_{i=1}^{N-k}(\boldsymbol{M}\odot\boldsymbol{C}^*)(i+k,i) = \sum_{m=0}^{L-1}\boldsymbol{v}_m^\dagger \boldsymbol{X}\boldsymbol{v}_m e^{jkm\theta},\ k = 1, \ldots, N-1. \tag{G.3}$$

It is clear that (G.2) can be further rewritten as

$$t = \mathrm{tr}\,(\boldsymbol{A}_0\boldsymbol{C}) - \mathrm{tr}\,(\boldsymbol{B}_0\boldsymbol{X}), \tag{G.4}$$

where

$$\boldsymbol{A}_0 = \boldsymbol{I} \odot \boldsymbol{M}, \qquad \boldsymbol{B}_0 = \sum_{m=0}^{L-1} \boldsymbol{v}_m \boldsymbol{v}_m^{\dagger}. \tag{G.5}$$

Observe that (G.3) has $2(N-1)$ equalities (counting the real part and imaginary parts):

$$\mathrm{tr}\,(\boldsymbol{A}_{k,1}\boldsymbol{C}) = \mathrm{tr}\,(\boldsymbol{B}_{k,1}\boldsymbol{X}),\ \ \mathrm{tr}\,(\boldsymbol{A}_{k,2}\boldsymbol{C}) = \mathrm{tr}\,(\boldsymbol{B}_{k,2}\boldsymbol{X}),\ k = 1, \ldots, N-1 \tag{G.6}$$

where

$$\boldsymbol{B}_{k,1} = \sum_{m=0}^{L-1} \boldsymbol{v}_m \boldsymbol{v}_m^{\dagger} \cos(km\theta),\ \ \boldsymbol{B}_{k,2} = \sum_{m=0}^{L-1} \boldsymbol{v}_m \boldsymbol{v}_m^{\dagger} \sin(km\theta),\ \ k = 1, \ldots, N-1, \tag{G.7}$$

and

$$\boldsymbol{A}_{k,1} = \frac{1}{2}\boldsymbol{M}_k, \qquad \boldsymbol{A}_{k,2} = \frac{1}{2}(\boldsymbol{M}_k \odot \boldsymbol{E}), \qquad k = 1, \ldots, N-1. \tag{G.8}$$

The $N \times N$ Hermitian matrices $\boldsymbol{M}_k$, $k = 1, \ldots, N-1$, are defined by

$$\boldsymbol{M}_k(i+k, i) = \boldsymbol{M}(i+k, i), \qquad i = 1, \ldots, N-k \tag{G.9}$$

and the diagonal elements and the other lower triangular elements of $\boldsymbol{M}_k$ are zero. The $N \times N$ Hermitian matrix $\boldsymbol{E}$ is defined by

$$\begin{cases} \boldsymbol{E}(i,i) = 1, \ \ i = 1, \ldots, N, \\ \boldsymbol{E}(i,l) = -j, \ \ \forall i > l. \end{cases} \tag{G.10}$$

By considering (G.2)-(G.4), (G.6), it is possible to rewrite problem (3.23) equivalently into the following form

$$\begin{array}{ll} \max\limits_{\boldsymbol{X},\boldsymbol{C}} & \mathrm{tr}\,(\boldsymbol{A}_0\boldsymbol{C}) - \mathrm{tr}\,(\boldsymbol{B}_0\boldsymbol{X}) \\ \text{s.t.} & \mathrm{tr}\,(\boldsymbol{A}_{k,1}\boldsymbol{C}) - \mathrm{tr}\,(\boldsymbol{B}_{k,1}\boldsymbol{X}) = 0, \ \ k = 1, \ldots, N-1 \\ & \mathrm{tr}\,(\boldsymbol{A}_{k,2}\boldsymbol{C}) - \mathrm{tr}\,(\boldsymbol{B}_{k,2}\boldsymbol{X}) = 0, \ \ k = 1, \ldots, N-1 \\ & \mathrm{tr}\,(\boldsymbol{E}_i\boldsymbol{C}) \le \gamma, \ i = 1, \ldots, N \\ & \mathrm{tr}\,(\boldsymbol{C}) = N \\ & \boldsymbol{C} \succeq \boldsymbol{0}, \ \boldsymbol{X} \succeq \boldsymbol{0} \end{array} \tag{G.11}$$

where $\boldsymbol{E}_i$ are the same as those in problem (3.9). Therefore, the dual problem of (G.11) is

$$\begin{array}{ll} \min\limits_{\{y(i)\},z,\{x_1(k)\},\{x_2(k)\}} & \gamma\sum_{i=1}^{N} y(i) + Nz \\ \text{s.t.} & z\boldsymbol{I} + \sum_{i=1}^{N} y(i)\boldsymbol{E}_i + \sum_{k=1}^{N-1}(x_1(k)\boldsymbol{A}_{k,1} + x_2(k) \\ & (\boldsymbol{A}_{k,2}) \succeq \boldsymbol{A}_0, \\ & \sum_{k=1}^{N-1}(x_1(k)\boldsymbol{B}_{k,1} + x_2(k)\boldsymbol{B}_{k,2}) \preceq \boldsymbol{B}_0, \\ & y(i) \geq 0,\ i = 1,\ldots,N,\ z \in \mathbb{R},\ x_1(k) \in \mathbb{R}, \\ & x_2(k) \in \mathbb{R},\ k = 1,\ldots,N-1. \end{array} \tag{G.12}$$

Take a point $\boldsymbol{c}$ satisfying $|c(i)| \leq \gamma$ for $i = 1,\ldots,N$ and $\|\boldsymbol{c}\| = N$, and set

$$t = \min_{\nu_d \in [0,1]} \boldsymbol{p}^{\dagger}(\boldsymbol{M} \odot (\boldsymbol{c}_0\boldsymbol{c}_0^{\dagger})^*)\boldsymbol{p},$$

which is a one-dimensional optimization. It follows from (3.26) that solving the one-dimensional optimization is equivalent to solving an SDP. Thus $(\boldsymbol{c}, t)$ is feasible for (3.19) and $(\boldsymbol{c}\boldsymbol{c}^{\dagger}, t)$ is feasible for (3.20), and thus (3.23) is feasible. It follows by the weak duality theorem that the dual SDP (G.12) is bounded below.

It is further seen that problem (G.12) is strictly feasible. In fact, let z be a sufficiently large positive number, y_i positive numbers sufficiently close to zero, $x_1(k)$, $x_2(k)$ equal to zero; then $(z, y(1),\ldots,y(N), x_1(1), x_2(1),\ldots,x_1(N-1), x_2(N-1))$ is a strictly feasible solution of (G.12). It is interesting to note that $\boldsymbol{B}_0 = \boldsymbol{W}^{\dagger}\boldsymbol{W}$ is the diagonal matrix with each diagonal element being L. Therefore, it is possible to conclude that problem (3.23) is solvable, because the dual is bounded below and strictly feasible.

Appendix H

Proof of Proposition 3.5.1

The present appendix is devoted to show that problem (3.28) includes the max-cut problem and the max-3-cut problem which are known to be NP-hard [45], [49], and [50]. In fact, problem (3.28) is equivalent to

$$\begin{array}{ll} \max\limits_{\boldsymbol{c}} & \boldsymbol{c}^{\dagger}\boldsymbol{R}\boldsymbol{c} \\ \text{s.t.} & |c(i)|^2 \leq 1 \\ & \arg\left(c(i)\right) \in \{0, \frac{1}{M}2\pi, \ldots, \frac{M-1}{M}2\pi\},\ i = 1, \ldots, N \\ & \|\boldsymbol{c}\|^2 = N/\gamma. \end{array} \tag{H.1}$$

The max-cut problem for a given undirected weighted graph (E, V) with P nodes, is cast as

$$\begin{array}{ll} \max\limits_{\boldsymbol{x}} & \sum_{k<l}\left(w_{kl}(1 - x(k)x(l))\right)/2 \\ \text{s.t.} & x(k) \in \{\pm 1\},\ k = 1, \ldots, P \end{array} \tag{H.2}$$

where $w_{kl} \geq 0$ is the weight on the edge between nodes k and l[1]. Let $\boldsymbol{Q}$ be the Laplacian matrix of the graph, i.e., $Q(k,l) = -w_{kl}$ for $k \neq l$ and $Q(k,k) = \sum_{l \neq k,\, l=1}^{P} w_{kl}$. Thus, $\boldsymbol{Q} \succeq \boldsymbol{0}$ and the objective function of max-cut problem (H.2) is equal to $\frac{1}{4}\boldsymbol{x}^T\boldsymbol{Q}\boldsymbol{x}$. Now, in (H.1), setting $M = 2$ (this means that $\arg\left(c(i)\right) \in \{0, \pi\}$, $\forall i$, i.e., any $c(i)$ is real-valued), $N = 2P$, $\gamma = 2$ (this implies that $\|\boldsymbol{c}\|^2 = P$), and

$$\boldsymbol{R} = \begin{bmatrix} \frac{1}{4}\boldsymbol{Q} & \boldsymbol{0} \\ \boldsymbol{0} & \boldsymbol{0}_{P\times P} \end{bmatrix}$$

[1] When there is no edge between k and l, one sets $w_{kl} = 0$.

(the so-defined $\boldsymbol{R}$, together with $\|\boldsymbol{c}\|^2 = P$ and $|c(i)| \leq 1 \; \forall i$, implies that an optimal solution $\boldsymbol{c}^\star$ of the maximization problem (56), has $|c(i)^\star| = 1$, $i = 1, \ldots, P$, and $|c_i^\star| = 0$, $i = P+1, \ldots, 2P$), it is possible to reduce (H.1) into the max-cut problem (H.2).

Bibliography

[1] A. De Maio, S. De Nicola, Y. Huang, S. Zhang, and A. Farina, "Code Design to Optimize Radar Detection Performance under Accuracy and Similarity Constraints", *IEEE Transactions on Signal Processing*, Vol. 56, No. 11, pp. 5618-5629, November 2008.

[2] N. Levanon and E. Mozeson, *Radar Signals*, John Wiley & Sons, 2004.

[3] R. A. Horn and C. R. Johnson, *Matrix Analysis*, Cambridge University Press, 1985.

[4] A. Farina, "Waveform Diversity: Past, Present, and Future", *Third International Waveform Diversity & Design Conference*, Plenary Talk, Pisa, June 2007.

[5] A. Nehorai, F. Gini, M. S. Greco, A. Papandreou-Suppappola, and M. Rangaswamy, "Adaptive waveform design for agile sensing and communications," *IEEE J. Sel. Topics Signal Process. (Special Issue on Adaptive Waveform Design for Agile Sensing and Communications)*, Vol. 1, No. 1, pp. 2-213, Jun. 2007.

[6] J. S. Bergin, P. M. Techau, J. E. Don Carlos, and J. R. Guerci, "Radar Waveform Optimization for Colored Noise Mitigation", *2005 IEEE International Radar Conference*, pp. 149-154, Alexandria, VA, 9-12 May 2005.

[7] J. Li, J. R. Guerci, and L. Xu, "Signal Waveforms Optimal-under-Restriction Design for Active Sensing", *IEEE Signal Processing Letters*, Vol. 13, No. 9, pp. 565-568, September 2006.

[8] A. De Maio, S. De Nicola, Y. Huang, Z. Q. Luo and S. Zhang, "Design of Phase Codes for Radar Performance Optimization With

a Similarity Constraint", *IEEE Transactions on Signal Processing*, Vol. 57, No. 2, pp. 610-621, February 2009.

[9] L. K. Patton and B. D. Rigling, "Modulus constraints in adaptive radar waveform design", *2008 IEEE Inter. Radar Conf.*, pp. 1-6, Rome, Italy, 26-30 May 2008.

[10] A. De Maio, S. De Nicola, Y. Huang, D. P. Palomar, S. Zhang and A. Farina, "Code Design for Radar STAP via Optimization Theory", *IEEE Transactions on Signal Processing*, Vol. 58, No. 2, pp. 679-694, February 2010.

[11] S. Boyd and L. Vandenberghe, Convex Optimization, *Cambridge University Press*, 2003.

[12] V. J. Amuso, P. Antonik, R. A. Schneible, and Y. Zhang, "Evolutionary Computation Approach to Multi-mission Waveform Design", *Radar 2002*, Edinburgh, Scotland, UK, pp. 454-458, October 2002.

[13] V. J. Amuso and J. Enslin, "An Evolutionary Algorithm Approach to Simultaneous Multi-Mission Radar Waveform Design", Chapter 5 in Principles of Waveform Diversity and Design, *Scitech Inc.*, pp. 110-125, 2010.

[14] I. S. Reed, J. D. Mallet, and L. E. Brennan, "Rapid convergence rate in adaptive arrays", *IEEE Transaction on Aerospace and Electronic Systems*, Vol. 10, No.6, pp. 853-863, November 1974

[15] J. S. Goldstein, I. S. Reed, and P. A. Zulch, "Multistage partially adaptive STAP CFAR detection algorithm", *IEEE Transaction on Aerospace and Electronic Systems*, Vol. 35, No. 2, pp. 645-661, Apr. 1999.

[16] A. Farina and S. Pardini, "A Track-While-Scan Algorithm Using Radial Velocity in a Clutter Environment", *IEEE Transactions on Aerospace and Electronic Systems,* Vol. 14, No. 5, pp. 769-779, September 1978.

[17] H. L. Van Trees, *Optimum Array Processing. Part IV of Detection, Estimation and Modulation Theory*, John Wiley & Sons, 2002.

[18] K. Deb, Multi-Objective Optimization Using Evolutionary Algorithms, *John Wiley & Sons*, 1st ed. , June 2001.

[19] M. Wicks, "A Brief History of Waveform Diversity", *Proceedings of the 2009 Radar Conference*, Pasadena, May 2009.

[20] A. Farina and F. A. Studer, "Detection with High Resolution Radar: Great Promise, Big Challenge", *Microwave Journal*, pp. 263-273, May 1991.

[21] S. U. Pillai, H. S. Oh, D. C. Youla, and J. R. Guerci, "Optimum Transmit-Receiver Design in the Presence of Signal-Dependent Interference and Channel Noise", *IEEE Transactions on Information Theory*, Vol. 46, No. 2, pp. 577-584, March 2000.

[22] S. Kay, "Optimal Signal Design for Detection of Point Targets in Stationary Gaussian Clutter/Reverberation", *IEEE Journal on Selected Topics in Signal Processing*, Vol. 1, No. 1, pp. 31-41, June 2007.

[23] Z. Q. Luo and T. H. Chang, "SDP Relaxation of Homogeneous Quadratic Optimization: Approximation Bounds and Applications," *Convex Optimization in Signal Processing and Communications*, D. P. Palomar and Y. Eldar, Eds, Cambridge, U.K.: Cambridge Univ. Press, 2010, ch. 4.

[24] B. Dumitrescu, *Positive Trigonometric Polynomials and Signal Processing Applications*, Springer, 2007.

[25] T. Roh and L. Vandenberghe, "Discrete Transforms, Semidefinite Programming, and Sum-of-Squares Representations of Nonnegative Polynomials," *SIAM Journal on Optimization*, Vol. 16, No. 4, pp. 939-964, 2006.

[26] A. Nemirovski, "Lectures on Modern Convex Optimization", *Class Notes, Georgia Institute of Technology*, Fall 2005.

[27] Y. Huang and S. Zhang, "Complex Matrix Decomposition and Quadratic Programming", *Mathematics of Operations Research*, Vol. 32, No. 3, pp. 758-768, Aug. 2007.

[28] J. F. Sturm, " Using SeDuMi 1.02, a MATLAB Toolbox for Optimization over Symmetric Cones," *Optimization Methods and Software*, Vol. 11-12, pp. 625-653, August 1999.

[29] R. Calderbank, S. Howard and B. Moran, “Waveform Diversity in Radar Signal Processing", *IEEE Signal Processing Magazine*, Vol. 26, No. 1, pp. 32-41, February 2009.

[30] D. Cochran, S. Suvorova, S. Howard and B. Moran, “Waveform Libraries", *IEEE Signal Processing Magazine*, Vol. 26, no. 1, pp. 12-21, February 2009.

[31] D. T. Gjessing, *Target Adaptive Matched Illumination Radar: Principles and Applications*, Peter Peregrinus: IEE Electromagnetic Waves Series, July 1986.

[32] A. De Maio, Y. Huang, and M. Piezzo, “A Doppler Robust Max-Min Approach to Radar Code Design", *IEEE Transactions on Signal Processing*, Vol. 58, No. 9, pp. 4943-4947, September 2010.

[33] H. He, P. Stoica, and J. Li, “Waveform Design with StopBand and Correlation Constraints for Cognitive Radar," *The 2nd International Workshop on Cognitive Information Processing*, Elba Island, Italy, June 2010.

[34] T. Jiang and Y. Wu, “An Overview: Peak-to-Average Power Ratio Reduction Techniques for OFDM Signals," *IEEE Transactions on Broadcasting*, Vol. 54, No. 2, pp. 257-268, February 2008.

[35] W. K. Ma, T. N. Davidson, K. M. Wong, Z. Q. Luo, and P. C. Ching, “Quasi-Maximum-Likelihood Multiuser Detection Using Semi-Definite Relaxation with Application to Synchronous CDMA", *IEEE Transactions on Signal Processing*, Vol. 50, No. 4, pp. 912 - 922, April 2002.

[36] E. Karipidis, N. D. Sidiropoulos, Z. Q. Luo, “Convex Transmit Beamforming for Downlink Multicasting to Multiple Co-Channel Groups", *Proceedings of the 2006 IEEE International Conference on Acoustics, Speech and Signal Processing*, Vol. 5, Toulouse, France, 14-19 May 2006.

[37] S. Zhang and Y. Huang, “Complex Quadratic Optimization and Semidefinite Programming," *SIAM Journal on Optimization*, Vol. 16, No. 3, pp. 871-890, 2006.

[38] Z. Q. Luo, N. D. Sidiropoulos, P. Tseng, and S. Zhang, "Approximation Bounds for Quadratic Optimization with Homogeneous Quadratic Constraints," *SIAM Journal on Optimization*, Vol. 18, pp. 1-28, February 2007.

[39] A. Nemirovski, C. Roos, and T. Terlaky, "On Maximization of Quadratic Form over Intersection of Ellipsoids with Common Center," Mathematcial Programming, Vol. 86, pp. 463-473, 1999.

[40] N. Sidiropoulos, T. Davidson, and Z.-Q. Luo, "Transmit Beamforming for Physical-Layer Multicasting," *IEEE Transactions on Signal Processing*, Vol. 54, No. 6, pp. 2239-2251, June 2006.

[41] A. So, J. Zhang, and Y. Ye, "On Approximating Complex Quadratic Optimization Problems Via Semidefinite Programming Relaxations," *Mathematical Programming*, Series B, Vol. 110, No. 1, pp. 93-110, June 2007.

[42] W.-K. Ma, B.-N. Vo, T. N. Davidson, and P.-C. Ching, "Blind ML Detection of Orthogonal Space-Time Block Codes: Efficient High-Performance Implementations", *IEEE Transactions on Signal Processing*, Vol. 54, No. 2, pp. 738-751, November 2008.

[43] Z.-Q. Luo, W.-K. Ma, A.M.-C. So, Y. Ye, and S. Zhang, "Semidefinite Relaxation of Quadratic Optimization Problems," *IEEE Signal Processing Magazine*, Vol. 27, No. 3, pp. 20-34, May 2010.

[44] M. Grant and S. Boyd, "CVX: Matlab Software for Disciplined Convex Programming (web page and software)," http://stanford.edu/∼boyd/cvx, December 2008.

[45] M. X. Goemans and D. P. Williamson, "Improved Approximation Algorithms for Maximum Cut and Satisfiability Problem using Semi-Definite Programming," *Journal of the ACM*, Vol. 42, pp. 1115-1145, 1995.

[46] S. Zhang, "Quadratic Maximization and Semidefinite Relaxation," *Mathematical Programming*, Ser. A, Vol. 87, No. 3, pp. 453-465, 2000.

[47] S. M. Kay, *Fundamentals of Statistical Signal Processing: Detection Theory*, Englewood Cliffs, NJ: Prentice-Hall, 1998, vol. II.

[48] M. R. Garey and D. S. Johnson, *Computers and Intractability: A Guide to the Theory of NP-Completeness*. San Francisco, CA: Freeman, 1979.

[49] M. X. Goemans and D. P. Williamson, "Approximation Algorithms for MAX-3-CUT and Other Problems Via Complex Semidefinite Programming", *Journal of Computer and System Sciences*, Vol. 68, No. 2, pp. 442-470, March 2004.

[50] A. Frieze and M. Jerrum, "Improved Approximation Algorithms for MAX k-CUT and MAX BISECTION", *Algorithmica*, Vol. 18, No. 1, pp. 67-81, May 1997.

[51] M. Skolnik, *Radar Handbook, 3rd Ed.*, Mc Graw Hill, 2008.

[52] P. Antonik, H. Shuman, P. Li, W. Melvin, and M. Wicks, "Knowledge-Based Space-Time Adaptive Processing," *1997 IEEE National Radar Conference*, Syracuse, NY, May 1997.

[53] P. A. Antonik, H. Griffiths, D. D. Wiener, and M. C. Wicks, "Novel Diverse Waveform," *Air Force Research Lab.*, New York, In-House Rep., June 2001.

[54] F. Gini and M. Rangaswamy, Editors, *Knowledge Based Radar Detection, Tracking and Classification*, John Wiley & Sons, Inc., 2008.

[55] J. R. Guerci, *Cognitive Radar, The Knowledge-Aided Fully Adaptive Approach*, Artech House, 2010.

[56] L. K. Patton, "On the Satisfaction of Modulus and Ambiguity Function Constraints in Radar Waveform Optimization for Detection," *Doctor of Philosophy (PhD) Dissertation*, Wright State University, Engineering PhD, 2009.

[57] A. De Maio, Y. Huang, M. Piezzo, S. Zhang, and A. Farina, "Design of Optimized Radar Codes with a Peak to Average Power Ratio Constraint," *IEEE Transactions on Signal Processing*, Vol. 59, No. 6, pp. 2683-2697, June 2010.

[58] W. D. Rummler, "A Technique for Improving the Clutter Performance of Coherent Pulse Trains Signals," *IEEE Transactions on Aerospace and Electronic Systems*, Vol. AES-3, No. 6, pp. 689-699, November 1967.

[59] D. F. Delong JR. and E. M. Hofstetter, " The Design of Clutter-Resistant Radar Waveforms with Limited Dynamic Range," *IEEE Transactions on Information Theory*, Vol. IT-15, No. 3, pp. 376-385, May 1969.

[60] J. S. Thompson and E. L. Titlebaum, "The Design of Optimal Radar Waveforms for Clutter Rejection Using the Maximum Principle," *Supplement to IEEE Trans. on Aerosp. Electron. Syst.*, Vol. AES-3, pp. 581-589, November 1967.

[61] A. I. Cohen, "An Algorithm for Designing Burst Waveforms with Quantized Transmitter Weights," *IEEE Transactions on Aerospace and Electronic Systems*, Vol. AES-11, No. 1, pp. 56-64, Jannuary 1975.

[62] A. Aubry, A. De Maio, A. Farina, and M. Wicks, "Knowledge-Aided (Potentially Cognitive) Transmit Signal and Receive Filter Design in Signal-Dependent Clutter", *IEEE Transactions on Aerospace and Electronic Systems*, Vol. 49, No. 1, pp. 93-117, January 2013.

[63] P. Stoica, H. He, and J. Li, "Optimization of the Receive Filter and Transmit Sequence for Active Sensing", *IEEE Transactions on Signal Processing*, Vol. 60, No. 4, pp. 1730-1740, April 2012.

[64] A. Kurekin, D. Radford, K. Lever, D. Marshall, and L. K. Shark, "New method for generating site-specific clutter map for land-based radar by using multimodal remote-sensing images and digital terrain data", *IET Radar, Sonar & Navigation*, Vol. 5, No. 3, pp. 374-388, March 2011.

[65] A. De Maio, Y. Huang, D. P. Palomar, S. Zhang, and A. Farina, "Fractional QCQP With Applications in ML Steering Direction Estimation for Radar Detection," *IEEE Transactions on Signal Processing*, Vol. 59, No. 1, pp. 172-185, January 2011.

[66] G. H. Golub and C. F. Van Loan, *Matrix Computations, 3rd Ed.*, The Johns Hopkins University Press, Baltimore and London, 1996.

[67] L. Bomer and M. Antweiler, "Polyphase Barker Sequences," *Electronics Letters*, Vol. 25, n. 23, pp. 1577-1579, November 1989.

[68] M. Friese, "Polyphase Barker Sequences up to Length 36," *IEEE Transactions on Information Theory*, Vol. IT-42, No. 4, pp. 1248-1250, July 1996.

[69] M. A. Richards, J. A. Scheer, and W. A. Holm, *Principles of Modern Radar: Basic Principles.* Raleigh, NC: Scitech Publishing, 2010.

[70] E. Mozeson and N. Levanon, "MATLAB Code for Plotting Ambiguity Functions," *IEEE Transactions on Aerospace and Electronic Systems*, Vol. AES-38, No. 3, pp. 1064-1068, July 2002.